Soft gluons and non-perturbative effects in QCD observables

A thesis submitted to the University of Manchester
for the degree of Doctor of Philosophy
in the Faculty of Engineering and Physical Sciences

2007

Yazid Delenda

School of Physics and Astronomy

Contents

Word count: 34,237

List of Tables

List of Figures

Abstract

In preparation to the commencement of the LHC considerable effort is devoted to improving the current understanding of QCD radiation. We are concerned here with this issue as manifested in soft gluon bremsstrahlung and non-perturbative effects. We study different observables that are sensitive to soft radiation and deduce the implications for current and future colliders.

We specifically address the possible small-x broadening effects, not accounted for in conventional Q_t resummations, in the Higgs Q_t spectrum at hadronic colliders. As a probe for this we study the DIS Breit current hemisphere Q_t spectrum at HERA. We resum the large logarithms to NLL accuracy, match the result to NLO predictions and smear it with a non-perturbative Gaussian function. Comparing our predictions to HERA data ought to reveal the existence or absence of such small-x effects.

Next we study the impact of jet algorithms on QCD resummation. There are very few resummed predictions for jet-defined quantities, which are often considered in QCD studies relevant (for instance) to the LHC, due to the lack of theoretical insight to all orders in the presence of jet algorithms. We consider the simple case of energy flow into a gap between two jets and compute the dependence of primary emissions on the k_t clustering algorithm. We show how non-global logarithms in this case are even more significantly reduced than suggested before in the literature and estimate the impact of our findings on ZEUS photoproduction data.

We then study the azimuthal correlation distribution for dijet production in DIS at HERA. We perform an NLL resummation and combine the result with NLO predictions. We point to the extension of this work to hadronic collisions at the Tevatron. The results of this analysis are important as this observable is commonly studied by experimentalists, e.g. to extract non-perturbative parameters.

Finally we calculate the power corrections to energy flows in hadronic collisions. This study provides the technology for further analyses of similar observables involving non-trivial colour algebra and dipole geometry.

Chapters 1 to 3 of this thesis are introductory and review chapters while chapters 4 to 7 represent the main results.

Declaration

No portion of the work referred to in the thesis has been submitted in support of an application for another degree or qualification of this or any other university or other institute of learning.

Copyright Statement

The Author

The author was educated at Lycée de Mohammed El-Tahar Qaddouri in Batna, Algeria, before joining the English Language Teaching Centre at UMIST in September 2000 and obtaining an IELTS certificate in April 2001. The author then enrolled in the School of Physics and Astronomy at the University of Manchester in September 2001 and obtained a first class Bachelor of Science with Honours in July 2004. The work presented in this thesis was undertaken at the University of Manchester.

Acknowledgments

I would like to thank my supervisor, Mrinal Dasgupta, for all the effort he made to ensure the success of the work presented in this thesis. Thanks to Jeff Forshaw and Fred Loebinger for administrative help and advise, and to Tim Coughlin for proofreading the thesis.

I also thank Gavin Salam for the assistance with the NLO program used in chapter 4 and Thomas Kluge for the preliminary HERA data for the distribution studied in the same chapter.

The work presented in chapter 5 was done in collaboration with Andrea Banfi and Robert Appleby. I would like to thank them both for the collaboration. Further thanks to Andrea for the collaboration and assistance in the work presented in chapter 6. The details of the contributions of collaborators is stated below.

I would also like to thank Magnus Hansson and Leif Jönsson for interesting discussions regarding the work presented in chapter 6.

The work presented in this thesis is sponsored by the Algerian government. I would like to thank the student affairs section in the Algerian consulate in London for their devotion to ensure a high level of service to the Algerian student community in the U.K.

The following details concern the contributions of collaborators to the work presented in this thesis:

- The numerical code used in chapter 5, originally described in ref. [21] with the modification of k_t clustering, and the analysis of the impact of k_t clustering on non-global logarithms, discussed in section 5.4, are contributions of Andrea Banfi and Mrinal Dasgupta (see ref. [20]).

- The analysis of the implications of our findings in chapter 5 for ZEUS photoproduction data, discussed in section 5.5, is a contribution of Robert Appleby (see ref. [20]).

- The program used for the numerical integration in chapter 6 and the NLO results (obtained from NLOJET++ [39, 40]) used in the same chapter are sup-

plied by Andrea Banfi. All the numerical analyses in that chapter were performed with a *detailed* assistance, in terms of both programming and physics, of Andrea Banfi (see ref. [38]).

List of Publications

- M. Dasgupta and Y. Delenda, *Aspects of power corrections in hadron-hadron collisions*, *submitted to J. High Energy Phys.* [arXiv: 0709.3309].

- Y. Delenda, *Dijet Azimuthal Correlations in QCD Hard Processes*, *To appear in the proceedings of* 15^{th} *International Workshop on Deep-Inelastic Scattering and Related Subjects (DIS 2007), Munich, Germany, 16-20 Apr 2007* [arXiv: 0706.2172].

- Y. Delenda, R. Appleby, A. Banfi and M. Dasgupta, *On QCD resummation with k_t clustering*, *J. High Energy Phys.* **12** (2006) 044 [hep-ph/0610242].

- M. Dasgupta and Y. Delenda, *The Q_t distribution of the Breit current hemisphere in DIS as a probe of small-x broadening effects*, *J. High Energy Phys.* **08** (2006) 080 [hep-ph/0606285].

- A. Banfi, G. Corcella, M. Dasgupta, Y. Delenda, G. P. Salam and G. Zanderighi, *Resummation*, *In the proceedings of HERA and the LHC: A Workshop on the Implications of HERA and LHC Physics, Hamburg, Germany, 21-24 Mar 2005* [hep-ph/0508096].

Dedication

The thesis is dedicated to my parents and my wife.

Chapter 1

Introduction

With the upcoming LHC collider valuable data are to be collected, providing the means for potential discoveries and advancements in various fields of particle physics. This machine will collide protons at a centre-of-mass energy of 14 TeV, thus becoming the largest and highest energy collider in the world. For comparison with the HERA collider we show in fig. 1.1 the kinematics regions that are accessible by two machines.

For optimal success of the program of searching for new physics (at the LHC) one needs to establish as good an understanding as possible of the physics involved in the comparison between such data and theory. In this context the role of the theory of strong interactions, quantum chromodynamics (QCD), is dominant since quarks and gluons are always involved in such studies. This theory describes the interactions between these particles with various approaches, e.g. lattice, perturbative and non-perturbative, that attempt to provide as accurately as possible theoretical predictions for many measured quantities.

The understanding of soft gluon radiation and non-perturbative effects, which form the bulk of QCD dynamics (e.g. in Higgs production), plays an important role in studies that aim to enhance QCD knowledge. To illustrate this point we show in fig. 1.2 a typical jet-event at the LHC in which two protons with momenta P_1 and P_2 collide head-on. Here we note that several sub-processes cannot be computed from first principles. In fact only the hard process, which contains potential new physics such as the Higgs production, can be dealt with from first principles to a few orders in α_s (the strong coupling) and in some cases the accompanying soft radiation to all

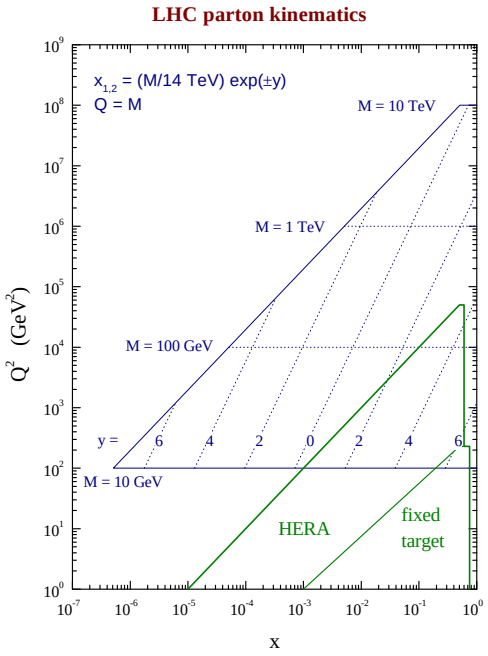

Figure 1.1: Comparison of the kinematics of HERA and the LHC. x and Q are the momentum fraction of the proton carried by the parton and the hard scale involved. Diagram is taken from ref. [1].

orders to a certain logarithmic accuracy. Precision in QCD is limited not just by what powers of α_s are controlled, but also by the lack of good understanding of dynamics such as the all-orders behaviour (manifested in the resummation of large logarithms) and the inevitable process of conversion of partons into hadrons, hadronisation.

It is even more difficult to get a grasp of this dynamics in hadronic collisions than in processes involving at least one lepton in the initial state, such as e^+e^- annihilation into hadrons and deep inelastic lepton-proton scattering (DIS). For instance in hadronic collisions interactions between remnants of both incoming protons, which are part of the underlying event, are also a major piece of non-perturbative effects. However these are absent in e^+e^- annihilation into jets and DIS studies.

It is therefore of benefit to use existing collider data such as those from HERA to probe QCD aspects that will still be relevant at the LHC. In this thesis we study observables that can be measured at both existing colliders and the LHC. We outline below the contents of this thesis referring the reader to fig. 1.2, which pinpoints the specific issues we are concerned.

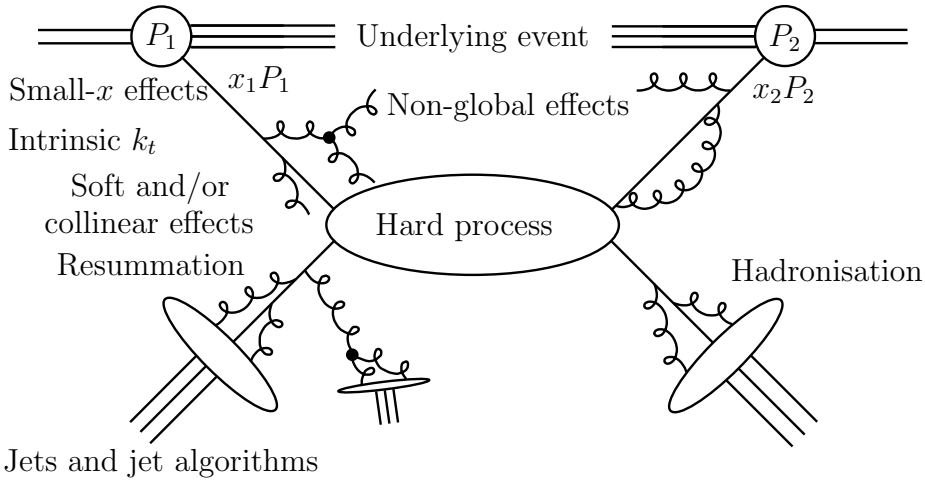

Figure 1.2: A typical jet-event at the LHC. This thesis is concerned with or related to the uncertainties associated with this process as shown here.

We begin by looking at the small-x enhancement[1] of non-perturbative intrinsic k_t effects, where x can be interpreted as the momentum fraction of the incoming hadron carried by the struck parton, in transverse momentum (Q_t) distribution of vector bosons (from Drell-Yan production) and Higgs boson. These distributions are often considered in identifying and studying the properties of massive bosons. Resummation of large logarithms that appear in the study of such distributions is established up to next-to-next-to-leading log (NNLL)[2] combined with next-to-leading order (NLO) accuracy for the Higgs Q_t spectrum [2, 3]. To account for non-perturbative effects one smears the perturbative result with a non-perturbative Gaussian function, representing the intrinsic k_t distribution of the incoming partons. It has been pointed out by Berge et al that such distributions may acquire a broader shape through Balitsky-Fadin-Kuraev-Lipatov (BFKL [4, 5, 6, 7]) enhancements of non-perturbative intrinsic-k_t effects, by means of modelling logarithms of $1/x$ to all orders into a Gaussian, as it has been observed for semi-inclusive deep inelastic

[1]Such small-x effects manifest themselves (in impact parameter space) as a factor proportional to $1/x$ in the exponent of the Gaussian function describing the intrinsic transverse momentum (k_t) distribution.

[2]Here we refer to NNLL accuracy in the logarithm of the integrated cross-section. For reference, most resummations, e.g. those for several event shapes at LEP and HERA, achieve only a next-to-leading logarithmic (NLL) accuracy.

scattering (SIDIS) Q_t distribution [8, 9]. These small-x effects may be particularly strong at the LHC and thus they are important for Higgs studies.

As a probe for this effect we study[3] the Q_t distribution of the DIS Breit current hemisphere in chapter 4. In the Breit frame [11, 12, 13] the incoming quark showers the remnant hemisphere, to NLL accuracy, with soft emissions giving rise to a transverse momentum for the incoming quark, which then scatters off the electron and showers the current hemisphere. The mechanism of acquiring a vectorial transverse momentum through recoil in this case is very similar to that of Q_t distributions in Drell-Yan vector boson and Higgs production at hadronic colliders. This similarity can be used to probe the non-perturbative (small-x) behaviour of such distributions. Furthermore the study we perform exploits a cleaner environment in terms of additional non-perturbative effects (as we stated before), such as multiple hard scattering and the underlying event. Thus we study this distribution resumming the large logarithms (in Q/Q_t, with Q being the hard scale) to NLL accuracy, performing an NLO matching and smearing the result with a non-perturbative (intrinsic-k_t) Gaussian function.

Next we look at jets in the final state and the impact of clustering algorithms on soft gluon resummation. For many observables that are valuable for LHC studies, one typically defines the final state in terms of clusters of jets rather than individual hadrons [14, 15, 16, 17]. This reconstruction has an impact on observables which are sensitive to emissions in a limited region of the phase-space [18, 19, 20] (non-global observables [21, 22]). Examples include energy flow into a gap between jets in hadronic collisions at the Tevatron [23, 24, 25] and in DIS photoproduction at HERA [26, 27, 28]. These observables receive extra single logarithms[4] (which are leading in the case of inter-jet energy flow) relative to "global" observables. Currently these extra logarithms can only be resummed numerically in the large N_c limit for two-jet[5] observables [21, 22], where N_c is the number of colour degrees of freedom.

It was shown by Appleby and Seymour [18] that employing a clustering algorithm

[3]Published in ref. [10].

[4]Super-leading (double) logarithms may also be present for these observables in processes involving four hard partons [29].

[5]In this thesis we count the number of jets including both initial and final-state ones.

on the final-state hadrons reduces the size of non-global logarithms in the case of energy flow into a gap between two jets. Furthermore it was noted by Banfi and Dasgupta [19] that the clustering requirement has a non-trivial impact on the global (primary) part of the resummed distribution, previously thought to just be the exponentiation of the single-gluon contribution. In this thesis we extend[6] the analysis of Banfi and Dasgupta [19] in chapter 5 and show that the result presented there in fact exponentiates and calculate additional terms that arise at higher orders. We also point out that the non-global component is even more reduced than previously claimed by Appleby and Seymour [18], after correction of an oversight in the numerical code, and estimate the impact of our findings on ZEUS photoproduction data. Thus we conclude that this method essentially makes any unaccounted-for $\mathcal{O}(1/N_c^2)$ terms in the non-global component negligible. This study gives us the technology to proceed with studies of non-global observables with jet-defined final states such as dijet azimuthal correlations.

Thus we proceed in chapter 6 with studying the dijet azimuthal correlation distribution ($\Delta\phi \equiv \pi - \delta\phi_{\text{jets}}$, with $\delta\phi_{\text{jets}}$ being the difference in azimuth between the leading hard jets in the final state) both in DIS and hadronic collisions. This quantity has recently been measured by the DØ collaboration at the Tevatron [30, 31] and the H1 collaboration at HERA [32, 33]. There have been many studies for this observable with various approaches aiming to extract non-perturbative parameters such as unintegrated parton distribution functions (PDFs) [34, 35], intrinsic k_t distributions [35] and small-x (BFKL) effects [36, 37]. However no resummed calculations have been performed due to the lack of theoretical insight to all orders in the presence of a jet algorithm. Now that we have the technology to deal with such algorithms [20] we can provide theoretical predictions for this observable.

Thus we perform[7] a full NLL resummation (we resum logarithms of $1/\Delta\phi$ in the small $\Delta\phi$ region) to this observable and match the resummed result to NLOJET++ [39, 40] predictions. In this study we concentrate on the DIS case and use the jet

[6]Published in ref. [20]. See the acknowledgment section for details of contributions of collaborators to this thesis.

[7]See ref. [38].

recombination method in which the azimuth of a jet is defined by the average E_t-weighted azimuths of particles in the jet [15]. This definition, as we shall show, makes the observable global and thus no non-global component is present and the resummed result, to NLL accuracy, has no dependence on the jet algorithm. This is the recombination scheme used by the H1 collaboration to measure this observable [32]. On the other hand the jet recombination scheme in which the four-momentum of a jet is defined by the addition of four-momenta of hadrons inside the jet, implies that the observable is non-global. The DØ collaboration employed the latter recombination scheme to measure the observable [30, 31]. In our study we point to the hadronic collisions case using both recombination schemes and briefly discuss the implications of our findings in chapter 5 on the result in the non-global case.

Finally we turn our attention to non-perturbative (hadronisation) effects. Such effects are incalculable from first principles and are usually estimated by models (for a review see ref. [41]). A popular and successful model that described the data well proved to be the renormalon (dispersive approach) model[8] [44]. Here one extrapolates the strong coupling, which diverges at the QCD scale ($\Lambda_{\rm QCD}$), into the non-perturbative domain and replaces the perturbative coupling below some infrared matching scale with this extrapolation. As a result of this, for example, event-shape variables receive "power corrections", amounting to a shift of their resummed distributions by an amount proportional to $1/Q$, where Q is the hard scale of the process [45, 46, 47]. Mean values of event shapes also receive corrections which are proportional to $1/Q$ [46, 47, 48, 49]. Q_t distributions acquire leading non-perturbative (intrinsic k_t) corrections through a Gaussian smearing function which can also be derived from the renormalon model [50].

The dispersive approach has in fact been successful for observables involving up to three jets [51, 52, 53, 54]. However for four-jet observables there are currently very few studies of non-perturbative power-behaved corrections (e.g. in ref. [55]) since they involve non-trivial colour algebra. Thus we investigate[9] in chapter 7 of this thesis non-perturbative power corrections to the energy flow distribution in hadronic

[8]For recent experimental reviews see refs. [42, 43].

[9]Published in ref. [56].

collisions. We find that the resummed distribution acquires a correction which is *not* a simple shift as in the case of event shapes in e^+e^- annihilation into two jets and DIS. The reason for this is the matrix structure of the colour flow in the resummed result [57, 58, 59, 60]. In our analysis we neglect the impact of non-global logarithms [21, 22] and the possible super-leading logarithms [29]. Nonetheless this work reveals the technology to further study non-perturbative power corrections in observables involving complicated colour flows and dipole geometry.

In the next chapter we provide a brief overview of QCD and the parton model. We use the process of DIS to illustrate the physics relevant to this thesis.

Chapter 2

Review of QCD, DIS and the parton model

2.1 Introduction

In this chapter we briefly discuss the basics of QCD. We review its Lagrangian and the derivation of Feynman rules. Then we discuss one of the most important processes that give us insight into QCD, namely DIS. We present the cross-section for this process and define the Breit frame of reference. We then discuss the property of collinear factorisation [61, 62, 63, 64] and Dokshitzer-Gribov-Lipatov-Altarelli-Parisi (DGLAP) evolution [65, 66, 67, 68].

2.2 Review of QCD

The theory of QCD is one of the building blocks of the Standard Model. It was introduced to explain the phenomenon of strong interactions between quarks and gluons. Its main feature is that it is a non-Abelian gauge theory with three colour degrees of freedom. The QCD Lagrangian is given by:

$$\mathcal{L} = \sum_f \left[\bar{q}_f^\alpha \left(i\gamma_\mu \partial^\mu - m_f \right) q_f^\alpha - g_s \left(\bar{q}_f^\alpha \gamma_\mu t^a_{\alpha\beta} q_f^\beta \right) \mathcal{A}_a^\mu \right] - \frac{1}{4} F^a_{\mu\nu} F_a^{\mu\nu}, \tag{2.2.1}$$

where the sum runs over all the flavours f, q are the quark fields (spinors[1]) with indices α and β running from 1 to N_c (quark colours), γ_μ are the Dirac matrices,

[1] We have suppressed spinor indices. The sum over repeated indices is assumed.

m_f are the quark masses, $g_s = \sqrt{4\pi\alpha_s}$, t^a are the SU(N_c) group generators in the fundamental representation ($N_c \times N_c$ matrices), with index a running from 1 to $N_c^2 - 1$ (gluon colours), $\mathcal{A}_\mu^a$ are the gauge fields and $F_{\mu\nu}$ is the gluon field strength tensor:

$$F_{\mu\nu}^a = \partial_\mu \mathcal{A}_\nu^a - \partial_\nu \mathcal{A}_\mu^a - g_s f_{abc} \mathcal{A}_\mu^b \mathcal{A}_\nu^c, \tag{2.2.2}$$

with f_{abc} being the structure constants.

From this Lagrangian Feynman rules can be derived. For instance the quark propagator can be read off from the first term by making the replacement $\partial^\mu \to -ip^\mu$ and taking the inverse of the term between the quark field and its Dirac conjugate and multiplying it by a factor i.

The interaction terms (those containing g_s) originate by imposing gauge invariance, that is the invariance of the Lagrangian under the local SU(N_c) transformation: $q^\alpha(x) \to [\exp(it^a\theta_a(x))]_{\alpha\beta} q^\beta(x)$, for arbitrary $\theta_a(x)$. These terms are used to derive Feynman rules for vertices. The last term in eq. (2.2.2) is absent in quantum electrodynamics (QED), and gives rise to gluon self-interactions and thus the property of asymptotic freedom [69, 70].

Feynman diagrams can then be used to predict measured cross-sections. In the next section we report on the DIS process and how its cross-section is calculated.

2.3 Deep inelastic electron-proton scattering

DIS[2] is one of the most powerful tools for testing the parton model of QCD. For instance it provides accurate measurements of variables that describe the structure of the proton and the strong coupling at different scales. In this process an electron scatters off a quark from the proton (at Born level) by the exchange of a virtual hard photon as shown in fig. 2.1. In all what follows we neglect the proton mass since it is much smaller than the photon virtuality.

[2]We explicitly use this process in chapters 4 and 6. Furthermore the results we derive in chapters 5 and 7 are relevant to dijet photoproduction in DIS.

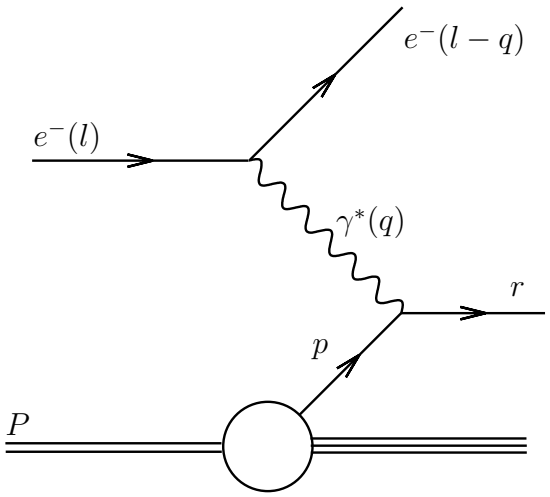

Figure 2.1: The process of DIS at Born level.

2.3.1 Leading-order kinematics

We consider the process in which a real gluon is emitted in DIS off a massless quark (fig. 2.2), or alternatively photon-gluon fusion (fig. 2.3).

We introduce the standard DIS variables: ξ, x and z. These satisfy the following relations: $p = xP/\xi$, $x = Q^2/(2P.q)$, $z = P.r/P.q = p.r/p.q$ and $Q^2 = -q^2$, where p, q , r and k are the momenta of the incoming parton, the virtual photon and the two outgoing partons respectively (as shown in figs. 2.2 and 2.3) and P is the momentum of the proton. The variable x represents the momentum fraction of the struck quark relative to the proton and x/ξ is the momentum fraction of the incoming parton relative to the proton. Thus $0 < x < \xi < 1$. We also define the variable $y = P.q/P.l = p.q/p.l \simeq Q^2/(xs)$, with s being the centre-of-mass energy squared and l being the momentum of the incoming electron. This variable describes the scattering angle of the electron.

2.3.2 Leading-order cross-section

The total cross-section for this process can be factored into a leptonic tensor, $L_{\mu\nu}$, corresponding to the Feynman amplitude squared for the emission of the virtual photon from the electron summed and averaged over spin, and a hadronic tensor, $W^{\mu\nu}$, corresponding to the Feynman amplitude squared for the diagrams in fig. 2.2

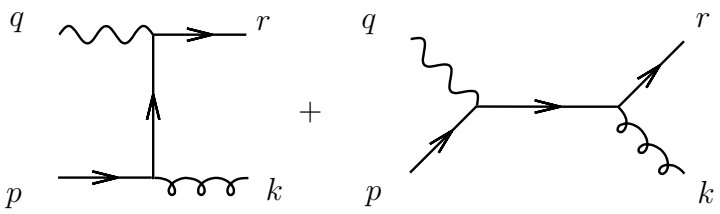

Figure 2.2: Leading-order Feynman diagrams for the emission of a real gluon in DIS with an incoming quark.

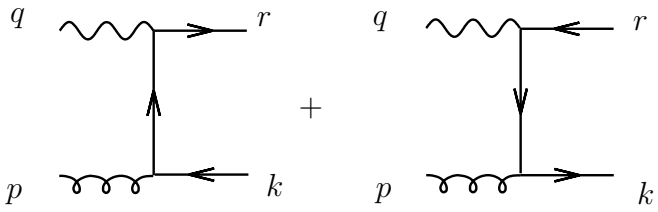

Figure 2.3: Leading-order Feynman diagrams for photon-gluon fusion in DIS with an incoming gluon.

or 2.3 summed and averaged over colours, spins and/or polarisations accordingly.

It is convenient to divide the hadronic tensor into two pieces contributing to the longitudinal and transverse structure functions. Namely:

$$W^{\mu\nu} = \left(-g^{\mu\nu} + \frac{q^\mu q^\nu}{q^2}\right) W_1 + \left(P^\mu + \frac{1}{2x}q^\mu\right)\left(P^\nu + \frac{1}{2x}q^\nu\right) W_2, \tag{2.3.1}$$

with $g_{\mu\nu}$ being the metric tensor. Hence:

$$W_1 = \frac{1}{2}\left(\frac{4\xi^2}{Q^2}p_\mu p_\nu - g_{\mu\nu}\right) W^{\mu\nu}, \tag{2.3.2}$$

$$W_2 = \frac{2x^2}{Q^2}\left(\frac{12\xi^2}{Q^2}p_\mu p_\nu - g_{\mu\nu}\right) W^{\mu\nu}. \tag{2.3.3}$$

The structure functions $\tilde{F}_1(x, Q^2)$ and $\tilde{F}_2(x, Q^2)$ are defined by: $\tilde{F}_1 = W_1$ and $\tilde{F}_2 = W_2\, Q^2/(2x)$. The transverse and longitudinal structure functions are given by: $\tilde{F}_T = 2\tilde{F}_1$ and $\tilde{F}_L = \tilde{F}_2/x - 2\tilde{F}_1$. Since we shall particularly be interested in the DIS final state (mainly in chapters 4 and 6) we utilise the *generalised* structure functions which do not contain virtual corrections and are unintegrated over z:

$$F_i(x, z, Q^2) = \frac{\alpha_s}{2\pi}\int_x^1 \frac{d\xi}{\xi}\left[C_F C_{i,q}(\xi, z) q\left(\frac{x}{\xi}, Q^2\right) + T_f C_{i,g}(\xi, z) g\left(\frac{x}{\xi}, Q^2\right)\right], \tag{2.3.4}$$

where $q(x, Q^2) = \sum_{j=1}^{n_f} e_j^2 (q_j(x, Q^2) + \bar{q}_j(x, Q^2))$, with q_j standing for the PDF for quark j and the sum extending over the n_f active quark flavours, and $T_f =$

$T_R \sum_{j=1}^{n_f} e_j^2$. Here C_F and T_R are the usual QCD colour factors, $C_F = (N_c^2 - 1)/(2N_c) = 4/3$ and $T_R = 1/2$ (where we assume $N_c = 3$).

The leading-order coefficient functions are given by [71]:

$$C_{T,q}(\xi, z) = \frac{z^2 + \xi^2}{(1-\xi)(1-z)} + 2z\xi + 2, \tag{2.3.5}$$

$$C_{L,q}(\xi, z) = 4z\xi, \tag{2.3.6}$$

$$C_{T,g}(\xi, z) = [\xi^2 + (1-\xi)^2]\frac{z^2 + (1-z)^2}{z(1-z)}, \tag{2.3.7}$$

$$C_{L,g}(\xi, z) = 8\xi(1-\xi). \tag{2.3.8}$$

After multiplying the hadronic tensor by the leptonic one and inserting the flux factors, the leading-order cross-section can be expressed as:

$$\frac{d^3\sigma}{dxdQ^2dz} = \frac{2\pi\alpha_{\rm em}^2}{Q^4}\left([1 + (1-y)^2]F_T(x,z) + 2(1-y)F_L(x,z)\right), \tag{2.3.9}$$

where $\alpha_{\rm em}$ is the electromagnetic coupling constant. Alternatively we can normalise the leading-order cross-section to the Born cross-section, σ_0, which satisfies:

$$\frac{d^2\sigma_0}{dxdQ^2} = \frac{2\pi\alpha_{\rm em}^2}{Q^4}[1 + (1-y^2)]q(x, Q^2). \tag{2.3.10}$$

Hence for a fixed x and Q we have:

$$\begin{aligned}\frac{1}{\sigma_0}\frac{d\sigma}{dz} &= \frac{1}{q(x,Q^2)}\left(F_T(x,z) + \frac{2(1-y)}{1+(1-y)^2}F_L(x,z)\right) \\ &= \frac{1}{q(x,Q^2)}\left(\frac{F_2(x,z)}{x} - \frac{y^2}{1+(1-y)^2}F_L(x,z)\right).\end{aligned} \tag{2.3.11}$$

We notice that the cross-section has soft and/or collinear singularities ($\xi \to 1$ and/or $z \to 1$ for the incoming quark channel and $z \to 1$ or 0 for the incoming gluon channel[3]). Soft singularities cancel when virtual corrections are considered, while collinear singularities do not. The uncancelled singularities are a sign of non-perturbative effects and are absorbed into PDFs. We discuss this in further detail in the next section.

2.3.3 The Breit frame

It proves convenient to introduce the Breit frame[4] of reference [11, 12, 13] which is defined by the rest frame of $2xP + q$. We choose to align the $+z$-axis along the

[3]Note that there are no soft singularities for the incoming gluon channel. Also note that there are no virtual corrections at $\mathcal{O}(\alpha_s)$ for this channel.

[4]We use this frame in chapters 4 and 6.

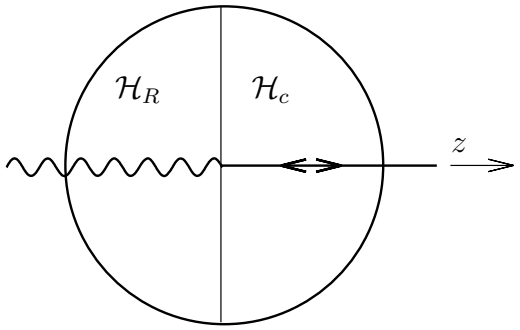

Figure 2.4: The Breit frame is the frame in which, at Born level, the momentum of the incoming quark is exactly reversed after absorbing the virtual photon. The current hemisphere (right) points in the current direction of the photon. The remnant hemisphere (left) contains all "remnants" of the proton (to a good accuracy).

photon momentum.

We divide the Breit space into two hemispheres whose plane of intersection is normal to the z-axis and define the remnant hemisphere, $\mathcal{H}_R$, to be the one pointing in the direction of motion of the incoming proton. We define the current hemisphere, $\mathcal{H}_c$, to be the opposite one. Fig. 2.4 shows a schematic diagram for the two hemispheres. To a good approximation the final-state particles that are present in the current hemisphere will come purely from the hard interaction whereas those in the remnant hemisphere are a mixture of remnants and scattered ones.

2.4 Collinear factorisation

The concepts of asymptotic freedom and confinement in QCD lead to the notions of perturbative and non-perturbative physics. The former describes high energy collisions of essentially free quarks and gluons, with calculable corrections expressed as an expansion in α_s, while the latter describes interactions at large scales and low energies, where α_s becomes large and cross-sections cannot be calculated with Feynman diagrams alone.

One of the main features of the theory of QCD is the ability to separate short distance perturbative physics effects from long distance non-perturbative ones. This means that, for processes containing hadrons in the initial state, one can study the

partonic sub-process separately from the overall interaction and then numerically convolute the hard cross-section with universal PDFs, which can only be extracted from experiments. For instance the leading-order cross-section for DIS is expressed in terms of structure functions. These are convolutions of coefficient functions (accounting for the partonic sub-process) with PDFs (e.g. eq. (2.3.4) which represents the real emission contribution). In hadronic collisions one can write the cross-section for an observable V as:

$$\sigma(V) \sim \int dx_a dx_b f_{a/A}(x_a, \mu_f^2) f_{b/B}(x_b, \mu_f^2) \sigma_{\text{hard}}(\mu_f^2, Q^2, V), \tag{2.4.1}$$

where Q is the hard scale and σ_{hard} is the cross-section for the observable at the partonic level. Here x_i represents the momentum fraction of the i^{th} incoming parton that undergoes the hard interaction with respect to its parent incoming hadron. The non-perturbative PDFs $f_{i/j}(x_i, \mu_f^2)$ are process-independent and (multiplied by dx_i) represent the probability of finding a parton i with momentum fraction between x_i and $x_i + dx_i$ in hadron j. They depend on a factorisation scale μ_f in analogy to the strong coupling which depends on a renormalisation scale μ_r.

The origin of this factorisation scale is the "renormalisation" of the bare PDFs by absorbing into them the collinear singularities to legs i. This is a similar idea to ultraviolet singularities being absorbed into the running of the strong coupling. Thus it is plausible that PDFs obey some sort of a renormalisation group equation that comes about due to the fact that the observable cross-section must ultimately be independent of the choice of μ_f. In fact such an equation in this case is called the DGLAP evolution equation and we shall discuss it in further detail in the next section.

2.5 DGLAP evolution

DGLAP evolution is an equation that governs the scale dependence of PDFs. It is a matrix equation in flavour space, with $(2n_f + 1) \times (2n_f + 1)$ dimensions. The full

matrix form of this equation is:

$$\mu^2\frac{\partial}{\partial\mu^2}\begin{pmatrix} u(x,\mu^2) \\ \bar{u}(x,\mu^2) \\ \vdots \\ g(x,\mu^2) \end{pmatrix} \equiv \frac{\alpha_s(\mu^2)}{2\pi}\boldsymbol{P}\otimes\boldsymbol{q}(x,\mu^2) = \frac{\alpha_s(\mu^2)}{2\pi}\int_x^1\frac{d\xi}{\xi}\times$$
$$\times\begin{pmatrix} P_{uu}(\xi,\alpha_s(\mu^2)) & P_{u\bar{u}}(\xi,\alpha_s(\mu^2)) & \cdots & P_{ug}(\xi,\alpha_s(\mu^2)) \\ P_{\bar{u}u}(\xi,\alpha_s(\mu^2)) & P_{\bar{u}\bar{u}}(\xi,\alpha_s(\mu^2)) & \cdots & P_{\bar{u}g}(\xi,\alpha_s(\mu^2)) \\ \vdots & \vdots & \ddots & \vdots \\ P_{gu}(\xi,\alpha_s(\mu^2)) & P_{g\bar{u}}(\xi,\alpha_s(\mu^2)) & \cdots & P_{gg}(\xi,\alpha_s(\mu^2)) \end{pmatrix}\begin{pmatrix} u(x/\xi,\mu^2) \\ \bar{u}(x/\xi,\mu^2) \\ \vdots \\ g(x/\xi,\mu^2) \end{pmatrix}, \tag{2.5.1}$$

where μ is the scale of the PDFs. The functions $P_{q_iq_j}$, P_{q_ig}, P_{gq_j}, and P_{gg} are known as the splitting functions. They respectively describe the probabilities of the transitions: $q_j \to q_i$, $g \to q_i$, $q_j \to g$ and $g \to g$ (by the emission of real and/or virtual partons). Here ξ is the momentum fraction of the final particle relative to the initial one, $\boldsymbol{P}$ and $\boldsymbol{q}$ are the matrices of splitting functions and PDFs. The leading-order splitting functions are given by[5] [67]:

$$P^{(0)}_{q_iq_j}(\xi) = \delta_{ij}C_F\left(\frac{1+\xi^2}{1-\xi}\right)_+, \tag{2.5.2}$$
$$P^{(0)}_{q_ig}(\xi) = T_R(\xi^2+(1-\xi)^2), \tag{2.5.3}$$
$$P^{(0)}_{gq_j}(\xi) = C_F\frac{1+(1-\xi)^2}{\xi}, \tag{2.5.4}$$
$$P^{(0)}_{gg}(\xi) = 2C_A\left(\frac{\xi}{(1-\xi)_+}+\frac{1-\xi}{\xi}+\xi(1-\xi)\right)+ +\delta(1-\xi)\frac{11C_A-4n_fT_R}{6}, \tag{2.5.5}$$

with $C_A = N_c$. The plus prescription is defined such that for any smooth function $f(\xi)$ and a divergent function $g(\xi)$ which has a singularity at $\xi = 1$, of the form $1/(1-\xi)$:

$$\int_0^1 f(\xi)[g(\xi)]_+d\xi = \int_0^1[f(\xi)-f(1)]g(\xi)d\xi. \tag{2.5.6}$$

The divergence in the function $g(\xi)$ is regularised by the plus prescription and the integral in eq. (2.5.6) is finite.

[5]These splitting functions include virtual corrections.

It proves convenient for solving the DGLAP equation to work in Mellin space conjugate to x. Here the convolution in eq. (2.5.1) becomes:

$$\mu^2 \frac{\partial \boldsymbol{q}_N(\mu^2)}{\partial \mu^2} = \frac{\alpha_s(\mu^2)}{2\pi} \boldsymbol{\gamma}_N(\alpha_s(\mu^2)) \boldsymbol{q}_N(\mu^2), \tag{2.5.7}$$

where N is the moment variable conjugate to x and $\boldsymbol{\gamma}_N(\alpha_s(\mu^2))$ is the matrix of anomalous dimensions[6]: $\gamma_{N,ij} = \int_0^1 \xi^{N-1} P_{ij}(\xi) d\xi$. Solving eq. (2.5.7) for an arbitrary scale Q and an initial scale Q_0 we obtain:

$$\boldsymbol{q}_N(Q^2) = \exp\left(\int_{Q_0^2}^{Q^2} \frac{d\mu^2}{\mu^2} \frac{\alpha_s(\mu^2)}{2\pi} \boldsymbol{\gamma}_N(\alpha_s(\mu^2)) \right) \times \boldsymbol{q}_N(Q_0^2). \tag{2.5.8}$$

One can now use the leading-order anomalous dimension matrix and the leading-order solution to the QCD β function (describing the running of the strong coupling) to achieve single logarithmic (SL) accuracy, in which $\mathcal{O}(\alpha_s^n \ln^n(Q/Q_0))$ terms are resummed. For this we exploit the relation:

$$\alpha_s(\mu^2) = \frac{\alpha_s(Q^2)}{1 - 2\varsigma}, \tag{2.5.9}$$

where $\varsigma = \alpha_s(Q^2)\beta_0 \ln(Q/\mu)$, with:

$$\beta_0 \;=\; \frac{11C_A - 2n_f}{12\pi}, \tag{2.5.10}$$

being the first coefficient of the QCD β function. The solution then reads:

$$\boldsymbol{q}_N(Q^2) = \exp\left(-\frac{1}{2\pi\beta_0} \ln(1 - 2\lambda) \boldsymbol{\gamma}_N^{(0)} \right) \times \boldsymbol{q}_N(Q_0^2), \tag{2.5.11}$$

where $\lambda = \alpha_s(Q^2)\beta_0 \ln(Q/Q_0)$. We remind the reader that this is a matrix equation and the order of matrices matters. One can now convert this equation to x space arriving finally at the formal equation (which is valid to SL accuracy):

$$\boldsymbol{q}(x, Q^2) = \exp\left(-\frac{1}{2\pi\beta_0} \ln(1 - 2\lambda) \boldsymbol{P}^{(0)} \otimes \right) \boldsymbol{q}(x, Q_0^2), \tag{2.5.12}$$

whose expansion to $\mathcal{O}(\alpha_s^2)$ yields[7]:

$$\boldsymbol{q}(x, Q^2) = \left[\mathbb{I} + 2\,\bar{\alpha}_s L \boldsymbol{P}^{(0)} + \bar{\alpha}_s^2 L^2 \left(4\pi\beta_0 \boldsymbol{P}^{(0)} + 2\boldsymbol{P}^{(0)} \otimes \boldsymbol{P}^{(0)} \right) \right] \otimes \boldsymbol{q}(x, Q_0^2), \tag{2.5.13}$$

[6]We do not explicitly show the expressions for the components of this matrix since we do not require them.

[7]This equation is useful for the procedure of "matching" in chapters 4 and 6.

with $\mathbb{I}(x) = \delta(1-x)\mathbb{1}$, $\bar{\alpha}_s = \alpha_s/(2\pi)$ and $L = \ln(Q/Q_0)$. Clearly PDFs are expressed here as a series in $\alpha_s L$ (to SL accuracy). Thus the result in eq. (2.5.13) is a good approximation only when $\alpha_s L$ is small. If $\alpha_s L \sim 1$ then the all-orders expression is the reliable approximation.

2.6 Summary

In this chapter we reviewed the theory that we shall use in this thesis (QCD). We briefly described the QCD Lagrangian and the process of DIS. We used this process to illustrate some important concepts of QCD. In particular we reviewed the subject of collinear factorisation and solved the DGLAP equation to SL accuracy.

In the next chapter we present the essential tools and techniques that are needed in this thesis. We shall provide an overview of resummation and non-global effects, illustrating the resummation of the energy flow distribution in e^+e^- annihilation into hadrons. We shall also give an example of resummation in the case of four-jet observables and discuss non-perturbative power corrections.

Chapter 3

Resummation and power corrections

3.1 Introduction

Although perturbation theory is valid at high energy (short distance) scales there is a subtlety in calculating observable distributions when two disparate scales are involved in the calculation, e.g a hard scale and a veto scale. The strong coupling becomes accompanied by large logarithms of the ratio of these scales. The origin of these logarithms is the break down of real-virtual cancellations of infrared singularities when a cut-off (veto) is introduced on real emissions. These logarithms become important at each order in perturbation theory when they are as large as the inverse of the coupling. Thus one cannot rely on a truncation of the perturbative series to a few orders to give the correct form of the spectrum and a resummation to all orders is necessary.

In this chapter we explain in detail the origin of these logarithms and how they are dealt with, illustrating the resummation of a simple observable, namely the energy flow into a gap between two jets in e^+e^- annihilation into two quarks. We then discuss the hadronic collisions case (complicated by the colour flow), calculating the matrices that enter the dynamical and colour flows in the process $q\bar{q} \to q\bar{q}$. Finally we discuss non-perturbative hadronisation effects in the renormalon model by introducing the non-perturbative coupling moment.

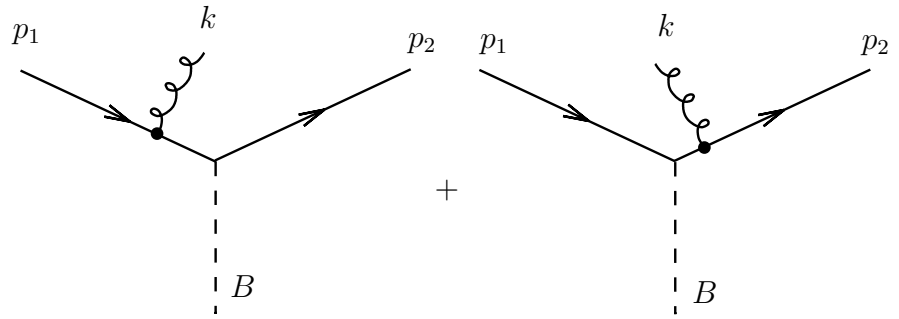

Figure 3.1: The scattering of a quark off an external field B, such as a photon.

3.2 Basics of soft gluon resummation

3.2.1 Soft gluon factorisation in hard processes

We consider the matrix element for the radiation of a gluon off a quark that undergoes a hard scattering with an external field B as shown in fig. 3.1. The external field could be for instance a photon coming from the electron in DIS. We write the Feynman amplitude for this process as follows:

$$\mathcal{M}^\mu = \bar{u}_i^{S'}(p_2)\epsilon_\lambda^{*a\alpha}(k)\left[(-ig_s t_a^{ij}\gamma_\alpha)\frac{i(\not{p}_2+\not{k})}{(p_2+k)^2}B^\mu + B^\mu\frac{i(\not{p}_1-\not{k})}{(p_1-k)^2}(-ig_s t_a^{ij}\gamma_\alpha)\right]u_j^S(p_1), \tag{3.2.1}$$

where u is the quark spinor, with indices i and j standing for quark colours and S and S' standing for spins, and ϵ is the gluon wave-function, with indices a and λ standing for the gluon colour and polarisation. We have defined $\not{p} = \gamma_\mu p^\mu$ and suppressed the spinor indices which are contained in the spinors, Dirac matrices and the external field B^μ.

We are interested in the case where the gluon is soft, meaning that we ignore terms which are $\mathcal{O}(\omega^0)$ and higher, with ω being the gluon energy, in the matrix element. Thus we simplify the matrix element to:

$$\mathcal{M}^\mu = g_s\bar{u}_i^{S'}(p_2)t_a^{ij}B^\mu u_j^S(p_1)\left(\frac{p_2.\epsilon_\lambda^{*a}}{p_2.k} - \frac{p_1.\epsilon_\lambda^{*a}}{p_1.k}\right), \tag{3.2.2}$$

where we use the relations $\not{p}u(p) = 0$ and $\gamma_\mu\gamma_\nu = -\gamma_\nu\gamma_\mu + 2g_{\mu\nu}$. We have kept the dominant piece of the amplitude in the soft limit, which goes like $\mathcal{O}(\omega^{-1})$.

Multiplying by the conjugate transpose, summing over final-state spins, polari-

sations and colours and averaging over initial-state spins and colours we arrive at:

$$\overline{\sum}_{S,\,S',\,\lambda,\,\text{colour}}|\mathcal{M}|^{2\,\mu\nu} = \frac{1}{2N_c}|\mathcal{M}_0|^{2\,\mu\nu} g_s^2 C_F N_c \frac{2p_1.p_2}{(p_1.k)(p_2.k)}, \tag{3.2.3}$$

where we define $|\mathcal{M}_0|^{2\,\mu\nu} \equiv \not{p}_2 B^\mu \ \not{p}_1 \overline{B}^\nu$ and used the relations $\sum_\lambda \epsilon_\lambda^{*a\alpha}(k)\epsilon_\lambda^{b\beta}(k) = -g^{\alpha\beta}\delta_{ab}$, $\sum_S u_j^S(p)\bar{u}_l^S(p) = \not{p}\delta_{jl}$ and $t_{ij}^a t_a^{ji} = C_F N_c$. The factor $1/(2N_c)$ comes from the averaging over the two spin states and the N_c colour states of the incoming quark. Note that $|\mathcal{M}_0|^{2\,\mu\nu}/2$ is simply the matrix element squared for the scattering shown in fig. 3.1 without the gluon dressing, summed and averaged over spins and colours.

Hence we have factored the amplitude squared (in the soft limit) into a hard contribution and a soft dressing. Note that virtual corrections (in the soft limit) also have exactly the same form with an overall minus sign. Furthermore this factorisation works in a similar way for processes where both quarks are in the final state, e.g. e^+e^- annihilation into a quark/anti-quark pair.

3.2.2 Probability of emission

The probability of the scattering shown in fig. 3.1 is given by the matrix element squared, summed and averaged over spins, polarisations and colours accordingly and multiplied by the phase-space. We write the probability of the scattering as follows:

$$d\Gamma = d\Gamma_{\text{hard}} d\Gamma_{\text{soft}}, \tag{3.2.4}$$

where $d\Gamma_{\text{hard}}$ is the probability of the hard scattering (without soft gluon dressing) and $d\Gamma_{\text{soft}}$ is given by:

$$\begin{aligned} d\Gamma_{\text{soft}} &= \frac{d^3\vec{k}}{2\omega(2\pi)^3} g_s^2 C_F \frac{2p_1.p_2}{(p_1.k)(p_2.k)} \\ &= \frac{d\omega}{\omega}\frac{d\cos\theta}{\sin^2\theta}\frac{d\phi}{2\pi}\frac{\alpha_s}{2\pi} C_F 2k_t^2 \frac{p_1.p_2}{(p_1.k)(p_2.k)} \\ &= \frac{dk_t}{k_t} d\eta \frac{d\phi}{2\pi}\frac{\alpha_s}{2\pi} C_F w_{12}, \end{aligned} \tag{3.2.5}$$

where we assume for simplicity that the hard legs are back-to-back and defined θ and ϕ to be the polar and azimuthal angles with respect to the incoming quark axis. Here $\eta = -\ln\tan(\theta/2)$ is the rapidity of the gluon with respect to the incoming quark axis, $k_t = \omega\sin\theta$ is the transverse momentum of the gluon with respect to the

quark axis and $w_{ij} = 2k_t^2\ p_i.p_j/(p_i.k\, p_j.k)$. In the case of a back-to-back dipole we have: $w_{12} = 4$.

There are two types of singularities in this expression: when $\omega \to 0$ (soft divergence) and when $\theta \to 0$ or π, or equivalently $\eta \to \pm\infty$ (collinear singularities). However for infrared and collinear-safe quantities [72] (those insensitive to soft and/or collinear real radiation) these singularities cancel with the virtual corrections since the matrix element squared in this case has exactly the same form as that in the real emission case with an overall minus sign.

This cancellation is broken if a veto is introduced on the final-state particles, e.g. when vetoing events with energy flowing into a gap between the two hard partons being above some scale Q_0. Thus virtual emissions which are emitted in the gap with energy above Q_0 are not vetoed and have nothing to cancel against[1]. This ultimately leads to large logarithms of the ratio of the veto scale and the hard scale, which implies the need for resummation to all orders when these scales are disparate. We discuss how this is done in the next section.

3.2.3 Multi-particle (primary) emissions

Having factored the probability of emission into hard and soft pieces we now proceed to higher orders in the logarithmically enhanced limit, i.e. when gluons are strongly ordered in energy [73].

The soft factorisation that we have demonstrated does not state anything about the vertex[2] B_μ as long as the emitted gluon is independent of the vertex. One can think of the emitted gluon as being part of the vertex and consider the emission of a softer gluon which is blind to the first gluon. Then we can see that the probability of this emission is also factored in the same way as before. Hence by iteration it is clear that the probability of emitting n soft gluons which are strongly ordered in

[1]Quantities with a veto scale are still infrared and collinear-safe since virtual emissions with scales below Q_0 cancel with real emissions.

[2]Note that the vertex could change the colour of the quark that undergoes the hard scattering, i.e. the external field being a gluon. The factorisation equally works in this case.

energy factorises as follows [73]:

$$d\Gamma_n = \frac{1}{n!} C_F^n w_{12}^n \prod_i^n \frac{dk_{t,i}}{k_{t,i}} d\eta_i \frac{d\phi_i}{2\pi} \frac{\alpha_s(k_{t,i}^2)}{2\pi}, \tag{3.2.6}$$

where we allow the coupling to run at a renormalisation scale $k_{t,i}$ for the i^{th} emission. The strong ordering is assumed because the logarithmically enhanced region of the phase-space originates when all the gluons have widely disparate scales. Here the gluons are essentially classical and are emitted independently except for multiple gluon branchings which are accounted for by the running of the coupling in the Catani-Marchesini-Webber (CMW) scheme [74]. The $1/n!$ term comes from the number of possible ways this energy-ordering could be achieved with n emitted gluons while allowing for the energy scales of the gluons to be interchanged. In other words we can either give a specific ordering (e.g. $k_1 \ll k_2 \cdots k_n \ll Q$) and remove the $1/n!$ factor or allow the interchanging of these gluons and keep the $1/n!$ factor.

3.3 Example: energy flow into gaps between jets in $e^+e^- \to q\bar{q}$

3.3.1 The global part

We now provide an example for the resummation of the "global" part of the energy flow distribution[3] in e^+e^- annihilation into two jets, which was computed by Dasgupta and Salam [22]. We write the integrated distribution for events with $\sum_{i\in\Omega} k_{t,i} < Q_0$, for some Q_0, with Ω being a gap of width $\Delta\eta$ which stretches over all azimuth and is centred about $\eta = 0$ in the rapidity-azimuth plane, as:

$$\Sigma(Q, Q_0) = \sigma(Q, Q_0)/\sigma_0 = \sum_n \int d\Gamma_n \theta\left(Q_0 - \sum_{i\in\Omega}^n k_{t,i}\right), \tag{3.3.1}$$

where σ_0 is the Born cross-section, Q is the hard scale and $d\Gamma_n$ is the differential phase-space for the emission of n gluons, given in eq. (3.2.6). We factorise the θ

[3] We use this observable in chapter 5 to describe the impact of jet algorithms on QCD resummation. We also use it in the case of hadronic collisions to estimate the non-perturbative power corrections.

function using the Mellin transform:

$$\theta\left(Q_0 - \sum_{i\in\Omega}^{n} k_{t,i}\right) = \int \frac{d\nu}{2\pi i\nu} e^{\nu Q_0} \prod_{i}^{n} e^{-k_{t,i}\nu}, \tag{3.3.2}$$

where the integral runs parallel to the imaginary axis to the right of all singularities of the integrand. Thus we can sum over all orders arriving at the result:

$$\Sigma(Q, Q_0) = \int \frac{d\nu}{2\pi i\nu} e^{\nu Q_0} \exp\left(4C_F \int \frac{dk_t}{k_t} d\eta \frac{d\phi}{2\pi} \frac{\alpha_s(k_t^2)}{2\pi} (e^{-k_t\nu} - 1)\right). \tag{3.3.3}$$

The term (-1) accounts for the virtual corrections. We can now make the substitution [75]: $\exp(-\nu k_t) - 1 \to -\theta\left(k_t\nu - 1\right)$ which is valid to SL accuracy. Thus we write:

$$\Sigma(Q, Q_0) = \int \frac{d\nu}{2\pi i\nu} e^{\nu Q_0} \exp\left(-4C_F \int_{1/\nu}^{Q/2} \frac{dk_t}{k_t} \frac{\alpha_s(k_t^2)}{2\pi} \int_\Omega d\eta \frac{d\phi}{2\pi}\right). \tag{3.3.4}$$

Performing the η, ϕ and k_t integrations we arrive at the result:

$$\int_{1/\nu}^{Q/2} \frac{dk_t}{k_t} \frac{\alpha_s(k_t^2)}{2\pi} \int_\Omega d\eta \frac{d\phi}{2\pi} = -\frac{1}{4\pi\beta_0} \ln(1 - 2\lambda)\Delta\eta, \tag{3.3.5}$$

with $\lambda = \alpha_s((Q/2)^2)\beta_0 \ln(\nu Q/2)$ and we expand $\alpha_s(k_t^2)$ using the QCD β function to SL accuracy. To solve the ν integration we use the saddle point method. It may be shown that the saddle point in the ν integral to SL accuracy is simply given by $1/Q_0$. Thus we can expand the exponent about this point and throw away all subleading logarithms, $\alpha_s^n \ln^m(Q/Q_0)$, with $m < n$, arriving finally the result:

$$\Sigma(Q, Q_0) = \exp\left(-4C_F \Delta\eta \tau(Q, Q_0)\right), \tag{3.3.6}$$

with:

$$\tau(Q, Q_0) = -\frac{1}{4\pi\beta_0} \ln\left(1 - 2\alpha_s((Q/2)^2)\beta_0 \ln\frac{Q}{2Q_0}\right). \tag{3.3.7}$$

We shall correct this result for non-global effects, which we introduce in the next subsection.

3.3.2 Non-global effects

Thus far we have only considered primary independent emissions from the hard dipole. For "global observables" (those which are sensitive to emissions in the entire

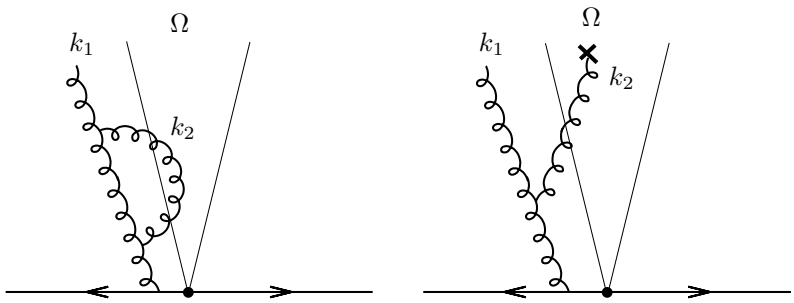

Figure 3.2: Gluon configurations that give rise to non-global logs at leading-order.

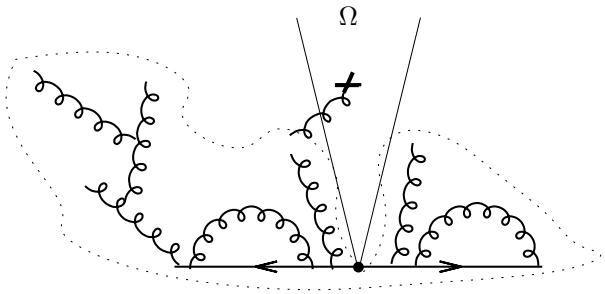

Figure 3.3: Gluon configurations that give rise to non-global logs at higher orders.

phase-space) this consideration is sufficient to produce all soft (collinear or wide-angle) logarithms. However for non-global observables (those which are sensitive to emissions in a limited region of the phase-space) there are other types of particle configurations that give rise to *extra* single logarithms which first appear at $\mathcal{O}(\alpha_s^2)$ [21, 22].

Consider the emission of a real or virtual softest gluon k_2 off a soft gluon k_1 which is emitted off a hard dipole as shown in fig. 3.2 ($k_2 \ll k_1 \ll Q$). The probability of emission for this configuration is logarithmically enhanced: if the emission k_1 is outside the gap region while k_2 is inside with energy $\omega_2 > Q_0$ then the right hand side diagram in fig. 3.2 receives a veto while the left hand side one does not. Thus we have a miscancellation which leads to large single logarithms.

At higher orders of this configuration the particles that are emitted outside the gap can take any complex geometrical structure while being energy-ordered. They coherently emit a single softest gluon into the gap as shown in fig. 3.3. It is only possible to deal with this configuration in the large N_c limit. Then one may write an evolution equation ([76]) to obtain the resummed form of these logarithms to all

orders numerically.

We now include the effect of non-global logarithms in the resummed result for the energy flow distribution in $e^+e^- \to q\bar{q}$. We write the result which corrects eq. (3.3.6) as [22]:

$$\Sigma(Q, Q_0) = \exp\left(-4C_F \Delta\eta \tau(Q, Q_0)\right) \mathcal{S}(Q, Q_0), \tag{3.3.8}$$

where we introduce the non-global component $\mathcal{S}$. This has been computed in ref. [22] and has the following approximation for large $\Delta\eta$:

$$\mathcal{S} \approx \exp\left(-2C_F C_A \frac{\pi^2}{3} \frac{1 + (A\tau)^2}{1 + (B\tau)^C} \tau^2 + \mathcal{O}(1/N_c^2)\right), \tag{3.3.9}$$

where $A = 0.85C_A$, $B = 0.86C_A$ and $C = 1.33$. Note that the values of τ are typically in the range $0 \leq \tau \lesssim 0.25$.

Note that the non-global component in this case contributes at leading-log level. We have ignored $\mathcal{O}(1/N_c^2)$ terms which are essentially leading logarithms.

3.4 Resummation

In general one may have soft *and* collinear double logarithms contributing to the observable cross-section. Here one may write the resummed result for the differential cross-section for an observable V (which vanishes in the Born limit) as [77]:

$$\frac{d\sigma}{dV} \propto \frac{d}{dV}\left(\left[\sum_n C_n \bar{\alpha}_s^n\right] \exp\left[L g_1(\alpha_s L) + g_2(\alpha_s L) + \alpha_s g_3(\alpha_s L) + \cdots\right] + D(V)\right), \tag{3.4.1}$$

where $\bar{\alpha}_s = \alpha_s/(2\pi)$, C_n are constants and L is the logarithm of the observable, $L = \ln(1/V)$.

The function $Lg_1(\alpha_s L)$ resums soft *and* collinear (double) logarithms, $\alpha_s^n L^{n+1}$, while the function $g_2(\alpha_s L)$ resums hard collinear or soft wide-angle (single) logarithms, $\alpha_s^n L^n$. Subleading logarithms, $\alpha_s^n L^m$, for $0 < m < n$, are resummed by $\alpha_s^i g_{i+2}$, for $i > 0$. These are usually uncontrollable by current resummation techniques.

The term $D(V)$ in the above equation vanishes in the limit of small V. It is usually obtained from fixed-order programs alongside the constants C_1 (if not available analytically) and C_2 . The procedure by which these are added to the distribution is

known as "matching" (we shall use this in chapters 4 and 6). Matching guarantees the correct behaviour of the spectrum in the region where resummation is not valid ($V \not\to 0$).

For observables which are unaffected by collinear emissions to the hard legs (e.g energy flows into gaps between jets) there are no double logarithms (the function g_1 vanishes) and single logarithms become the leading ones.

3.5 Colour flow in hadronic collisions

Let us now consider the resummation in processes which are complicated by the colour flow[4]. For simplicity we work with the energy flow into a gap Ω between the jets in the process $q\bar{q} \to q\bar{q}$ (this was computed by Berger et al [78] and by Banfi et al [76] including the non-global component in the large N_c limit).

3.5.1 Born matrix element

We begin by looking at the matrix element for the Born process which is shown in fig. 3.4. We decompose the matrix element into s and t-channel pieces. We write the matrix element as follows:

$$\mathcal{M} = \mathcal{M}_s t^a_{ij} t^a_{kl} + \mathcal{M}_t t^a_{li} t^a_{jk}, \tag{3.5.1}$$

with a being the colour of the internal gluon and i, j, k and l being the colours of the external quarks. Here $\mathcal{M}_s$ and $\mathcal{M}_t$ are the colour-blind matrix elements for the s and t-channel processes, which are calculable using QED-like Feynman rules. We can represent this matrix element in a colour-flow diagram as shown in fig. 3.4.

Note that $t^a_{li} t^a_{jk} = \delta_{ij}\delta_{kl}/2 - 1/(2N_c)\delta_{il}\delta_{jk}$. This identity is known as the Fierz identity and can be represented in graphical form as in fig. 3.5. Thus we can decompose the matrix element in terms of the elements $c_1 = \delta_{il}\delta_{jk}$ and $c_2 = \delta_{ij}\delta_{kl}/2 - 1/(2N_c)\delta_{il}\delta_{jk}$, which form a basis for the colour flow. We thus write:

[4]This study is useful for chapter 7, where we calculate the power corrections to the energy flow distribution in hadronic collisions.

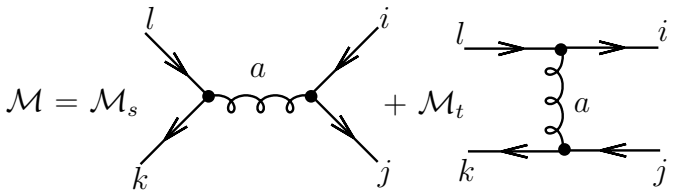

Figure 3.4: Decomposition of the matrix element for the process $q\bar{q} \to q\bar{q}$ into s and t-channel components.

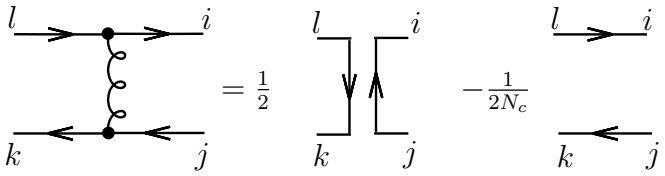

Figure 3.5: The Fierz identity in graphical representation.

$$\begin{aligned} \mathcal{M} &= \mathcal{M}_s \left(\frac{C_F}{N_c} c_1 - \frac{1}{N_c} c_2 \right) + \mathcal{M}_t c_2 \\ &= \frac{C_F}{N_c} \mathcal{M}_s c_1 + \left(\mathcal{M}_t - \frac{1}{N_c} \mathcal{M}_s \right) c_2. \end{aligned} \tag{3.5.2}$$

We can equivalently express the matrix element in terms of a vector in colour space whose orthogonal basis is (c_1, c_2). We write this vector as:

$$\mathbf{M} = \begin{pmatrix} \frac{C_F}{N_c} \mathcal{M}_s \\ \mathcal{M}_t - \frac{1}{N_c} \mathcal{M}_s \end{pmatrix}. \tag{3.5.3}$$

The matrix element squared is given by $\mathbf{M}^\dagger \mathbf{S} \mathbf{M}$, with $\mathbf{S}$ being a diagonal matrix with elements $c_1^2 = N_c^2$ and $c_2^2 = (N_c^2 - 1)/4$. This can be seen by expanding $\mathcal{M}^*.\mathcal{M}$ using eq. (3.5.2) and the fact that $c_1.c_2 = 0$. Thus the final result for the Born matrix element squared, summed and averaged over spins and colours, is given by:

$$\begin{aligned} \Sigma_0 &= \frac{1}{N_c^2} \overline{\sum}_{\text{spin}} \mathbf{M}^\dagger \mathbf{S} \mathbf{M} \\ &= \frac{C_F}{2N_c} \left(\overline{\sum}_{\text{spin}} |\mathcal{M}_s|^2 + \overline{\sum}_{\text{spin}} |\mathcal{M}_t|^2 \right) - \frac{C_F}{N_c^2} \overline{\sum}_{\text{spin}} \mathcal{M}_t^* \mathcal{M}_s, \end{aligned} \tag{3.5.4}$$

where we have:

$$\overline{\sum}_{\text{spin}} |\mathcal{M}_s|^2 = 2 \frac{\hat{u}^2 + \hat{t}^2}{\hat{s}^2}, \tag{3.5.5}$$

$$\overline{\sum}_{\text{spin}} |\mathcal{M}_t|^2 = 2 \frac{\hat{u}^2 + \hat{s}^2}{\hat{t}^2}, \tag{3.5.6}$$

$$\overline{\sum}_{\text{spin}} \mathcal{M}_{t,\,\alpha\beta}^* \mathcal{M}_s^{\alpha\beta} = 2 \frac{\hat{u}^2}{\hat{s}\hat{t}}, \tag{3.5.7}$$

with $\overline{\sum}_{\text{spin}}$ denoting the sum over final-state spins and average over initial-state spins. Here $\hat{s} = (p_1 + p_2)^2$, $\hat{t} = (p_1 - p_3)^2$ and $\hat{u} = (p_1 - p_4)^2$ are the usual Mandelstam variables, with p_n standing for the momentum of the n^{th} quark and we label the quarks whose colour indices are l, k, i and j by 1, 2, 3 and 4 respectively. The factor $1/N_c^2$ in eq. (3.5.4) stands for the averaging over the N_c^2 colour states of the incoming quark/anti-quark pair.

3.5.2 Soft gluon factorisation and resummation

Let us consider the dressing of the matrix element under consideration with a soft virtual gluon, whose energy is greater than the veto scale Q_0, in the gap region in all possible ways such that the virtual gluon connects two external legs. This will then be multiplied by the conjugate transpose of the Born matrix element and then added to the conjugate transpose of the result (i.e. $\mathcal{M}_0^\dagger.\mathcal{M}_1 + \mathcal{M}_1^\dagger.\mathcal{M}_0$, with $\mathcal{M}_0$ standing for the Born matrix element and $\mathcal{M}_1$ standing for the Born matrix element with virtual dressing) to produce the $\mathcal{O}(\alpha_s)$ virtual corrections. This consideration is sufficient to capture all single logarithms [57, 58, 59, 60] except non-global logarithms [21, 29, 76]. The attachments can be translated to the basis itself instead of the actual matrix elements. This ultimately leads to a rotation of the basis (in colour space) which has the form:

$$c_i' = c_j \tilde{\Gamma}_{ji}, \tag{3.5.8}$$

where c_i' is formed by dressing c_i with virtual gluons as described before. Note that the matrix $\tilde{\mathbf{\Gamma}}$ describes both dynamical and colour flows. To calculate this matrix one uses the identity $t_{ij}^a t_{jk}^a = C_F \delta_{ik}$. Thus we write the result as follows:

$$\begin{aligned}
c_1' &= C_F(\tilde{w}_{13} + \tilde{w}_{24})c_1 + (\tilde{w}_{12} - \tilde{w}_{14} - \tilde{w}_{32} + \tilde{w}_{34})c_2, \\
c_2' &= \frac{C_F}{2N_c}(\tilde{w}_{12} - \tilde{w}_{14} - \tilde{w}_{32} + \tilde{w}_{34})c_1 + \\
&\quad +(C_F[\tilde{w}_{12} + \tilde{w}_{34}] - 1/(2N_c)[\tilde{w}_{12} + \tilde{w}_{13} - 2\tilde{w}_{14} - 2\tilde{w}_{23} + \tilde{w}_{24} + \tilde{w}_{34}])c_2,
\end{aligned} \tag{3.5.9}$$

with [51, 52, 53, 79, 80]:

$$\begin{aligned}\tilde{w}_{ij} &= -\frac{1}{2}\int_{Q_0}^{Q}\frac{dk_\perp}{k_\perp}\frac{\alpha_s(k_\perp^2)}{2\pi}\int_\Omega d\eta\frac{d\phi}{2\pi}w_{ij} \\ &= -\frac{1}{2}\tau(Q,Q_0)\int_\Omega d\eta\frac{d\phi}{2\pi}w_{ij}, \end{aligned} \tag{3.5.10}$$

where τ is defined in eq. (3.3.7)[5], $k_\perp$ is the invariant transverse momentum of the dipole (ij), which is given by $k_\perp^2 = 4k_t^2/w_{ij}$, and k_t, η and ϕ are measured with respect to the axis formed by the incoming quarks[6]. The hard scale Q is the transverse momentum of the outgoing hard jets. The minus sign in the expression for $\tilde{w}_{ij}$ accounts for the fact that virtual corrections have a negative sign with respect to real emissions and the factor $1/2$ accounts for the fact that we only considered attachments of the virtual gluon to the external legs of the matrix element, but not its conjugate transpose. We shall include the attachments to the conjugate transpose of the Born matrix element presently.

Now the matrix element squared (the $\mathcal{M}_0^\dagger\mathcal{M}_1$ piece) is give by $\mathbf{M}^\dagger\mathbf{S}^{(1)}\mathbf{M}$, where the matrix $\mathbf{S}^{(1)}$ has the elements $S_{ij}^{(1)} = c_i^*.c_j' = c_i^* c_k\tilde{\Gamma}_{kj} = S_{ik}\tilde{\Gamma}_{kj} = (\mathbf{S}\tilde{\mathbf{\Gamma}})_{ij}$. Similarly we can attach the virtual gluon to the conjugate transpose Born matrix element and multiply it by the Born matrix element (i.e. the $\mathcal{M}_1^\dagger\mathcal{M}_0$ piece) arriving at a contribution of $\mathbf{M}^\dagger\tilde{\mathbf{\Gamma}}^\dagger\mathbf{S}\mathbf{M}$. By summing the two contributions we arrive at the one-loop result for the energy flow distribution (normalised to the Born cross-section) as follows:

$$\Sigma^{(1)}(Q,Q_0) = -\frac{1}{N_c^2}\overline{\sum}_{\text{spin}}\mathbf{M}^\dagger\left(\mathbf{\Gamma}^\dagger\mathbf{S}+\mathbf{S}\mathbf{\Gamma}\right)\mathbf{M}/\Sigma_0\,, \tag{3.5.11}$$

where $\mathbf{\Gamma} = -\tilde{\mathbf{\Gamma}}$. The 2×2-dimensional matrix $\mathbf{\Gamma}$ is defined by:

$$\mathbf{\Gamma} = \begin{pmatrix} C_F T & \frac{C_F}{2N_c}(S-U) \\ S-U & C_F S - \frac{1}{2N_c}(T-2U+S)\end{pmatrix}, \tag{3.5.12}$$

where:

$$S = \tilde{w}_{12}+\tilde{w}_{34}, \tag{3.5.13}$$

$$T = \tilde{w}_{13}+\tilde{w}_{24}, \tag{3.5.14}$$

$$U = \tilde{w}_{23}+\tilde{w}_{14}. \tag{3.5.15}$$

[5]Note that the difference between $Q/2$ and Q in the upper limit of the $k_\perp$ integration is sub-leading.

[6]Note that $k_\perp = k_t$ only when the legs of the dipole are back-to-back.

By iteratively attaching energy-ordered virtual gluons to the hard matrix element it becomes apparent that the result exponentiates in a similar fashion to the two-jet case in e^+e^- annihilation into two quarks. Hence we finally arrive at the resummed result:

$$\Sigma(Q,Q_0) = \frac{1}{N_c^2}\overline{\sum}_{\text{spin}} \mathbf{M}^\dagger \exp\left(-\mathbf{\Gamma}^\dagger\right) \mathbf{S} \exp\left(-\mathbf{\Gamma}\right) \mathbf{M}/\Sigma_0. \tag{3.5.16}$$

Alternatively we can express this in the standard form:

$$\Sigma(Q,Q_0) = \text{Tr}\left[\mathbf{H} \exp\left(-\mathbf{\Gamma}^\dagger\right) \mathbf{S} \exp\left(-\mathbf{\Gamma}\right)\right] / \text{Tr}(\mathbf{HS}), \tag{3.5.17}$$

where the matrix $\mathbf{H}$ has the components $H_{ij} = 1/N_c^2 \sum_{\text{spins}} \mathcal{M}_i^* . \mathcal{M}_j$, with $\mathcal{M}_i$ being the components of the vector $\mathbf{M}$. The matrices $\mathbf{H}$, $\mathbf{\Gamma}$ and $\mathbf{S}$ are provided in refs. [57, 58, 59, 60].

3.6 Non-perturbative effects

In this section we illustrate the calculation of the power corrections to the energy flow distribution in e^+e^- annihilation into two jets[7]. We begin by observing that the k_t integration in eq. (3.3.3) is perturbatively divergent since $\alpha_s(k_t^2)$ diverges when $k_t \to \Lambda_{\text{QCD}}$. The origin of this singularity is the factorial divergences associated with renormalon chains [81]. We have only been able to perform this integration by neglecting the region of integration $k_t < Q_0$, with $Q_0 \gg \Lambda_{\text{QCD}}$, on the grounds that it is subleading.

To account for non-perturbative effects we introduce an effective coupling α_{eff} [44] which is equivalent to the perturbative coupling at high scales while being convergent at low scales. We introduce an infrared matching scale μ_I characterising the scale at which the effective coupling starts to differ from the perturbative coupling. This is usually chosen to be 2 GeV.

We split the k_t integration in the exponent of eq. (3.3.3) into perturbative and non-perturbative contributions as follows (respectively):

$$\int_0^{Q/2} \frac{dk_t}{k_t}(e^{-\nu k_t} - 1)\frac{\alpha_s(k_t^2)}{2\pi} + \int_0^{\mu_I} \frac{dk_t}{k_t}(e^{-\nu k_t} - 1)\frac{\alpha_{\text{eff}}(k_t^2) - \alpha_s(k_t^2)}{2\pi}, \tag{3.6.1}$$

[7]We shall study the power corrections to energy flows in the case of hadronic collisions in chapter 7.

where we subtract the contribution to the k_t integration for $k_t < \mu_I$ and added it back using the effective coupling. We perform the integration in the first term of eq. (3.6.1) perturbatively as before (i.e. using $\exp(-\nu k_t) - 1 \to -\theta\left(k_t\nu - 1\right)$).

To obtain the leading power corrections we expand $\exp(-\nu k_t) - 1 \simeq -\nu k_t$, in the second term of eq. (3.6.1), where we are interested in the region $\nu k_t \ll 1$, which corresponds $k_t \ll Q_0$. Thus we write the second term of eq. (3.6.1) as:

$$-\nu \int_0^{\mu_I} dk_t \frac{\alpha_{\rm eff}(k_t^2) - \alpha_s(k_t^2)}{2\pi} = -\nu\mathcal{P}, \tag{3.6.2}$$

with:

$$\begin{aligned}\mathcal{P} &= \frac{\mu_I}{2\pi}\left(\alpha_0(\mu_I) - \frac{1}{\mu_I}\int_0^{\mu_I} dk_t \alpha_s(k_t^2)\right) \\ &= \frac{\mu_I}{2\pi}\left(\alpha_0(\mu_I) - \alpha_s(Q^2) - \frac{\beta_0}{2\pi}\left(\ln\frac{Q}{\mu_I} + \frac{K_F}{\beta_0} + 1\right)\alpha_s^2(Q^2) + \mathcal{O}(\alpha_s^3)\right),\end{aligned} \tag{3.6.3}$$

and $\alpha_0(\mu_I) = 1/\mu_I \int_0^{\mu_I} dk_t\, \alpha_{\rm eff}(k_t^2)$. The parameter α_0 is only measured through experiments (see e.g. [42, 43]). In going from the first line of eq. (3.6.3) to the second one we convert the coupling from the CMW scheme to the modified minimal subtraction ($\overline{\rm MS}$) scheme. In the above equation we have:

$$K_F = C_A\left(\frac{67}{18} - \frac{\pi^2}{6}\right) - \frac{5}{9}n_f. \tag{3.6.4}$$

We therefore write the ν integration (eq. (3.3.3)) as follows:

$$\Sigma(Q, Q_0) = \int \frac{d\nu}{2\pi i\nu} e^{\nu(Q_0 - 4C_F\Delta\eta\mathcal{P})} \exp\left(-4C_F\int_{1/\nu}^{Q/2}\frac{dk_t}{k_t}\frac{\alpha_s(k_t^2)}{2\pi}\int_\Omega d\eta\frac{d\phi}{2\pi}\right). \tag{3.6.5}$$

Hence we arrive at the same result as before with the replacement $Q_0 \to Q_0 - 4C_F\Delta\eta\mathcal{P}$, which amounts to a shift of the distribution to the right by an amount equal to $4C_F\Delta\eta\mathcal{P}$. If we one measures Q_0 in units of Q the shift of the distribution would be proportional to $1/Q$.

Note that we did not account for the "Milan factor" [82], which arises when considering a two-loop analysis for the argument of the coupling. When a two-loop calculation for the power corrections is performed it is found that, for event shapes, the result is equal to that computed using one-loop analysis (such as that we calculated above) rescaled by a universal constant factor [83, 84] ($\mathcal{M} \simeq 1.49$). This factor has not been yet accounted for in hadronic collisions.

3.7 Summary

In this chapter we provided an overview of the various techniques and methods that we use in this thesis. We now proceed with studying various QCD observables that give us more insight into QCD radiation and non-perturbative effects.

In the next chapter we look at the Q_t distribution of the Breit frame in DIS and perform a resummation and correct the result for non-perturbative effects to probe the small-x enhancement of Q_t spectra at hadron colliders.

Chapter 4

The Q_t distribution of the Breit current hemisphere in DIS as a probe of small-x broadening effects

4.1 Introduction

With the imminent advent of the LHC, considerable effort has been dedicated to utilising existing collider data and theoretical predictions for QCD observables to foster an even better knowledge of crucial parameters such as the strong coupling and parton distributions in hadrons (see e.g. [85]).

An invaluable source for such data is the HERA collider, which continues to play an important role in phenomenological studies of QCD. The HERA-LHC workshop[1] was in fact dedicated towards the aim of directly linking HERA QCD studies to those that will be important in a discovery context at the LHC.

In the present chapter we shall highlight one such study. To illustrate our point we choose the Q_t spectrum of the Higgs boson for which very accurate theoretical predictions exist in the literature [2, 3], as we highlighted in the introduction chapter. Such accurate studies are important in the context of formulating improved strategies to extract the signal and to enhance its statistical significance over backgrounds.

One concern that has been a point for some discussion (see e.g. ref. [8]) is the

[1] http://www.desy.de/~heralhc

role that might be played by neglected small-x effects that one may expect could be relevant at the x values involved in vector boson and Higgs production at the LHC. Here x is the momentum fraction of struck parton relative to the incoming hadron. As we stated in chapter 1, if neglected small-x effects are indeed important in this context, they could in principle lead to broader Q_t spectra than those predicted by conventional resummations (sometimes also referred to as Collins-Soper-Sterman or CSS formalism [86]) alone. Henceforth we shall refer to these resummations involving Q_t spectra in hadron-hadron collisions with the generic label Drell-Yan Q_t resummations.

It was observed for instance by Berge et al [8] that effects due to small-x enhancements that were suggested by phenomenological studies [9] for SIDIS Q_t distributions, could be very significant (especially in the context of massive vector boson production) when extrapolated to the smaller x values that will be important at the LHC. It was also suggested in ref. [8] that such effects could be visible with Tevatron (Run II) data if one concentrates on forward production of vector bosons alone, rather than integrating over all rapidities. On the other hand, studies for many event-shape variables in the current hemisphere of the Breit frame in DIS have been very successful, down to moderately small x values ($x \approx 10^{-2}$), based on resummation [47, 87, 88] that did not account for BFKL small-x effects. The comparison to HERA data for several event-shape variables can be found in [47].

It is also clear however that event shapes are somewhat different from Q_t spectra of the Drell-Yan type, significantly due to their direct sensitivity to gluon emissions, rather than purely through recoil. This difference means that event-shape variables receive non-perturbative corrections that scale as $1/Q$ [49], where Q is the DIS hard scale. These power corrections arise in a way similar to that we described in section 3.6, and are due to soft gluon emissions alone and hence are independent of x. The quantity we shall study in the present chapter is closer in nature to the Drell-Yan Q_t spectra since the leading non-perturbative effects here scale as $1/Q^2$ and can be associated with what is commonly known as "intrinsic k_t" of partons inside hadrons. Thus one would expect any missing small-x effects that appear in the present context (perhaps as suggested by Berge et al [8] in terms of a small-x enhanced smearing

of the conventional resummation), to manifest themselves in a very similar way in the Drell-Yan case. It is thus conceivable that for the Q_t distribution we present here, deviations are seen from the resummed form, even at x values already studied successfully for event-shape variables.

To be more precise, the observable we study here is the distribution $1/\sigma\, d\sigma/dQ_t$, with Q_t being the modulus of the transverse momentum vector of all particles in the current hemisphere ($\mathcal{H}_c$) of the DIS Breit frame:

$$\vec{Q}_t = \sum_{i \in \mathcal{H}_c} \vec{k}_{t,i}\,, \tag{4.1.1}$$

where $\vec{k}_t$ is measured with respect to the photon axis. Note that the addition over particles mentioned above is *vectorial* in nature, in contrast to say that involved in event shapes like the jet broadening observable [87], where one adds the moduli of individual particle transverse momenta. This is also a different quantity from the resummed z flow studied in refs. [8, 9] while also being directly related to the Drell-Yan Q_t spectra and thus should provide an independent probe of small-x broadening effects.

To relate the quantity here to Q_t spectra in Drell-Yan type processes one notes that in the Drell-Yan case one has the massive vector boson recoiling against emissions from two incoming hard partons, while for our DIS example the transverse momentum of the current hemisphere is equal and opposite to that of the remnant hemisphere. If one assumes the remnant hemisphere Q_t spectrum to be entirely generated by emissions from a single incoming leg the relationship to Drell-Yan Q_t is obvious: we just have to account for the form-factor of one incoming parton instead of two and thus we have, at the level of form-factors, $\Delta^N_{\rm DIS}(Q, Q_t) = \sqrt{\Delta^N_{\rm DY}(Q, Q_t)}$. The variable N indicates moment space, conjugate to x.

This simple relationship breaks down at NLL level, due to the non-global nature [21, 22] of the DIS observable. Non-globalness in the present case is a consequence of looking at just a single hemisphere and provides an extra factor in the DIS case, to do with soft emissions at large angles, which is absent for the global Drell-Yan quantity. We shall of course account for this factor, but we stress here that the fundamental relationship of our quantity to Drell-Yan Q_t (which is exactly of the

square-root form we wrote above, at leading-logarithmic accuracy) is unchanged by this complication. In particular any neglect of terms that are enhanced at small x ought to be of similar significance in the two cases.

To further this investigation we obtain here a resummed result for the above quantity, to NLL accuracy[2] and combine it with fixed-order predictions to $\mathcal{O}(\alpha_s^2)$ accuracy. Our result is thus suitable for comparison with data over the entire measured range of Q_t values. We also comment on the effect of smearing our result with a Gaussian function, as is usual to accommodate the so-called intrinsic k_t of the incoming parton, which has a non-perturbative origin. The resultant prediction can then be directly compared to data which should be of interest especially at lower x values. If discrepancies are visible at low x then one may consider a small-x enhanced smearing function as was the case in refs. [8, 9]. This is certainly not a substitute for a detailed treatment based on a physical understanding of the small-x region, but merely a phenomenological investigation into how such effects may be parameterised if present in the first place. Subsequently one may also consider the extrapolation of our findings to hadron colliders. We note that preliminary data from H1 are already available [89] and await the final versions together with potential data from the ZEUS collaboration.

The outline of this chapter is as follows: in section 4.2 we put together the different ingredients required to obtain our NLL resummed result which we compute in impact parameter or b space as is most convenient for Q_t resummations. Once we obtain the b-space answer we find, in section 4.3, its transform to Q_t space and comment on its main features. In section 4.4 we carry out the matching of our resummed result to the full $\mathcal{O}(\alpha_s^2)$ result from the fixed-order program DISENT [90, 91]. Finally we comment on the potential role of non-perturbative effects that are expected to take the form of a smearing of the Q_t distribution with a function representing the "intrinsic transverse momentum" of partons inside hadrons. Here one may try different choices for the smearing function and search for any discrepancies at lower x values, between our results and the data. We shall leave the details of this to our

[2]Equivalently we seek SL accuracy in the resummed exponent that we shall compute subsequently.

forthcoming phenomenological investigation [92].

4.2 Resummation

At Born level the struck quark is aligned along the photon axis, the quantity in question (Q_t) vanishes and the distribution is essentially a delta function: $d\sigma/dQ_t \sim \delta(Q_t)$.

At small Q_t the emission of soft and collinear gluons deform the delta function. One may, on general grounds, expect this deformation to take the form of a Sudakov form-factor. This is essentially true over a large range of Q_t values with the caveat that at very small Q_t, the correct result is no longer of Sudakov form. The reason for this is the Parisi-Petronzio observation that the smallest Q_t values are in fact obtained by vectorial cancellation of emissions, rather than by suppressing the transverse momenta of each individual emission [93]. We shall explain this issue more quantitatively, with reference to our observable, in section 4.3. For now we proceed with resumming the large logarithms that arise at small Q_t.

To carry out the resummation we have to address two distinct kinematic regimes:

- collinear emissions (soft or hard) along the directions of the incoming and scattered quark directions.

- soft emissions at large angles to the incoming and scattered (outgoing) quark axis (since in the Breit frame the incoming and scattered quarks are back-to-back at Born level). This contribution arises due to the non-global nature [21, 22] of the observable and is a correlated multi-gluon emission term, that can only be computed in the large N_c limit.

We shall treat each region in turn starting with the collinear enhanced contribution and then including the non-global term that arises from the piece of the fixed-order matrix elements with only soft enhancement (i.e. is integrable over soft gluon *directions*).

4.2.1 Pure collinear contribution

The collinear contribution is simple to assess since one can, to the NLL accuracy we seek, consider collinear radiation as being included in the evolution of the incoming and outgoing hard quark jets. In order to derive the NLL pure collinear contribution it proves useful to first consider the observable as defined in eq. (4.1.1). Since we deal with soft and/or collinear gluon emissions alone, we look at a tiny deviation from the Born configuration. Thus the sum over current hemisphere emissions, on the right hand side of eq. (4.1.1), includes a contribution from the transverse momentum of the outgoing current quark. To work in terms of secondary emissions alone one uses conservation of transverse momentum to write eq. (4.1.1) as:

$$\vec{Q}_t = -\sum_{i\in\mathcal{H}_R} \vec{k}_{t,i}\,, \tag{4.2.1}$$

where the sum now runs over all final-state particles in the *remnant* hemisphere.

In the collinear region there is an important simplification, in that all these emissions can, to our accuracy, be attributed to the showering of the incoming quark. Note that since one is now inclusive over current-hemisphere emissions, we can neglect the collinear evolution of the outgoing quark. This will correct our resummed result by a factor of relative order α_s, but not enter into the NLL form-factor we aim to compute.

The next step is to consider multiple collinear gluon branchings on the incoming hard leg. In this region the squared matrix element can be approximated to NLL accuracy by a product in N space of individual gluon emissions from the hard incoming quark, where N is the moment variable conjugate to Bjorken x. Taking first just *soft and collinear* emissions[3], where we can just as well work in x space, one can write:

$$\frac{1}{\sigma_0}\frac{d\sigma}{dQ_t^2} \approx \sum_n \int dP_n\, \delta(p_t^2 - Q_t^2)\, d^2\vec{p}_t\, \delta^2\left(\vec{p}_t + \sum_{i\in\mathcal{H}_R}^{n} \vec{k}_{t,i}\right), \tag{4.2.2}$$

where dP_n is the differential n gluon emission probability and we introduce the vector $\vec{p}_t$, which is the vectorial sum of transverse momenta of particles in $\mathcal{H}_R$. Note that for purely soft and collinear emissions the PDF cancels with that in σ_0, the Born cross-section. This is not correct in the hard collinear region and we will re-introduce the

[3]The subsequent extension to hard and collinear emissions will be straightforward.

PDF while considering those emissions. For the final result we shall also normalise to the cross-section including up to $\mathcal{O}(\alpha_s)$ corrections, rather than merely the Born cross-section.

We first compute the integrated quantity:

$$\frac{1}{\sigma_0}\sigma(Q,Q_t) = \frac{1}{\sigma_0}\int_0^{Q_t^2}\frac{d\sigma}{dQ_t'^2}dQ_t'^2 \approx \sum_n \int dP_n\,\theta(Q_t-p_t)\,d^2\vec{p}_t\,\delta^2\left(\vec{p}_t+\sum_{i\in\mathcal{H}_R}\vec{k}_{t,i}\right). \tag{4.2.3}$$

One can then express:

$$\delta^2\left(\vec{p}_t+\sum_{i\in\mathcal{H}_R}\vec{k}_{t,i}\right) = \int\frac{d^2\vec{b}}{(2\pi)^2}e^{i\vec{b}.\vec{p}_t}\prod_{i\in\mathcal{H}_R}e^{i\vec{b}.\vec{k}_{t,i}}\,. \tag{4.2.4}$$

Having achieved our aim of factorising the delta function constraint into a product of individual gluon contributions, we integrate over $\vec{p}_t$ which reduces the above to:

$$\frac{1}{\sigma_0}\sigma(Q,Q_t) \approx \sum_n \int dP_n\,Q_t\,J_1(b\,Q_t)\,db\prod_{i\in\mathcal{H}_R}e^{i\vec{b}.\vec{k}_{t,i}}\,, \tag{4.2.5}$$

where in writing the above we make use of $\int_0^{2\pi}d\theta\,\exp\left(i\,b\,p_t\cos\theta\right) = 2\pi J_0(b\,p_t)$, and $uJ_1(u) = \int_0^u u'J_0(u')du'$, with J_0 and J_1 being the zeroth and first-order Bessel functions.

The emission probability dP_n factorises for *soft and collinear* emissions into an essentially classical independent emission pattern (see eq. (3.2.6) in chapter 3):

$$dP_n = \frac{1}{n!}\prod_{i\in\mathcal{H}_R}C_F\frac{\alpha_s(k_{t,i}^2)}{\pi}\frac{d^2\vec{k}_{t,i}}{\pi k_{t,i}^2}d\eta_i\,, \tag{4.2.6}$$

where $\vec{k}_{t,i}$ and η_i refer to the transverse momenta and rapidity of the i^{th} emission with respect to the incoming quark direction . Since the incoming quark is anti-parallel to the photon axis, in the Breit frame, the k_t immediately above is the same to NLL accuracy as that measured with respect to the photon axis and we do not distinguish the two. The coupling α_s is defined in the CMW scheme [74]. We note that the rapidity integration is bounded by $\eta = 0$ at large angles to the incoming quark since we consider emissions in the remnant hemisphere alone.

Summing over all emissions in the remnant hemisphere using the factorised forms (4.2.4) and (4.2.6) and inserting virtual corrections according to the emission pattern (4.2.6) (with an additional factor $(-1)^n$) we arrive at the resummed soft and collinear

contribution to $\sigma(Q, Q_t)/\sigma_0$:

$$\int Q_t \, J_1(b\, Q_t) \, \exp[-R_{\rm sc}(b)] \, db \,, \tag{4.2.7}$$

where $R_{\rm sc}(b)$ is the "radiator" accounting for soft and collinear emissions by the incoming quark:

$$R_{\rm sc}(b) = -\frac{C_F}{\pi} \int \frac{d^2\vec{k}_t}{\pi k_t^2} \, d\eta \, \alpha_s(k_t^2) \, \left(e^{i\vec{b}.\vec{k}_t} - 1 \right) . \tag{4.2.8}$$

We remind the reader that one needs to correct the above expression to obtain single logarithms arising from hard collinear radiation as well as those that arise in the large-angle region from soft emissions, which we shall do presently.

Let us for the moment concentrate on the quantity $R_{\rm sc}(b)$, which is the most important piece of the result since it contains the leading (double) logarithms. Integrating over the polar angle variable in eq. (4.2.8) we obtain:

$$R_{\rm sc}(b) = -\frac{2C_F}{\pi} \int \frac{dk_t}{k_t} d\eta \, \alpha_s(k_t^2) \, (J_0(b\, k_t) - 1) \, . \tag{4.2.9}$$

Further to SL accuracy, it suffices to make the substitution [75]: $(J_0(bk_t) - 1) \to -\theta(k_t - 2e^{-\gamma_E}/b)$, with γ_E being the Euler constant, and arrive at:

$$R_{\rm sc}(b) = \frac{2C_F}{\pi} \int_{1/\bar{b}}^{Q} \alpha_s(k_t^2) \frac{dk_t}{k_t} \ln \frac{Q}{k_t} \,, \qquad \bar{b} = b\, e^{\gamma_E}/2 \,, \tag{4.2.10}$$

where we perform the rapidity integration.

Next we extend the soft-collinear result above to the full collinear one by including hard emissions. As is easy to show (see e.g. [88]), hard emissions collinear to the incoming quark lead to a modification of the factorisation scale μ^2 in the PDFs to the scale $1/\bar{b}^2$, $q(x, \mu^2) \to q(x, 1/\bar{b}^2)$, and contribute an additional finite term which can be absorbed by the replacement of Q in eq. (4.2.10) by $Q\, e^{-3/4}$. Thus the extension of the soft-collinear result, eq. (4.2.7), to the full collinear one is:

$$\frac{1}{q(x, \mu^2)} \int q\left(x, 1/\bar{b}^2\right) Q_t \, J_1(b\, Q_t) \, \exp[-R(\bar{b}\, Q)] db \,, \tag{4.2.11}$$

with:

$$R(\bar{b}\, Q) = \frac{2C_F}{\pi} \int_{1/\bar{b}}^{Q} \alpha_s(k_t^2) \frac{dk_t}{k_t} \left(\ln \frac{Q}{k_t} - \frac{3}{4} \right) . \tag{4.2.12}$$

4.2.2 Non-global corrections

We also have to include the effects of soft emissions at large angles. Thus far we have identified remnant emissions as those belonging to the incoming quark while current-hemisphere emissions (over which we claim to be inclusive) are associated to the struck final-state quark. As is the case for single-hemisphere observables, this identification is not correct at SL level due to correlations between soft emissions at large angles [21, 22]. Thus the remnant hemisphere distribution is affected at SL level by soft gluons at large angles to the current quark, but still in the current hemisphere, emitting into the remnant hemisphere.

As we stated earlier, the computation of this piece has been carried out in the large N_c approximation[4] and is universal for all observables having a linear dependence on k_t of soft large-angle emissions. We label this non-global piece $\mathcal{S}(\bar{b}\,Q)$, which can be parameterised as [21]:

$$\mathcal{S}\left(\bar{b}\,Q\right) \simeq \exp\left[-C_F C_A \frac{\pi^2}{3}\left(\frac{1+(At)^2}{1+(Bt)^C}\right) t^2\right], \tag{4.2.13}$$

where:

$$t(\bar{b}\,Q) = -\frac{1}{4\pi\beta_0}\ln\left(1-2\alpha_s(Q^2)\beta_0\ln(\bar{b}\,Q)\right), \tag{4.2.14}$$

with $A = 0.85\,C_A$, $B = 0.86\,C_A$ and $C = 1.33$.

Thus our final form for the resummed result to NLL accuracy can be expressed as:

$$\frac{1}{\sigma_0}\sigma(Q,Q_t) = \frac{1}{q(x,Q^2)}\int q\left(x,1/\bar{b}^2\right)\mathcal{S}(\bar{b}\,Q)\,e^{-R(\bar{b}\,Q)}\,Q_t\,J_1(b\,Q_t)\,db\,, \tag{4.2.15}$$

where we chose $\mu = Q$. The above result now incorporates all the sources of logarithmic enhancements to NLL or SL accuracy, specifically soft and hard collinear emissions and soft emissions at large angles. The result for the NLL radiator $R(\bar{b}\,Q)$ is explicitly given in appendix A.2. In the following section we shall take the b-space result above and convert it to one valid in Q_t space over the range of Q_t values that interest us.

[4]Strictly speaking the full result has been computed at $\mathcal{O}(\alpha_s^2)$ and the large N_c approximation starts $\mathcal{O}(\alpha_s^3)$.

4.3 Result in Q_t space

We start by noting that one commonly used method to derive a Q_t-space result from the b-space form is simply to evaluate the complete b integral in eq. (4.2.15) numerically. This method is not without several well-documented shortcomings [94, 95] that are usually circumvented by "reasonable" prescriptions that are not derived from first principles of QCD.

For instance the b integral stretches from 0 to ∞, but the function $R(\bar{b}\,Q)$ has a Landau pole singularity at $\bar{b}\,Q = \exp\left[1/\left(2\,\beta_0\,\alpha_s\right)\right]$, which means it is perturbatively undefined for large b values. To get around this problem one introduces a parameter b^* and substitutes[5] $b \to b^* = b/\sqrt{1 + b^2/b_{\rm lim}^2}$ [86]. This ensures one never evaluates $R(\bar{b}\,Q)$ or the structure functions at scales larger than some cut-off $b_{\rm lim}$, whose value is adjustable. Additionally we smear the b-space result with a non-perturbative Gaussian function that is also not obtained from first principles, but typically through fits to data sets [96, 97, 98, 99, 100, 101]. These prescriptions are needed in order to do the b integral and obtain a result for finite Q_t, even at relatively large Q_t values where one might expect to trust perturbative predictions and where additional non-perturbative parameters or ad-hoc inputs should not play any significant role. Moreover the matching to fixed-order Q_t-space results is complicated by not having an analytical resummed result in Q_t space.

In what follows we provide an analytical Q_t-space result which is valid for use over a large range of Q_t values and represents a clean extraction of the NLL resummed Q_t-space result, from the b integral [102, 103]. The price we pay for not evaluating the complete b integral in detail is a formal divergence at small Q_t, which one can anticipate quite generally through considerations based on the work of Parisi and Petronzio [93]. Thus we cannot use our result at very small Q_t values since in this region our answer is no longer a good approximation to the b integral. For quantitative studies however, with the specified Q_t range over which data is available, our formula is valid for use as it stands. The region over which we start to see a problem with our approximation occurs at Q_t values that are too small ($Q_t \lesssim 1.5$

[5] In chapter 6 we use this method to compute the resummed dijet azimuthal correlation distribution in DIS.

GeV, see later) to study accurately via perturbative methods and in any case below the lowest Q_t data.

To obtain a resummed result in Q_t space we expand the function $R(\bar{b}\,Q)$ in eq. (4.2.15), about the point $\hat{b}(\equiv b\,Q_t) = 2e^{-\gamma_E}$ to obtain:

$$R(\bar{b}\,Q) = R\,(Q/Q_t) + R'(Q/Q_t)\left(\gamma_E - \ln 2 + \ln \hat{b}\right) + \cdots\,, \tag{4.3.1}$$

where we use $R'(\bar{b}\,Q) = \partial R(\bar{b}\,Q)/\partial \ln b$ and neglected R'' and higher derivatives as they contribute only to subleading (below SL) accuracy. The non-global function $\mathcal{S}$ and the b dependent parton distributions are straightforwardly expressed in Q_t space with the substitution $\bar{b} \to 1/Q_t$, since logarithmic derivatives of these SL functions, analogous to R' above, only contribute at subleading accuracy.

Using the Taylor expansion for R above, one can cast the result (4.2.15) as:

$$\begin{aligned}\frac{1}{\sigma_0}\sigma(Q,Q_t) &= \frac{q\,(x,Q_t^2)}{q(x,Q^2)}\mathcal{S}(Q/Q_t)\,e^{-R(Q/Q_t)+(\ln 2-\gamma_E)R'(Q/Q_t)}\int_0^\infty d\hat{b}J_1(\hat{b})\,\hat{b}^{-R'(Q/Q_t)} \\ &= \frac{q\,(x,Q_t^2)}{q(x,Q^2)}\mathcal{S}(Q/Q_t)\,e^{-R(Q/Q_t)-\gamma_E R'(Q/Q_t)}\frac{\Gamma(1-R'/2)}{\Gamma(1+R'/2)}\,. \end{aligned}\tag{4.3.2}$$

Incorporating, as a factor, the $\mathcal{O}(\alpha_s)$ constant pieces (see appendix A.1) we can write the result as:

$$\begin{aligned}\frac{1}{\sigma_0}\sigma(Q,Q_t) = \frac{1}{q(x,Q^2)}\left(\boldsymbol{C}_0\otimes\boldsymbol{q}(x,Q_t^2) + \frac{\alpha_s}{2\pi}\boldsymbol{C}_1\otimes\boldsymbol{q}(x,Q^2)\right)\times \\ \times\,\mathcal{S}(Q/Q_t)\,e^{-R(Q/Q_t)-\gamma_E R'(Q/Q_t)}\frac{\Gamma\,(1-R'/2)}{\Gamma\,(1+R'/2)}\,,\end{aligned}\tag{4.3.3}$$

where $\boldsymbol{C}_0$ and $\boldsymbol{C}_1$ are matrices in flavour space of coefficient functions (see appendix A.1). While the $\boldsymbol{C}_0$ terms are merely proportional to delta functions the $\boldsymbol{C}_1$ pieces are important to correct the soft-collinear resummed result for hard real and virtual emissions at the leading $\mathcal{O}(\alpha_s)$ accuracy. They are straightforward to compute and are presented in appendix A.1.

We immediately note that the above result diverges at $R' = 2$, an entirely expected feature. The reason for this divergence (encountered also in the Drell-Yan Q_t resummations and the jet broadening in DIS [87]) is merely the fact that at very small Q_t the result one obtains is not described by exponentiation of the leading-order result, which is essentially the form we have derived above [93]. As $Q_t \to 0$ the mechanism of vectorial cancellation between emissions of formally arbitrary hardness

takes over from the Sudakov suppression of soft and collinear radiation as the dominant mechanism for producing a small Q_t. However the divergence does not play a major role for phenomenological purposes[6], since over the values of Q_t we intend to study we are sufficiently away from the point $R' = 2$. This will be further elaborated in the subsection below.

4.3.1 Position and impact of the divergence

As we mentioned above, for the particular case at hand, the divergence occurs at rather small values of Q_t for the Q values[7] of interest to us. The corresponding Q_t values, at and near the divergence, fall in a region that is either neglected for phenomenological purposes or modelled with the introduction of non-perturbative parameters, since one expects non-perturbative effects to be large here. In the Q_t region where the divergence does not have any significant numerical impact, we still probe small enough Q_t to test the perturbative resummation and non-perturbative corrections, as is our aim.

To be precise the divergence occurs at $R' = 2$. In terms of the variable Q_t, using the expression for R' given in appendix A.2, this results in:

$$Q_t = Q \exp\left(-\frac{\pi}{\alpha_s(C_F + 2\pi\beta_0)}\right), \tag{4.3.4}$$

which for the illustrative value of $Q = 90$ GeV gives $Q_t = 0.52$ GeV, with $\alpha_s = 0.118$. Since this region is in any case perturbatively unsafe, being quite close to the QCD scale, we do not expect to obtain sensible results with the perturbative methods we use. However we can safely study Q_t values of a few GeV without worrying about the impact of the formal divergence at $R' = 2$.

We note that the scale associated with the divergence varies only very slowly with the hard scale Q, since substituting the one-loop result for $\alpha_s(Q^2)$ in eq. (4.3.4) one obtains $Q_t \sim \Lambda_{\rm QCD}(Q/\Lambda_{\rm QCD})^{1/4}$. Thus for the scale of the divergence to exceed even 1 GeV one has to increase the hard scale Q to beyond the TeV limit.

[6] We contrast this with the dijet azimuthal correlation distribution which we shall study in chapter 6. There the position of the divergence is too high to be ignored. In that case we resort to the numerical method we highlighted before.

[7] There are data in the range $17\,\text{GeV} \leq Q \leq 116\,\text{GeV}$.

We can quantify this statement as follows: in the region where $R' = 2$ there is a complete breakdown of the hierarchy between leading, next-to-leading, etc. logarithms. In order to determine up to which value of R' one can use the usual hierarchy, where N^{n}LL terms are suppressed by α_s^n with respect to leading logarithmic terms, one can follow the procedure outlined by Dasgupta and Salam [87].

From those arguments one can infer that terms that are formally NNLL contribute a correction that is of the same order as the terms that one keeps in the NLL resummed result in the region where $2 - R' = \sqrt{\alpha_s}$. The NNLL terms contribute at relative $\mathcal{O}(\alpha_s)$ when $R' = 1$ or more. Thus for $R' \leq 1$ we can safely use our resummed Q_t-space formula since omitted NNLL terms contribute as usual, at relative $\mathcal{O}(\alpha_s)$.

We can work out the position of both points in terms of Q_t for a given Q. For $Q = 90$ GeV we obtain that the critical value, where all terms in the formal hierarchy are in fact of the same order, is $Q_t = 0.68$ GeV and that the region where the usual hierarchy is respected is $Q_t \geq 1.5$ GeV. This still allows the full range of available data to be safely probed, including the lowest measured Q_t bins.

4.4 Matching to fixed-order

Having obtained the NLL perturbative estimate we now need to combine it with the exact $\mathcal{O}(\alpha_s^2)$ perturbative result to obtain accurate predictions over the entire range where data exist. This will allow us to arrive at a result which has the form given by eq. (3.4.1). We follow the matching prescription known as M_2 matching introduced by Dasgupta and Salam [87]. Here the final result is given by:

$$\sigma_r + \bar{\alpha}_s \left(\sigma_e^{(1)} - \sigma_r^{(1)}\right) + \bar{\alpha}_s^2 \left(\sigma_e^{(2)} - \sigma_r^{(2)}\right) \Sigma(Q, Q_t)\,, \tag{4.4.1}$$

where $\bar{\alpha}_s = \alpha_s/(2\pi)$ and $\sigma_r^{(1),(2)}$ denote the coefficients of the resummed result, σ_r, expanded to first and second order in $\bar{\alpha}_s$ respectively, while $\sigma_e^{(1),(2)}$ are the corresponding coefficients obtained from fixed-order Monte Carlo programs such as DISENT [90, 91]. The above matching formula adds the resummed and exact results and subtracts the double-counted terms (up to $\mathcal{O}(\bar{\alpha}_s^2)$) that are included in the resummation.

Note that terms such as $\alpha_s^2 \ln(Q/Q_t)$, which are formally subleading and hence not included in the resummation, are present in the piece $\bar{\alpha}_s^2 \left(\sigma_e^{(2)} - \sigma_r^{(2)}\right)$ of eq. (4.4.1).

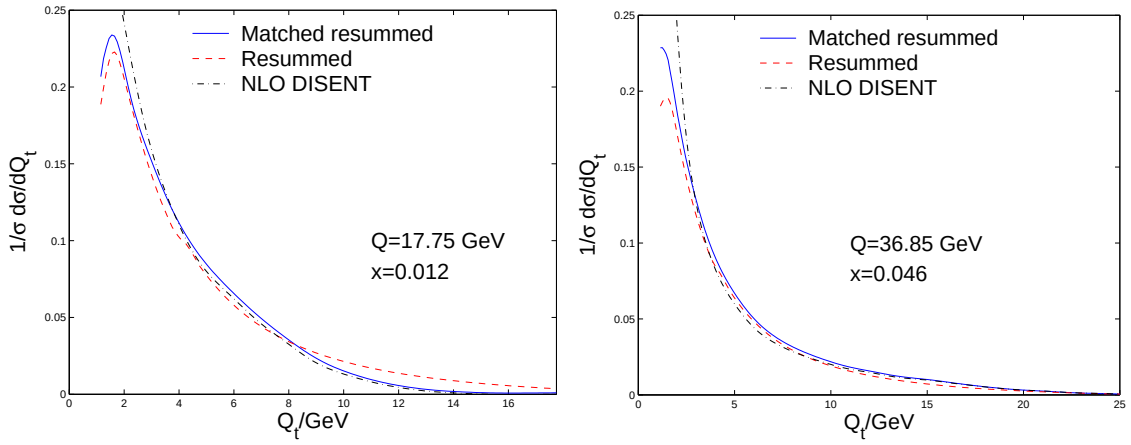

Figure 4.1: Comparison between DISENT, matched resummed and pure resummed differential distributions. MRST NLO PDFs are used with $\alpha_s(M_Z^2) = 0.1205$ [104].

This piece is divergent as $Q_t \to 0$ and thus we multiply it by the resummed form-factor $\Sigma(Q, Q_t) \equiv q(x, Q_t^2)/q(x, Q^2)\, \mathcal{S}(Q/Q_t) \exp\left[-R\left(Q/Q_t\right)\right]$, to ensure sensible behaviour at small Q_t. This procedure is obviously ad-hoc but only affects the result at subleading-logarithmic accuracy, which is in any case beyond our quantitative control.

Another point that needs to be re-emphasised is that the factor Σ, as we use it here, is just an approximation to the resummed result given by a full evaluation of the b integral. The approximation is intended for use (and is valid to NLL accuracy) only sufficiently away from $R' = 2$, the position of the divergence. As we explained in the last section, this covers the range over which can make reasonable comparisons with the data.

4.5 Results

The aim of this section is to display the results obtained for an NLL resummed prediction matched to NLO predictions from DISENT. Additionally we comment on the role that might be played by a non-perturbative Gaussian smearing function and that small-x effects may effectively give an enhanced smearing of the spectrum leading to a broader prediction than the one provided here as was observed also in the SIDIS case [8, 9].

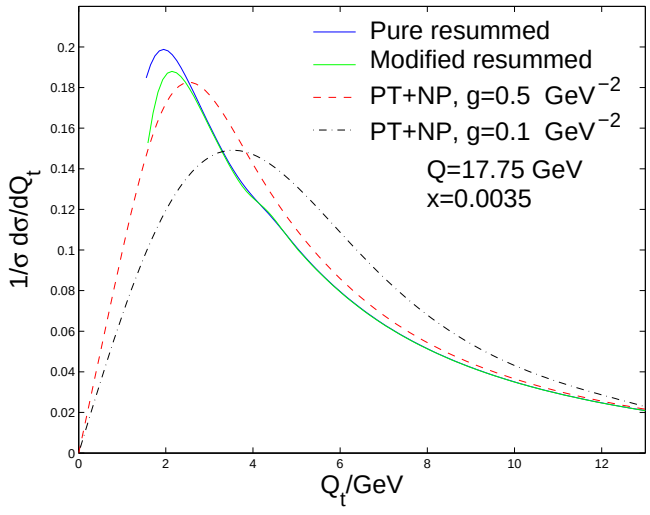

Figure 4.2: Non-perturbative smearing of the modified resummed prediction with a Gaussian function in k_t, $\exp[-gk_t^2]$. Here PT and NP stand for perturbative and non-perturbative respectively. Two different choices of the smearing parameter g are illustrated. Also shown is the pure resummed result. It can be seen that the modification, as described in the text, does not affect the resummed result over its region of validity.

In fig. 4.1, we display the fixed-order NLO results along with the pure resummed and matched results for two values of the hard scale Q and corresponding Bjorken x values. The choice of the x and Q values correspond to bins where preliminary data already exist [89]. There one notes the divergent NLO result and the correct small-Q_t behaviour as given by the resummation as well as the role of matching in the high-Q_t tail of the distribution. We also point out that the role of the non-global term is limited to a few percent effect after the matching to fixed-order has been performed. Thus missing uncalculated SL terms in the non-global piece $\mathcal{S}$, which are suppressed as $1/N_c^2$, are not expected to change our quantitative conclusions.

We also present here the effect of smearing or convoluting our resummation with a b-space or equivalent k_t-space Gaussian function representing non-perturbative effects. Such intrinsic k_t effects have been the subject of much phenomenological investigation in Drell-Yan–like processes [86, 99, 105, 106]. The non-perturbative smearing function we choose has the simple form: $F^{\rm NP}(k_t) = \exp[-gk_t^2]$, and we perform a two-dimensional convolution: $\int d^2\vec{k}_t\, g/\pi F^{\rm NP}\left(|\vec{Q}_t - \vec{k}_t|\right) I(k_t)$ with the re-

summed distribution $I(k_t) = 1/\sigma\, d\sigma/dk_t^2$, to obtain the smeared result as a function of Q_t. We carry out the smearing with different values of g, two of which are illustrated in fig. 4.2. The value of $g = 0.5\,\mathrm{GeV}^{-2}$ corresponds to a reasonable mean intrinsic k_t value of 1.25 GeV. We also illustrate the effect of using a smaller g value of $0.1\,\mathrm{GeV}^{-2}$, which leads as shown to a broader Q_t distribution. Ideally one would need to compare our predictions with the data at different x values in order to ascertain whether one sees any visible broadening of the NLL resummed spectra at smaller x, such as that mimicked by a change in the smearing parameter g. If this is the case one may investigate the dependence of the smearing parameter g on Bjorken x, a step we leave to forthcoming work [92].

We should point out that in convoluting the resummed prediction with the non-perturbative Gaussian (intrinsic k_t) distribution it was necessary to provide an extrapolation of our resummed result for $I(k_t)$ down to $k_t = 0$. We have chosen this extrapolation as introduced by Ellis and Veseli [94] so as not to modify the NLL resummed result as well as to obtain the correct limiting behaviour of the integrated cross-section $\propto k_t^2$, as determined by evaluating the b integral for the integrated quantity $\sigma(k_t)$, in the limit $k_t \to 0$.

Thus we substitute for k_t an effective variable $(k_t^*)^2 = k_t^2 + Q_0^2 \exp(-k_t^2/Q_0^2)$ and make the replacement $\sigma(k_t) \to \sigma(k_t^*)\,(1 - \exp(-ak_t^2))$, where Q_0 and a should be chosen so as not to modify the resummed result in the range where it is valid, as in ref. [94]. These additional parameters should only modify the very low (non-perturbative) Q_t region where our NLL result is in any case not valid as it stands. One can think of the parameters a and Q_0 as being non-perturbative inputs that can be varied alongside the smearing parameter g to obtain a good fit to data in the lowest Q_t region.

For the plot in fig. 4.2 we chose to take $Q_0 = 1.2\,\mathrm{GeV}$ and $a = 1/Q_0^2$ as these choices do not impact our resummed result over most of its range of validity. This can be clearly seen from fig. 4.2 where we plot the pure resummed and modified resummed results with these choices of parameters. The dominant impact in the very low Q_t region, beyond the control of NLL resummation, is in fact that of the smearing function $\exp(-gk_t^2)$, for which different choices have been already mentioned.

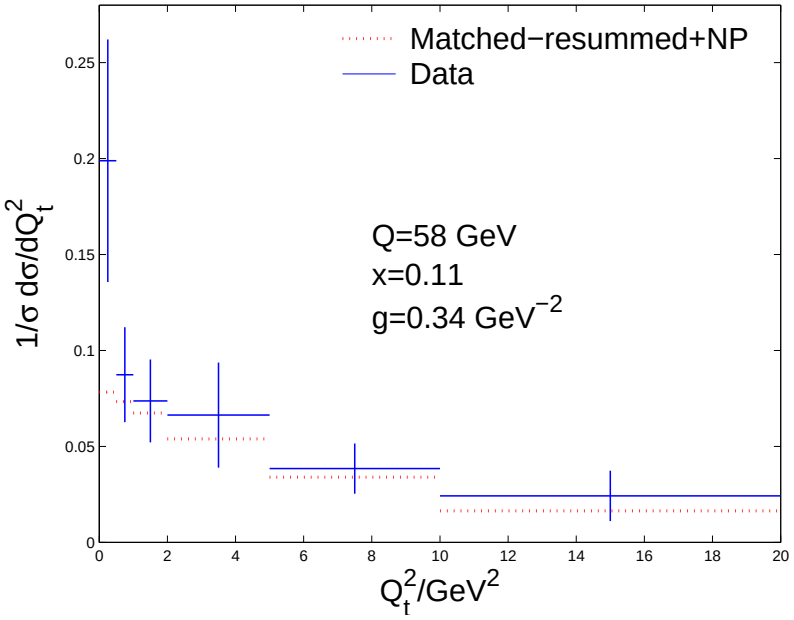

Figure 4.3: Comparison between H1 data [89] and the matched-resummed result including the non-perturbative correction. Note that the differential distribution in Q_t^2 is shown (rather than in Q_t as before).

Finally we show in fig. 4.3 a comparison between preliminary H1 data [89] and our theoretical prediction which is valid both at NLL and NLO accuracies, and accounts for non-perturbative intrinsic k_t effects.

4.6 Conclusions

We have introduced here a DIS variable that, as we have explained, has a very simple relationship to vector boson and Higgs Q_t spectra at hadron colliders. The aim of doing this has been to use HERA data to compare resummed theoretical predictions with experiment, keeping an eye on comparisons at lower x values. This complements the extensive studies of DIS event shapes that have been carried out thus far which employed the standard resummation formalism (and non-global logarithms), supplemented by $1/Q$ power corrections [49]. We recall that the program of comparing DIS event shapes to the data was quite successful without any special role visible for small-x effects [47].

Given however that only moderately small x values, $x \sim 10^{-2}$, can be reasonably

accessed in these studies, it is clearly better to choose a variable that is potentially more sensitive to small-x dynamics than event-shape variables, in order to determine the role of these effects. We expect such a variable to be the Q_t spectrum we have defined here, where it will be interesting to establish if a small-x enhanced broadening of the resummation we presented is indeed visible in the data. This was apparently the case in SIDIS studies [9] and, if present, we expect these effects to manifest themselves for our observable too. Given the simple relationship of our results to those for Drell-Yan–like observables it should then be easy to extrapolate our conclusions to hadron collider studies, where it is important to reach a firm conclusion on the issue of small-x broadening.

We have shown a comparison between our result and preliminary H1 prediction [89], and we await the data in its final form before making detailed phenomenological analyses and drawing conclusions on this issue. This will be the subject of forthcoming work.

In the next chapter we proceed with revisiting the energy flow distribution in e^+e^- annihilation into two jets to investigate the impact of jet algorithms on QCD resummation.

Chapter 5

On QCD resummation with k_t clustering

5.1 Introduction

One of the most commonly studied QCD observables is the flow of transverse energy (E_t) into gaps between jets in various QCD hard processes. Since the E_t flow away from jets is infrared and collinear-safe it is possible to make perturbative predictions for the same, which can be compared to experimental data for a given hard process. However since one typically examines configurations where E_t is small compared to the hard scale Q of the process (e.g. jet transverse momenta in hadronic collisions) the perturbative predictions involve large logarithms in the ratio Q/E_t. We have seen in section 3.3 that the resummation of logarithmically enhanced terms of the form $\alpha_s^n \ln^n(Q/E_t)$ has proved a challenge that is still to be fully met - complete calculations are available only in the large N_c limit [21, 22, 76]. Studies of the E_t flow have in fact directly led to developments in the theoretical understanding of QCD radiation and this process is still ongoing [29].

Another feature of the energy flow away from jets is its sensitivity to non-perturbative effects[1]. We showed in section 3.6 that one may expect significant $1/Q$ power corrections to energy flow distributions of a similar origin to those ex-

[1]In fact we use this observable to study non-perturbative effects in hadronic collisions. See chapter 7.

tensively studied for various jet-shape observables [47]. Moreover the E_t flow in hadronic collisions is a standard observable used to develop an understanding of the underlying event and to assess its role after accounting for perturbatively calculable QCD radiation [78, 107].

Given that E_t flow studies potentially offer so much valuable information on QCD over disparate scales, involving perturbative parameters such as the strong coupling α_s, QCD evolution, coherence properties of QCD radiation and non-perturbative effects, it is not surprising that they have been the subject of substantial theoretical effort over the last decade.

In this chapter we focus on the aspect of resummed predictions for the E_t flow into gaps between jets. Perhaps the most significant problem involved in making such predictions is the non-global nature of the observable [21, 22]. As we stated before, in order to resum the leading single logarithms one has to address not just a veto on soft emissions coupled to the underlying primary hard parton antennae (the primary emission term), but additionally correlated emissions or non-global contributions such as those represented in fig 3.3. For this latter contribution one has to resort to the large N_c limit to provide merely a leading-logarithmic estimate for the away-from-jet E_t flow. This situation can be contrasted with the case of event shapes and Drell-Yan Q_t resummations which have been pushed to NLL and NNLL accuracy respectively. The impact of finite N_c corrections in non-global observables is thus a factor in the theoretical uncertainty involved in the corresponding resummed predictions.

Given that the non-global component has a substantial quantitative impact over a significant range of E_t values for a given hard scale Q and that it is computable only in the large N_c approximation, it is clearly desirable to reduce the sensitivity of a given observable to non-global logarithms. An important observation in this regard, which we highlighted in the introduction chapter, was made by Appleby and Seymour [18]: if one employs the k_t clustering algorithm [14, 15] to define the final state such that the energy flow into a gap between jets is due to soft k_t-clustered mini-jets (rather than individual hadrons), the non-global logarithms are significantly

reduced in magnitude[2]. This observation was exploited to study the case of E_t flow in dijet photoproduction at HERA where a result was provided for the primary emission component of the E_t distribution and the reduced non-global component was modelled [108].

However it has subsequently been found by Banfi and Dasgupta that the k_t clustering algorithm also has a non-trivial impact on the primary emission component of the result [19]. This was not taken into account by Appleby and Seymour [18, 108] and also affects the ability to make resummed predictions for a host of other jet observables such as dijet azimuthal correlations between jets ($\Delta\phi$), which we shall study in the next chapter. In fact the findings of Banfi and Dasgupta [19] are not just specific to the k_t algorithm but would also crop up in the case of jet observables defined using iterative cone algorithms.

In the present chapter we shed more light on the resummation of the primary or independent emission component of the result and its dependence on the clustering algorithm. While the leading $\mathcal{O}\left(\alpha_s^2 \ln^2(Q/E_t)\right)$ clustering-dependent behaviour was computed analytically by Banfi and Dasgupta [19], the full resummed result for the primary emission component was computed only numerically in the case of a single hard emitting dipole ($e^+e^- \to 2$ jets or DIS $1+1$ jets). Here while sticking to a single hard dipole we shed more light on the structure of the primary emission term and analytically compute it to an accuracy that is sufficient for a wide range of phenomenological applications.

The analytical insight and calculations we provide here will also make the generalisation of the k_t-clustered primary emission result to the case of several hard emitters (dijets produced in photoproduction or hadron-hadron processes), involving a non-trivial colour flow, relatively straightforward.

The above resummation of the primary component of the answer assumes greater significance when we discuss our second observation: once an error is corrected in the numerical code used for the purposes of refs. [18, 108] the non-global component of the result is reduced even more compared to the earlier estimate. With a very small non-global component (which can be numerically computed in the large N_c limit)

[2]For recent progress on aspects of the k_t algorithm itself see refs. [16, 17].

and a primary emission component that correctly treats the dependence on the jet algorithm, one is better placed to make more accurate resummed predictions than has been the case till now. This is true not just for the E_t flow but also as we mentioned for a variety of jet observables for which there are either no resummed predictions as yet, or only those employing jet algorithms not directly used in experimental studies [109].

This chapter is organised as follows. In the following section we define the observable in question and revisit the issue of the dependence of the primary and non-global pieces on the jet clustering algorithm. Following this we demonstrate how the primary or independent emission piece can be computed to all orders in α_s, accounting to sufficient accuracy for the effects of the clustering algorithm. We explicitly describe the case of three and four-gluon emission contributions to demonstrate the steps leading to our all-orders result. Following this we re-examine the non-global component of the answer and find that this is significantly smaller than earlier calculations of the same [18]. We put our findings together to examine their impact on photoproduction data for the ZEUS collaboration [28] and lastly point to the conclusions one can draw and future extensions of our work.

5.2 Resummation of the primary emissions

Let us consider for simplicity the process $e^+e^- \to 2$ jets. The calculations for processes involving a larger number of jets and more complex jet topologies can be done along similar lines.

We examine the E_t flow in a region Ω which we choose as a slice in rapidity[3] of width $\Delta\eta$ centred on $\eta = 0$. We then define the gap transverse energy as:

$$E_t = \sum_{i \in \Omega} E_{t,i}\,, \tag{5.2.1}$$

where the index i refers to soft jets obtained after k_t clustering of the final state. We

[3]Since we deal with back-to-back jets we can define the rapidity with respect to the jet axis or equivalently, for our purposes, the thrust axis.

shall concentrate on the integrated E_t cross-section which is defined as:

$$\Sigma(Q, Q_\Omega) = \frac{1}{\sigma} \int_0^{Q_\Omega} \frac{d\sigma}{dE_t} dE_t \,, \tag{5.2.2}$$

with σ being the total cross-section for $e^+e^- \to$ hadrons, with centre-of-mass energy Q.

The SL result for the above, without k_t clustering (where the sum over i in eq. (5.2.1) refers to hadrons in the gap rather than jet clusters), was computed by Dasgupta and Salam [22] and is presented in section 3.3. The result can be expressed as:

$$\Sigma(Q, Q_\Omega) = \Sigma_P(t)\, S(t) \,, \qquad t = \frac{1}{2\pi} \int_{Q_\Omega}^{Q/2} \frac{dk_t}{k_t}\, \alpha_s(k_t^2) \,. \tag{5.2.3}$$

The above result contains a primary emission or "Sudakov" term[4] $\Sigma_P(t)$ and a non-global term $S(t)$.

The primary emission piece is built up by considering only emissions attached to the primary hard partons, namely those emitted from the hard initiating $q\bar{q}$ dipole in our example, while the non-global term arises from coherent soft emission from a complex ensemble of energy-ordered soft emitters alongside the hard initiating dipole. More precisely we have:

$$\Sigma_P(t) = e^{-4C_F t \Delta\eta} \,, \tag{5.2.4}$$

which is the result of resumming uncancelled k_t-ordered virtual emission contributions in the gap region. The non-global component, as we stated before, is computed numerically in the large N_c limit.

Next we turn to the k_t-clustered case. The result stated by Appleby and Seymour [18] defines the primary or Sudakov piece to be unchanged by clustering since it appears to be the exponentiation of a single gluon emitted inside the gap. The remainder is recomputed numerically implementing clustering [18]. As already shown by Banfi and Dasgupta [19], this remainder comprises the genuine non-global contribution and corrections to primary emissions due to clustering. The corrections to the primary emission term first appear while considering two gluons emitted by

[4]We use the term "Sudakov" in a loose sense since the primary emission result leads to an exponential that is analogous to a Sudakov form-factor.

the hard $q\bar{q}$ dipole and persist at all orders. Below we provide a reminder of the two-gluon emission case (discussed in ref. [19]) and subsequently consider explicitly the three and four-gluon emission cases before writing down the result to all orders as a function of the radius parameter R.

5.2.1 Two-gluon emission

In order to examine the role of the k_t algorithm we point out that in our case (k_t-ordered soft limit) one can start the clustering procedure with the lowest transverse-energy parton or equivalently the softest parton. One examines the "distances" of this particle (i) from its neighbours in the rapidity-azimuth plane (η-ϕ), defined by $d_{ij} = E_{t,i}^2 \left((\delta\eta_{ij})^2 + (\delta\phi_{ij})^2 \right)$, where $E_{t,i}$ is the transverse energy of the softest parton. If the smallest of these distances is less than $E_{t,i}^2 R^2$, particle i is recombined or clustered into its nearest neighbour and the algorithm is iterated. On the other hand if all d_{ij} are greater than $E_{t,i}^2 R^2$, particle i is counted as a jet and removed from the process of further clustering. The process continues until the entire final state is made up of jets. Also in the limit of strong energy ordering, which is sufficient to obtain the leading logarithms we are concerned with here, the recombination of a softer particle with a harder one gives a jet that is aligned along the harder particle.

The dependence of the primary emission term on the jet algorithm starts naturally enough from the two-gluon emission level. While the Sudakov result $\exp\left(-4C_F t\Delta\eta\right)$ comes about due to assuming real-virtual cancellations such that one is left with only virtual emissions with $k_t \geq Q_\Omega$ in the gap region (for the integrated distribution), k_t clustering spoils this cancellation.

Specifically let us take two real gluons k_1 and k_2 that are ordered in energy ($\omega_1 \gg \omega_2$). We consider as in ref. [19] the region where the softer gluon k_2 is in the gap whilst the harder k_1 is outside. Additionally we take the case that the gluons are clustered by the jet algorithm which happens when $(\delta\eta)^2 + (\delta\phi)^2 \leq R^2$ with $\delta\eta = \eta_2 - \eta_1$ and similarly $\delta\phi = \phi_2 - \phi_1$. We shall denote this condition with the symbol θ_{21}. Since k_2 is clustered to k_1 it gets pulled outside the gap, the recombined jet being essentially along k_1. Thus the double real emission term does not contribute to the gap energy *differential* distribution $d\sigma/dE_t$. Now let k_1 be a virtual gluon. In

this case it cannot cluster k_2 out of the gap and we do get a contribution (proportional to C_F^2) to the gap energy differential distribution. Thus a real-virtual cancellation which occurs for the unclustered case fails here and the mismatch for the integrated quantity ($\Sigma(t)$) amounts to:

$$C_2^p = \frac{(-4C_F t)^2}{2!}\int_{k_1\notin\Omega} d\eta_1 \frac{d\phi_1}{2\pi}\int_{k_2\in\Omega} d\eta_2 \frac{d\phi_2}{2\pi}\theta_{21} = \frac{(-4C_F t)^2}{2!}\frac{2}{3\pi}R^3\,, \qquad (5.2.5)$$

where we report the result computed by Banfi and Dasgupta [19] for $R \leq \Delta\eta$. Here we introduce the primary emission term C_n^p that corrects the Sudakov result at $\mathcal{O}(\alpha_s^n)$ due to the clustering requirement.

The fact that the result scales as the third power of the jet radius parameter is interesting in that by choosing a sufficiently small value of R one may hope to virtually eliminate this piece and thus the identification of the primary result with the Sudakov exponent would be at least numerically accurate. However for such small R the non-global term would then be significant which defeats the main use of clustering. If one chooses to minimise the non-global component by choosing e.g. $R = 1$, then one must examine the primary emission terms in higher orders in order to estimate their role. To this end we start by looking at the three and four-gluon emission cases below.

5.2.2 Three-gluon emission

Consider the emission of three energy-ordered gluons k_1, k_2 and k_3 with $\omega_3 \ll \omega_2 \ll \omega_1$, off the primary $q\bar{q}$ dipole and employing the inclusive k_t clustering algorithm [14, 15] as explained previously.

We consider all the various cases that arise when the gluons (which could be real or virtual) are in the gap region or outside. We also consider all the configurations in which the gluons are affected by the clustering algorithm. We then look for all contributions where a real-virtual mismatch appears due to clustering, that is not included in the exponential Sudakov term. The Sudakov itself is built up by integrating just virtual gluons in the gap, above the scale Q_Ω. The corrections to this are summarised in table 5.1.

In order to obtain the various entries of the table one just looks at the angular

θ_{32}	θ_{31}	θ_{21}	$k_3 \in \Omega$	$k_2 \in \Omega$	$k_1 \in \Omega$	$k_3\,,\, k_2 \in \Omega$	$k_3\,,\, k_1 \in \Omega$	$k_2\,,\, k_1 \in \Omega$
0	0	0	0	0	0	0	0	0
1	0	0	0	0	0	0	W	0
0	1	0	0	0	0	W	0	0
0	0	1	0	0	0	W	0	0
1	1	0	W	0	0	W	W	0
1	0	1	0	0	0	0	W	0
0	1	1	0	0	0	W	0	0
1	1	1	W	0	0	W	W	0

Table 5.1: Contributions of different configurations of particles to Σ_P at $\mathcal{O}(\alpha_s^3)$. We define $\theta_{ij} = \theta\,(R^2 - (\eta_i - \eta_j)^2 - (\phi_i - \phi_j)^2)$, e.g. $\theta_{13} = 1$ means $(\eta_1 - \eta_3)^2 + (\phi_1 - \phi_3)^2 \leq R^2$. We also define $W = (-4C_F t)^3/3!$, so the entries "W" indicate a miscancellation which leads to a SL correction to the Sudakov result, while the entries "0" indicate a complete real-virtual cancellation. We have discarded the case where all particles are in the gap since such configurations are already included in the exponential Sudakov result.

configuration in question, draws all possible real and virtual contributions and looks for a mismatch between them generated by the action of clustering. We translate table 5.1 to:

$$\begin{aligned} C_3^p \;=\; & \frac{1}{3!}(-4C_F t)^3 \times \\ & \times\Bigg(\int_{k_1\notin\Omega} d\eta_1 \frac{d\phi_1}{2\pi} \int_{k_2\notin\Omega} d\eta_2 \frac{d\phi_2}{2\pi} \int_{k_3\in\Omega} d\eta_3\, \theta_{32}\, \theta_{31} + \\ & + \int_{k_1\notin\Omega} d\eta_1 \frac{d\phi_1}{2\pi} \int_{k_2\in\Omega} d\eta_2 \frac{d\phi_2}{2\pi} \int_{k_3\in\Omega} d\eta_3\, [\theta_{31} + (1-\theta_{31})(1-\theta_{32})\theta_{21}] + \\ & + \int_{k_1\in\Omega} d\eta_1 \frac{d\phi_1}{2\pi} \int_{k_2\notin\Omega} d\eta_2 \frac{d\phi_2}{2\pi} \int_{k_3\in\Omega} d\eta_3\, \theta_{32} \Bigg), \end{aligned} \tag{5.2.6}$$

where we use the freedom to set $\phi_3 = 0$. We identify three equal contributions consisting of the integrals in which there is only one theta function constraining only two particles: the integral over θ_{31} and that over θ_{21} in the third line and the last integral over θ_{32}. The set of configurations θ_{32}, θ_{31} and θ_{21} is just the set of constraints on all possible pairs of gluons. In fact we can generalise the number of

these configurations to the case of any number n of gluons by $n(n-1)/2$, which will enable us to resum R^3 terms to all orders. We shall return to this observation later. The integrals of the above type reduce essentially to the clustered two-gluon emission case, as calculated in eq. (5.2.5), and the integral over the third "unconstrained" gluon is just $\Delta\eta$.

Explicitly we write eq. (5.2.6) as:

$$\begin{aligned} C_3^p &= \frac{1}{3!}(-4C_F t)^3 \times \\ &\quad \times\Bigg(\int_{k_1\notin\Omega} d\eta_1 \frac{d\phi_1}{2\pi} \int_{k_2\notin\Omega} d\eta_2 \frac{d\phi_2}{2\pi} \int_{k_3\in\Omega} d\eta_3\, \theta_{32}\,\theta_{31} + \\ &\quad + \int_{k_1\notin\Omega} d\eta_1 \frac{d\phi_1}{2\pi} \int_{k_2\in\Omega} d\eta_2 \frac{d\phi_2}{2\pi} \int_{k_3\in\Omega} d\eta_3\, [\theta_{31}\theta_{32} - \theta_{31} - \theta_{32}]\,\theta_{21} + \\ &\quad + 3 \times \int_{k_1\in\Omega} d\eta_1 \frac{d\phi_1}{2\pi} \int_{k_2\notin\Omega} d\eta_2 \frac{d\phi_2}{2\pi} \int_{k_3\in\Omega} d\eta_3\, \theta_{32} \Bigg). \end{aligned} \tag{5.2.7}$$

Computing the various integrals above (for simplicity we take $R \leq \Delta\eta/2$, which is sufficient for our phenomenological purposes) one obtains:

$$\begin{aligned} C_3^p &= \frac{1}{3!}(-4C_F t)^3 \times \\ &\quad \times \left[\left(\frac{\pi}{3} - \frac{32}{45}\right)\frac{R^5}{\pi^2} + \tilde{f}_2 \frac{R^5}{\pi^2} - \left(\frac{\pi}{3} - \frac{32}{45}\right)\frac{R^5}{\pi^2} - \frac{32}{45}\frac{R^5}{\pi^2} + 3 \times \frac{2}{3\pi}\Delta\eta\, R^3 \right], \end{aligned} \tag{5.2.8}$$

with $\tilde{f}_2 \simeq 0.2807$ and we have written the results in the same order as the five integrals that arise from the various terms in eq. (5.2.7). Hence:

$$C_3^p = \frac{1}{3!}(-4C_F t)^3 \left(3 \times \frac{2}{3\pi}\Delta\eta\, R^3 + f_2\, R^5 \right), \tag{5.2.9}$$

where $f_2 \simeq -0.04360$. We note the appearance of an R^5 term which, as we shall presently see, persists at higher orders. This term is related to a clustering constraint on *three* gluons at a time via the product of step functions $\theta_{32}\,\theta_{21}(\theta_{31} - 1)$ with $k_2,\, k_3 \in \Omega$ and $k_1 \notin \Omega$.

Next we look at the emission of four soft, real or virtual energy-ordered gluons. This will help us move to a generalisation with any number of gluons.

5.2.3 Four-gluon emission case and beyond

Now we take the case of four-gluon emission and identify the patterns that appear at all orders. A table corresponding to table 5.1 is too lengthy to present here. The

result can however be expressed in an equation similar to that for the three-gluon emission case. We have:

$$
\begin{aligned}
C_4^p \;=\; & \frac{1}{4!}(-4C_F t)^4 \times \\
& \times\Bigg(\int_{1\,\mathrm{in}}\int_{2\,\mathrm{in}}\int_{3\,\mathrm{out}}\int_{4\,\mathrm{in}} \theta_{43} + \\
& + \int_{1\,\mathrm{in}}\int_{2\,\mathrm{out}}\int_{3\,\mathrm{in}}\int_{4\,\mathrm{in}} (\theta_{42} + \theta_{32}[1-\theta_{43}][1-\theta_{42}]) + \\
& + \int_{1\,\mathrm{out}}\int_{2\,\mathrm{in}}\int_{3\,\mathrm{in}}\int_{4\,\mathrm{in}} (\theta_{41} + \theta_{-41}[\theta_{31}\,\theta_{-43} + \theta_{43}\,\theta_{21}\,\theta_{-42} + \\
& \qquad\qquad + \theta_{21}\,\theta_{-42}\,\theta_{-43}\,\theta_{-31}\theta_{-32}]) + \\
& + \int_{1\,\mathrm{in}}\int_{2\,\mathrm{out}}\int_{3\,\mathrm{out}}\int_{4\,\mathrm{in}} \theta_{42}\,\theta_{43} + \\
& + \int_{1\,\mathrm{out}}\int_{2\,\mathrm{in}}\int_{3\,\mathrm{out}}\int_{4\,\mathrm{in}} \theta_{43}\,(\theta_{41} + \theta_{-41}\,\theta_{-42}\,\theta_{21}) + \\
& + \int_{1\,\mathrm{out}}\int_{2\,\mathrm{out}}\int_{3\,\mathrm{in}}\int_{4\,\mathrm{in}} (\theta_{41}\,\theta_{42} + \theta_{41}\,\theta_{-42}\,\theta_{-43}\,\theta_{32} + \\
& \qquad\qquad + \theta_{-41}\,\theta_{-43}\,\theta_{31}\,[\theta_{42} + \theta_{-42}\,\theta_{32}]) + \\
& + \int_{1\,\mathrm{out}}\int_{2\,\mathrm{out}}\int_{3\,\mathrm{out}}\int_{4\,\mathrm{in}} \theta_{41}\,\theta_{42}\,\theta_{43}\Bigg)\,,
\end{aligned}
\tag{5.2.10}
$$

where $\theta_{-ij} = 1 - \theta_{ij}$ and "in" or "out" pertains to whether the gluon is inside the gap region or out. For brevity we do not write the differential phase-space factor for each gluon which is as always $d\eta\, d\phi/(2\pi)$. We identify six R^3 terms exactly of the same kind as computed before and similarly four R^5 terms. Explicitly we have:

$$
\begin{aligned}
C_4^p \;=\; & \frac{1}{4!}(-4C_F t)^4 \times \\
& \times\Bigg(6 \times \int_{1\,\mathrm{in}}\int_{2\,\mathrm{in}}\int_{3\,\mathrm{out}}\int_{4\,\mathrm{in}} \theta_{43} + \\
& + 4 \times \Bigg[\int_{1\,\mathrm{in}}\int_{2\,\mathrm{out}}\int_{3\,\mathrm{out}}\int_{4\,\mathrm{in}} \theta_{42}\,\theta_{43} + \\
& \qquad + \int_{1\,\mathrm{in}}\int_{2\,\mathrm{out}}\int_{3\,\mathrm{in}}\int_{4\,\mathrm{in}} \theta_{32}\,(\theta_{43}\,\theta_{42} - \theta_{43} - \theta_{42}) \Bigg] + \\
& + 3 \times \int_{1\,\mathrm{out}}\int_{2\,\mathrm{in}}\int_{3\,\mathrm{out}}\int_{4\,\mathrm{in}} \theta_{21}\,\theta_{43}\,(1 - \theta_{41} - \theta_{42} + \theta_{41}\,\theta_{42}) + \\
& + \int_{1\,\mathrm{out}}\int_{2\,\mathrm{in}}\int_{3\,\mathrm{in}}\int_{4\,\mathrm{in}} \theta_{21}\big(\theta_{42}\,\theta_{43} - \theta_{42} - \theta_{43} - \theta_{41}\,\theta_{-42}\,\theta_{-43}\big) \times \\
& \qquad\qquad \times\big(\theta_{31}\,\theta_{32} - \theta_{31} - \theta_{32}\big) + \\
& + \int_{1\,\mathrm{out}}\int_{2\,\mathrm{out}}\int_{3\,\mathrm{in}}\int_{4\,\mathrm{in}} \theta_{32}\,\theta_{31}\,[\theta_{41}(1-\theta_{43})(\theta_{42}-2) - \theta_{43}] + \\
& + \int_{1\,\mathrm{out}}\int_{2\,\mathrm{out}}\int_{3\,\mathrm{out}}\int_{4\,\mathrm{in}} \theta_{41}\,\theta_{42}\,\theta_{43}\Bigg)\,.
\end{aligned}
\tag{5.2.11}
$$

We discuss below each set of integrals, generalise the result to the case of n emitted gluons and then resum all orders.

- The integral:
$$\frac{1}{4!}(-4C_F t)^4\, 6 \times \int_{1\,\text{in}}\int_{2\,\text{in}}\int_{3\,\text{out}}\int_{4\,\text{in}} \theta_{43}\,. \tag{5.2.12}$$
The integrals over particles 1 and 2 give $(\Delta\eta)^2$. The remaining integrals reduce to the result computed for the two-gluon emission case, i.e. the R^3 term. The factor 6 accounts for the number of pairs of gluons $n(n-1)/2$, for $n = 4$. Explicitly we have for this term:
$$\frac{1}{4!}(-4C_F t)^4 \frac{4\times 3}{2}\Delta\eta^{4-2}\frac{2}{3\pi}R^3\,. \tag{5.2.13}$$
For n emitted gluons the R^3 term, which is always related to the clustering of two gluons, is given by:
$$\frac{1}{n!}\frac{n(n-1)}{2}(-4C_F t\Delta\eta)^n\Delta\eta^{-2}\frac{2}{3\pi}R^3\,, \quad n\geq 2\,. \tag{5.2.14}$$
Hence to all orders one can sum the above to obtain:
$$e^{-4C_F t\Delta\eta}\frac{(-4C_F t)^2}{2}\frac{2}{3\pi}R^3\,. \tag{5.2.15}$$

- The integrals:
$$\frac{1}{4!}(-4C_F t)^4\, 4 \times \Bigg(\int_{1\,\text{in}}\int_{2\,\text{out}}\int_{3\,\text{out}}\int_{4\,\text{in}} \theta_{42}\,\theta_{43} + \\ + \int_{1\,\text{in}}\int_{2\,\text{out}}\int_{3\,\text{in}}\int_{4\,\text{in}} \theta_{32}\,[\theta_{43}\,\theta_{42} - \theta_{43} - \theta_{42}]\Bigg)\,. \tag{5.2.16}$$
The integral over particle 1 gives $\Delta\eta$, while the rest of the integrals reduce to the ones we calculated earlier which gave the R^5 result. The factor 4 stands for the number of triplet combinations formed by four gluons. For n emitted gluons this factor is $n(n-1)(n-2)/3!$. Explicitly we have for this case:
$$\frac{1}{4!}(-4C_F t)^4\frac{4\times 3\times 2}{6}\Delta\eta^{4-3}f_2\,R^5\,. \tag{5.2.17}$$
At the n^{th} order we obtain:
$$\frac{1}{n!}(-4C_F t\Delta\eta)^n\frac{n(n-1)(n-2)}{6}\Delta\eta^{-3}f_2\,R^5\,, \quad n\geq 3\,. \tag{5.2.18}$$
Summing all orders we get:
$$e^{-4C_F t\Delta\eta}\frac{(-4C_F t)^3}{6}f_2\,R^5\,. \tag{5.2.19}$$

- The integral:

$$\frac{1}{4!}(-4C_F t)^4\, 3 \times \int_{1\,\mathrm{out}} \int_{2\,\mathrm{in}} \int_{3\,\mathrm{out}} \int_{4\,\mathrm{in}} \theta_{21}\, \theta_{43}\,. \tag{5.2.20}$$

This integral can be factored into two separate integrals involving the constraint on k_1 and k_2 and on k_3 and k_4 respectively. Each of these reduces to the R^3 result obtained in the two-gluon emission case. Thus we get:

$$\frac{1}{4!}(-4C_F t)^4\, 3 \times \left(\frac{2}{3\pi}\right)^2 R^6\,. \tag{5.2.21}$$

At n^{th} order this becomes:

$$\frac{1}{n!}\frac{n(n-1)(n-2)(n-3)}{8}(-4C_F t\Delta\eta)^n \Delta\eta^{-4} \left(\frac{2}{3\pi}\right)^2 R^6\,, \quad n \geq 4\,, \tag{5.2.22}$$

which can be resummed to:

$$e^{-4C_F t\Delta\eta}\frac{(-4C_F t)^4}{8}\left(\frac{2}{3\pi}\right)^2 R^6. \tag{5.2.23}$$

The factor 3 (and generally $n(n-1)(n-2)(n-3)/8$) is the number of configurations formed by four (and generally n) gluons such that we have two pairs of gluons, each being formed by a soft in-gap gluon clustered to a harder out-of-gap one.

- The remaining integrals give at most an $\mathcal{O}(R^7)$ term because they constrain all the four gluons at once. In fact for gap sizes $\Delta\eta \geq 3R$, these integrals go purely as R^7 with no dependence on $\Delta\eta$. Since here however we use the condition $\Delta\eta \geq 2R$, which allows us to make use of the whole range of HERA data, these integrals do not depend purely on R. They are a function of R and $\Delta\eta$ which have an upper bound of order R^7. This can be seen by noting that there are three azimuthal integrations that each produce a function which has a maximum value proportional to R, so the result of integrating over all azimuthal variables is a factor that is bounded from above by $\mathcal{O}(R^3)$. Similarly there are four rapidity integrations with a clustering constraint on all four gluons implying that they can produce an $\mathcal{O}(R^4)$ term at most. In general the result at n^{th} order of constraining n gluons at once, is bounded from above by a factor of order R^{2n-1}.

We can write the result for all these as $(-4C_F t)^4/4!\, y(R,\Delta\eta)$, and resum such terms to all orders (in the same manner as before) to:

$$e^{-4C_F t\Delta\eta}\frac{(-4C_F t)^4}{4!}y(R,\Delta\eta)\,, \tag{5.2.24}$$

where $y(R,\Delta\eta)$ is at most $\mathcal{O}(R^7)$. We do not calculate these terms (though it is possible to do so) since the accuracy we achieve by retaining the R^3, R^5 and R^6 terms, we have already computed, is sufficient as we shall show.

The five-gluon emission case is too lengthy to analyse here. The same patterns as pointed out above persist here, but new terms that are at most $\mathcal{O}(R^9)$ appear when all five gluons are constrained. There is also an R^8 term, coming from the combination of R^3 and R^5 terms in the same manner that the R^6 term arose as a combination of two R^3 terms.

5.3 All-orders result

From the above observations we can assemble an all-orders result to R^6 accuracy, where we shall consider R to be at most equal to unity. The final result for primary emissions alone and including the usual Sudakov logarithms (for $\Delta\eta \geq 2R$) is:

$$\begin{aligned}\Sigma_P(t) &= e^{-4C_F t\Delta\eta}\times \\ &\times\left(1+(-4C_F t)^2\frac{R^3}{3\pi}+(-4C_F t)^3\frac{f_2}{6}R^5+(-4C_F t)^4\frac{R^6}{18\pi^2}+\frac{(-4C_F t)^4}{4!}\mathcal{O}(R^7)\right).\end{aligned} \tag{5.3.1}$$

Formally one may extend this accuracy by computing a few more terms such as those integrals that directly give or are bounded by an R^7 behaviour and this is possible though cumbersome. It should also be unnecessary from a practical viewpoint, especially keeping in mind that $R = 0.7$ is a preferable value to $R = 1$, in the important case of hadron collisions[5]. In fact even at $R = 1$ the R^3 term significantly dominates the result over the range of t values of phenomenological interest, as we shall see below.

[5]This is because the underlying event will contaminate jets less if one chooses a smaller R.

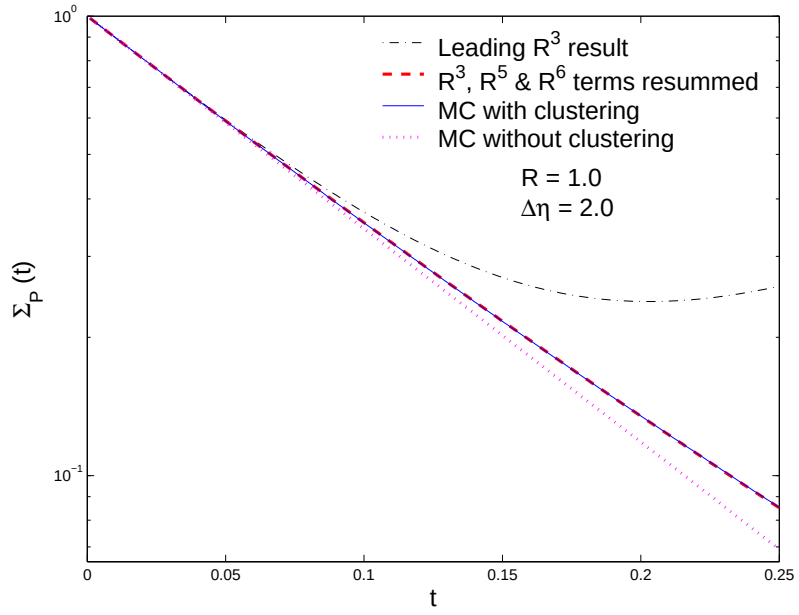

Figure 5.1: Comparison of the analytical results to a numerical Monte Carlo (MC) estimate.

We further note that if one keeps track of all the terms that come about as a combination of R^3 and/or R^5 terms in all possible ways at all orders, one ends up with the following form for eq. (5.3.1):

$$\Sigma_P(t) = e^{-4C_F t\Delta\eta} \exp\left(\frac{(-4C_F t)^2}{2!}\frac{2}{3\pi}R^3 + \frac{(-4C_F t)^3}{3!} f_2\, R^5 + \frac{(-4C_F t)^4}{4!}\mathcal{O}(R^7)\right), \tag{5.3.2}$$

the expansion of which agrees with eq. (5.3.1). In the above by $\mathcal{O}(R^7)$ we mean terms that, while they may depend on $\Delta\eta$, are at most as significant as an R^7 term. We also mention that in the formal limit $\Delta\eta \to \infty$, there is no dependence of the clustering terms on $\Delta\eta$ and they are a pure power series in R. The limit of an infinite gap appears in calculations where the region considered includes one of the hard emitting partons. An example of such cases (which have a leading double-logarithmic behaviour) is once again the quantity $\Delta\phi$ in e.g. DIS or hadron collisions.

Fig. 5.1 represents a comparison between the leading R^3 result (i.e. the pure fixed-order result of ref. [19] combined with the resummed Sudakov exponent), the resummed R^3, R^5 and R^6 result (eq. (5.3.1)) and a numerical Monte Carlo estimate with and without clustering. The Monte Carlo program in question is essentially that

described in ref. [21] with the modification of k_t clustering where we compute just emissions off the primary dipole "switching off" the non-global correlated emission.

We note that the resummed analytical form (5.3.1) is in excellent agreement with the numerical result which contains the full R and $\Delta\eta$ dependence. We have tested this agreement with a range of values of R. We take this agreement as indicating that uncomputed R^7 and higher terms can safely be ignored even at $R = 1$ and even more so at fractional values of R, e.g. $R = 0.7$. To provide an idea about the relative role of terms at different powers of R in eq. (5.3.1) we note that for $R = 1$ and $t = 0.25$ the resummed R^3 term increases the Sudakov result $\exp(-4C_F t\Delta\eta)$ by 19%, the R^5 term represents a further increase of 1.5% to the result after inclusion of the resummed R^3 term and the R^6 term has a similar effect on the result obtained after including up to R^5 terms.

Next[6] we comment on the size of the non-global component at different values of R.

5.4 Revisiting the non-global contribution

We have seen above how the primary emission piece is dependent on the jet clustering algorithm. It was already noted by Appleby and Seymour [18] that the non-global contribution is significantly reduced by clustering. Here we point out that after correction of an oversight in the code used there, the non-global component is even more significantly reduced than previously stated in the literature. Indeed for $R = 1$ and the illustrative value of $t = 0.15$, which corresponds to a gap energy $Q_\Omega = 1$ GeV for a hard scale $Q = 100$ GeV, the non-global logarithms are merely a 5% effect as opposed to the 20% reported previously [18] and the over 65% effect in the unclustered case.

In fig. 5.2 we plot the curves for the primary and full results (in the large N_c limit) for the integrated quantity $\Sigma(t)$ as a function of t defined earlier. We note that for $R = 0.5$ the primary result is essentially identical to the Sudakov result. The

[6]See the acknowledgment section for details of contributions of collaborators to the work presented in this thesis.

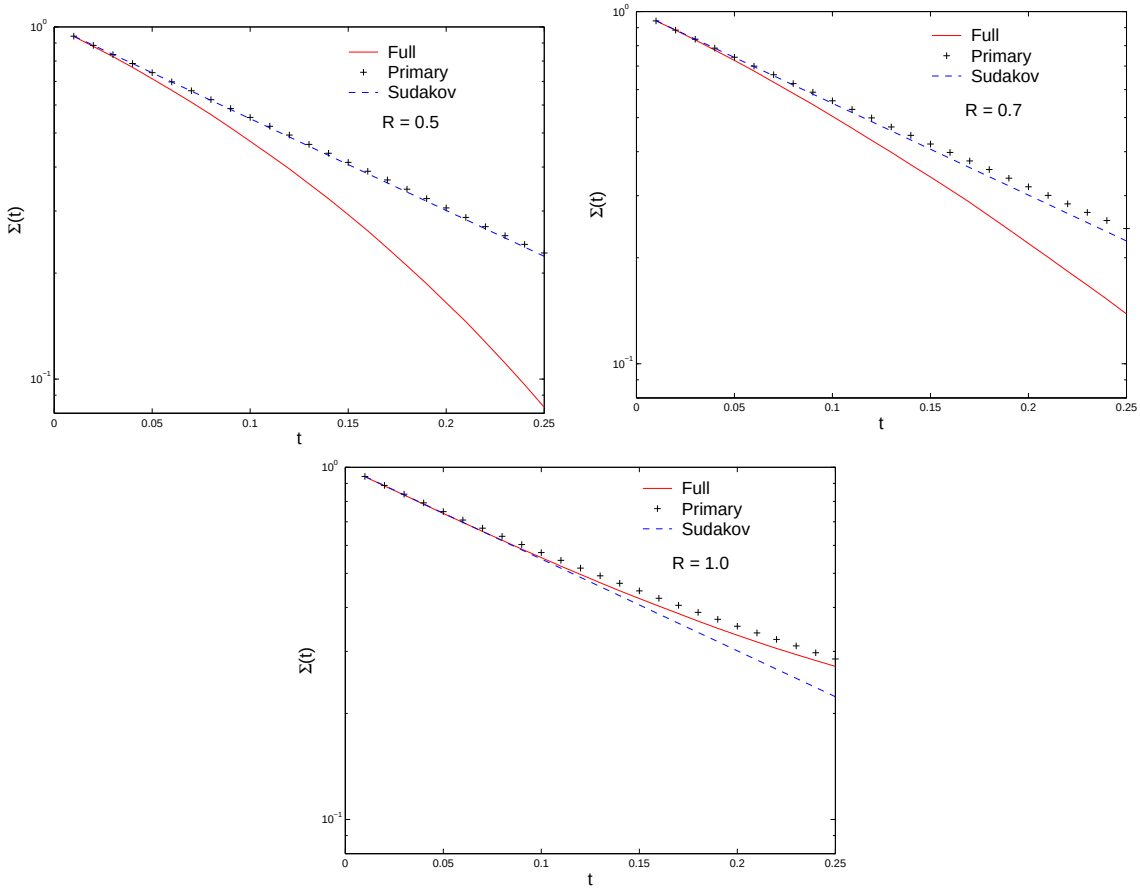

Figure 5.2: Comparison of the Sudakov result, the correct primary result and the full result including non-global logarithms, for different values of R and with $\Delta\eta = 1$. All quantities are shown in the large N_c limit for ease of comparison.

non-global contribution (which is the ratio of the full and primary curves) is however still quite significant. Neglecting it leads to an overestimate of 40% for $t = 0.15$. Increasing the jet radius in a bid to lower the non-global component we note that for $R = 0.7$ the impact of the non-global component is now just over 20% while the difference between the full primary result and the Sudakov result is small (less than 5%). The situation for $R = 1$ is a bit different. Here it is the non-global logarithms that are only a 5% effect (compared to the 20% claimed earlier [18]) while the full primary result is bigger than the Sudakov term by around 11%.

The value $R = 1$ is in fact the one used in the HERA analysis of gaps-between-jets in photoproduction. It is now clear that such analysis will have a very small non-global component and a moderate effect on primary emissions due to clustering. In

order to completely account for the primary emission case for dijet photoproduction one would need to generalise the calculations presented here for a single $q\bar{q}$ dipole to the case of several hard emitting dipoles. An exactly similar calculation would be needed for the case of hadron-hadron collisions and this is work in progress. It is straightforward however to at least estimate the effect of our findings on the photoproduction case and we deal with this in the following section.

5.5 Gaps between jets at HERA- the ZEUS analysis

We can test the perturbative framework presented in this chapter with energy flow measurements in the photoproduction of dijets. These energy flow observables are defined with two hard jets in the central detector region separated by a gap in pseudorapidity. A gap-event is defined when the sum of the hadronic transverse energy in the gap is less than a cut-off, and the gap fraction is defined as the ratio of the gap cross-section to the total inclusive cross-section. The energy flow observables measured by H1 [27] and ZEUS [28] use the k_t clustering definition of the hadronic final state, and the transverse energy in the gap is given by the sum of the mini-jet contributions. In this section we focus on the ZEUS measurements and provide revised theoretical estimates for them. These revisions lead to changes that are minor in the context of the overall theoretical uncertainty, but should become more significant once the matching to fixed higher orders is carried out and an estimate of the next-to-leading logarithms is obtained. The H1 data was considered in ref. [108], where the theoretical analysis consisted of only the resummed primary emission contribution without taking into account the effect of k_t clustering.

The ZEUS data was obtained by colliding 27.5 GeV positrons with 820 GeV protons, with a total integrated luminosity of 38.6 pb^{-1} in the 1996-1997 HERA running period. The full details of the ZEUS analysis can be found in ref. [28], but

the cuts relevant to the calculations in this section are:

$$\begin{aligned} 0.2 < y < 0.75\,, \\ Q^2 < 1\,\mathrm{GeV}^2\,, \\ E_{T,\,1} > 6\,\mathrm{GeV}\,, \\ E_{T,\,2} > 5\,\mathrm{GeV}\,, \\ |\eta_{1,\,2}| < 2.4\,, \\ |0.5(\eta_1 + \eta_2)| < 0.75\,, \\ 2.5 < \Delta\eta < 4\,, \end{aligned} \tag{5.5.1}$$

where y is the inelasticity (as defined in subsection 2.3.1), Q^2 is the virtuality of the photon, $E_{T,\,1}$ and $E_{T,\,2}$ are the transverse energies of the two outgoing hardest jets with respect to the proton axis, η_1 and η_2 are the pseudorapidities of the two hardest jets (in the final state) with respect to the proton axis and $\Delta\eta$ is the gap size (which is chosen to equal the rapidity difference between the leading jets $|\eta_1 - \eta_2|$). The further requirement for the gap sample is $E_{t,\,\mathrm{gap}} < Q_\Omega$, for $Q_\Omega = 0.5$, 1, 1.5 and 2 GeV, and the clustering parameter R is always taken to be unity.

The theoretical prediction for the gap fraction is composed of the primary piece, with corrections due to clustering, and the non-global piece. We shall now describe each in turn.

The resummed primary contribution, ignoring the clustering corrections, is obtained from the factorisation methods of Sterman et al [57, 58, 59, 60, 109] and is described in ref. [108]. The four-jet case of photoproduction requires a matrix formalism similar to that we discussed in section 3.5 and the exponents of the Sudakov factors in the gap cross-section are anomalous dimension matrices over the basis of possible colour flows of the hard sub-process. The emissions of soft gluons cause mixing of the colour basis (eq. (3.5.8)). Diagonalisation of the anomalous dimension matrices (by consideration of the eigenvectors and eigenvalues), allows the resummed four-jet primary emission differential cross-section to be written as [108]:

$$\frac{d\sigma}{d\eta} = \sum_{L,I} \widetilde{H}_{IL} \widetilde{S}_{LI} \exp\left(- \left(\lambda_L^*(\eta,\Omega) + \lambda_I(\eta,\Omega)\right) \int_{Q_\Omega}^{p_t} \frac{d\mu}{\mu} \frac{\alpha_s(\mu^2)}{2\pi} \right), \tag{5.5.2}$$

where the sums extends over the components of the hard and soft matrices $\widetilde{H}$ and

$\widetilde{S}$ (defined in the colour basis in which the anomalous dimension matrices are diagonal[7]), λ denotes the eigenvalues of the anomalous dimension matrices, $\eta = \Delta\eta/2$ and p_t is the hard scale of the process. This was computed by Appleby and Seymour [108] for the case of photoproduction and energy flow observables measured by H1. In this section we recompute this differential gap cross-section for the observable defined by the ZEUS collaboration. The uncertainty in the renormalisation scale is quantified by varying the hard scale in the resummation by a factor of 2 (upper bound) and 0.5 (lower bound).

We now need to account for the effect of clustering on eq. (5.5.2). Since we do not have as yet the full result for the four-jet case of photoproduction we simply estimate the full correction as the square of the correction arising in the two-jet case we have dealt with, using the appropriate colour factors for each hard sub-process. This was also the method used by Appleby and Seymour to approximate the non-global contribution for the four-jet case in ref. [108]. While we emphasise that this is only a rough way of examining the impact of the clustering-dependent terms, given the size of the effects we deal with, it is clear that no significant differences ought to emerge if one were to properly compute the various dipole contributions. We also include the revised and virtually negligible non-global component in an identical fashion to arrive at the best current theoretical estimates.

The results for the ZEUS gap-fraction with a k_t-defined final state are shown[8] in figs. 5.3 and 5.4. We consider here two different values for the gap energy Q_Ω. For the value of $Q_\Omega = 0.5$ GeV one notes that the full prediction, accounting approximately for all additional sources of SL enhancements, is somewhat higher than the pure "Sudakov-type" prediction. This is due to the extra primary terms we computed here, non-global corrections being negligible. For a larger value of $Q_\Omega = 1.0$ GeV, the difference between the clustered and unclustered primary results is negligible. We also note the large theoretical uncertainty on the predictions as represented by the renormalisation scale dependence. This is to be expected in light of the fact that

[7]See chapter 7 for a detailed treatment of the diagonalisation of the anomalous dimensions.

[8]The predictions we display here are readily made available for the ZEUS collaboration as the current best theoretical estimate.

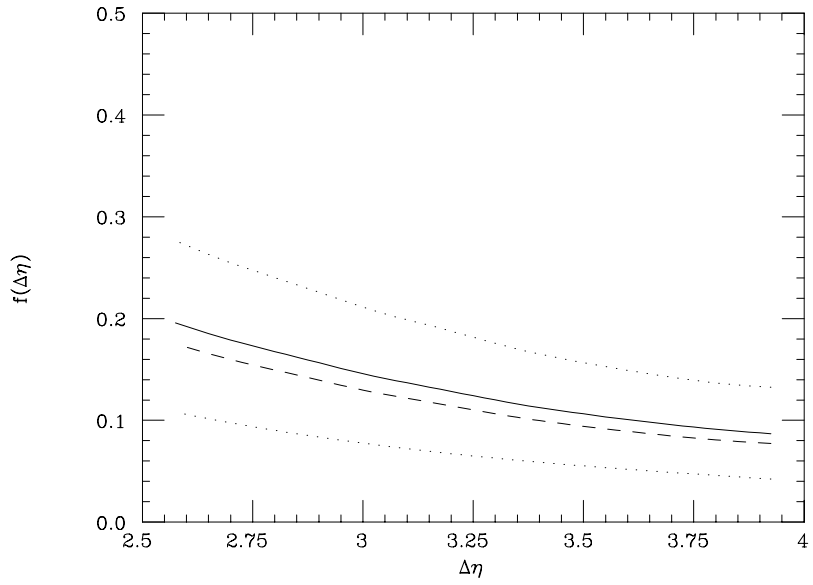

Figure 5.3: The gap fraction for the ZEUS analysis with a k_t-defined final state ($R = 1.0$ and $Q_\Omega = 0.5$ GeV). The solid line shows the effect of resummed primary emissions, the primary emission clustering correction factor and the non-global suppression factor. The overall theoretical uncertainty in all three contributions is shown by the dotted lines. The dashed line indicates the gap fraction obtained by only including primary resummed emissions without accounting for clustering.

these predictions are not matched to fixed-order results and account only for the leading logarithms. Improvements along both these directions should be possible in the immediate future after which the role of the various effects we highlighted here should be revisited.

5.6 Conclusions

In the present chapter we have shed further light on resummations of k_t-clustered final states. We have shown that both the primary and non-global components of the resummed result are affected by clustering and dealt with the resummation of each in turn. For the non-global component we found that the results after applying clustering are different from those presented earlier [18]. The new results we presented here indicate an even smaller non-global component than previously believed.

We have also shown how the primary emission clustering effects can be resummed

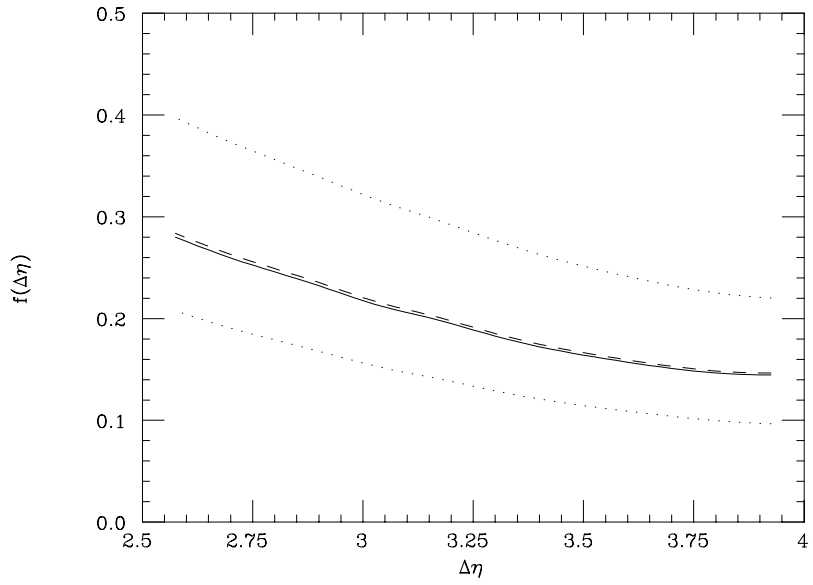

Figure 5.4: The gap fraction for the ZEUS analysis with a k_t-defined final state ($R = 1.0$ and $Q_\Omega = 1.0$ GeV). The solid line shows the effect of resummed primary emissions, the primary emission clustering correction factor and the non-global suppression factor. The overall theoretical uncertainty in all three contributions is shown by the dotted lines. The dashed line indicates the gap fraction obtained by only including primary resummed emissions without accounting for clustering.

to all orders as an expansion in the clustering parameter R and computed a few terms of the series. The analytical results we have provided here for a single emitting dipole should be generalisable to the case of several hard dipoles (multi-jet processes). This should then enable one to write a correct resummed result for primary emissions to a high accuracy and deal with the reduced non-global component in the large N_c limit. Such progress is relevant not just to energy flow studies but to any jet observable of a non-global nature, requiring resummation. An example is the azimuthal angle between jets ($\Delta\phi$) we mentioned previously, which we shall study in the next chapter. The work we have carried out should enable NLL calculations of such jet observables to sufficient accuracy to enable phenomenological studies of the same.

Lastly we have also mentioned the impact of our new findings on the ZEUS gaps-between-jets analysis. Since the non-global effects are very small for $R = 1$ the main new effect is the additional clustering-dependent primary terms we computed here. Approximating the effect of these terms for the case of photoproduction somewhat

changes the theoretical predictions, but this change is insignificant given the large theoretical uncertainty that arises due to missing higher orders and unaccounted for next-to-leading logarithms. We consider both these areas as avenues for further work and hope that more stringent comparisons can thus be made in the very near future.

Chapter 6

Dijet azimuthal correlations in QCD hard processes

6.1 Introduction

As we emphasised at length in the introduction chapter, studies of soft gluon radiation and non-perturbative effects in QCD observables are of vital importance. They help us better understand the dynamics of QCD and enhance the accuracy of theoretical predictions for measured quantities.

Successful examples of such studies are manifested in event-shape variables at LEP and HERA. Resummed estimates for these observables, combined with NLO predictions and corrected for non-perturbative effects, have been very successful in describing the data [46, 47]. Parameters such as the strong coupling and the effective non-perturbative coupling [48] can then be consistently extracted by studying distributions and mean values of such observables [42, 43].

Going beyond the case of two hard partons is more challenging in terms of theory but is also a more stringent test of our understanding of QCD dynamics. Multi-jet event-shape variables have been studied by Banfi et al [51, 52, 53, 54, 79]. However for jet-defined quantities, e.g. several dijet distributions, there are currently very few resummed predictions because of the lack of theoretical insight to all orders in the presence of a jet algorithm. Many measurements are already established (see e.g. [30, 32]) and await comparison to theoretical estimates.

Effort has recently been devoted to improve the understanding of the effect of jet algorithms on QCD resummation [18, 19, 20, 108]. As we have seen in chapter 5, a clustering algorithm has an impact on the resummation of observables which are sensitive to emissions in a limited region of the phase-space (non-global observables [21, 22]), such as energy flow outside jets. These receive single logarithms which are currently accounted for numerically in the large N_c limit for processes involving only two hard partons. It was shown in ref. [18] that employing a k_t algorithm on the final-state particles reduces these logarithms in the case where only two hard partons are present. However the resummation of jet-defined quantities proved to be non-trivial [19] and we have explained the full impact of the k_t clustering algorithm on resummation in chapter 5.

With the technique of resummation using a clustering algorithm one can proceed with studying jet-defined quantities. In the present chapter we focus on the dijet azimuthal correlation distribution. We consider the process of production of two hard jets (in the final state) in DIS or hadronic collisions. We study the azimuthal correlation defined by the azimuthal angle between the two leading hard jets in the final state. This study is similar to that of the DIS angular correlation introduced and analysed by Banfi et al [110], however our observable here is a jet-defined quantity being sensitive to the final-state jets (not hadrons).

This observable has been measured by the H1 collaboration [32]. The data obtained in these measurements were compared to fixed-order NLO predictions which showed the necessity of higher-order corrections. A resummation has therefore been suggested and it is this we aim to do here. A different approach, namely that employing unintegrated PDFs, has been followed by Hansson and Jung and it is interesting to compare our predictions with those of ref. [35].

In the soft and/or collinear region, i.e. close to the Born configuration in which the outgoing jets are back-to-back in the hadronic centre-of-mass frame, the dijet azimuthal correlation distribution receives large logarithms. This region is also strongly affected by non-perturbative effects. In this chapter we calculate the resummed distribution to NLL accuracy both in DIS and hadronic collisions. We find that the differential cross-section tends to a constant in the logarithmically enhanced region.

We also provide a matching to NLO results obtained from NLOJET++ [39, 40] in the DIS case.

This chapter is organised as follows. In the next section we discuss the kinematics of dijet production in DIS and the observable definition in the soft and collinear limit. We then provide a resummed prediction for the DIS case in section 6.3 and discuss the numerical approach we use to obtain the result in section 6.4. In section 6.5 we match the resummed result to NLO result and in section 6.6 we discuss our findings. Finally we briefly describe the extension of this work to hadronic collisions in section 6.7.

6.2 Kinematics

We consider the process in which soft gluons are emitted in dijet production in DIS ($q + p_0 \to p_1 + p_2 + \sum_i^n k_i$), with q, p_0, p_1, p_2 and k_i standing for the momenta of the virtual photon, the incoming parton, the two outgoing hard partons and the i^{th} soft gluon. We write the transverse momenta of particles with respect to the photon axis in the Breit frame (or equivalently the hadronic centre-of-mass frame), in which the incoming parton and virtual photon collide head-on, as:

$$\begin{aligned}
\vec{p}_{t,0} &= (0,0), \\
\vec{q}_t &= (0,0), \\
\vec{p}_{t,1} &= p_{t,1}(1,0), \\
\vec{p}_{t,2} &= p_{t,2}(-\cos\epsilon, \sin\epsilon), \\
&= p_{t,2}(\cos(\pi-\epsilon), \sin(\pi-\epsilon)), \\
\vec{k}_{t,i} &= k_{t,i}(\cos\phi_i, \sin\phi_i),
\end{aligned} \tag{6.2.1}$$

where we define the $+z$-axis to be parallel to the photon axis and consider the outgoing hard particle "1" to be at azimuthal angle $\phi_1 = 0$. We also consider a small recoil (azimuthal) angle, ϵ (positive or negative), of the hard outgoing partons, due to the emission of soft gluons. We define p_t as the transverse momentum of the outgoing hard partons ($p_t = p_{t,1} \approx p_{t,2}$ to NLL accuracy).

The azimuthal angle of a jet in the "E_t-weighted scheme" is defined by [14, 15]:

$$\phi_{\rm jet} = \frac{\sum_{i\in{\rm jet}} E_{t,i}\phi_i}{\sum_{i\in{\rm jet}} E_{t,i}}\,, \tag{6.2.2}$$

where the sum runs over all final-state particles inside the jet with $E_{t,i}$ and ϕ_i being the transverse energy and azimuthal angle of the $i^{\rm th}$ particle as defined above. At leading order we have two back-to-back hard jets in the final state. Thus $\Delta\phi \equiv |\pi - \delta\phi_{\rm jets}| = 0$.

Thus we write the azimuths of the leading outgoing jets, in the soft and/or collinear regime, as:

$$\phi_{\rm jet1} \approx \sum_{i\in{\rm jet1}} k_{t,i}\,\phi_i/p_t, \tag{6.2.3}$$

$$\phi_{\rm jet2} \approx \pi + \sum_{i}^{n} k_{t,i}\sin\phi_i/p_t + \sum_{j\in{\rm jet2}} k_{t,j}(\phi_j-\pi)/p_t, \tag{6.2.4}$$

where we use $\epsilon \approx -\sum_i^n k_{t,i}\sin\phi_i/p_t$, which is sufficient for NLL accuracy. Hence the observable we study has the following approximation (in the soft and/or collinear region):

$$\begin{aligned}\Delta\phi &= |\pi - \delta\phi_{\rm jets}|\,,\\ &= \left|\sum_i \frac{k_{t,i}}{p_t}\left(\sin\phi_i - \theta_{i1}\phi_i - \theta_{i2}(\pi-\phi_i)\right)\right|,\end{aligned} \tag{6.2.5}$$

where $\theta_{ij} = 1$ if particle i is clustered to jet j and is zero otherwise.

In the next section we discuss the definition of the observable with respect to the axes defined by the outgoing legs. This will help us confirm the continuous globalness of the observable, compare our predictions with CAESAR [111] and determine the radiator (see appendix B).

6.2.1 Globalness of the observable

A "continuously global" observable [21, 22, 47, 111] (V) is one that satisfies, for the emission of a single soft and collinear gluon to an external leg (l) ($l = \{0,1,2\}$),

$$\frac{\partial \ln V(k_t^{(l)},\phi^{(l)},\eta^{(l)})}{\partial \ln k_t^{(l)}} = a_0, \tag{6.2.6}$$

where $k_t^{(l)}$, $\phi^{(l)}$ and $\eta^{(l)}$ are the transverse momentum, azimuthal angle and rapidity of the emission with respect to leg (l). Here a_0 represents the power of k_t in the observable definition with respect to the incoming leg "0".

To show that our observable is continuously global we write its definition in terms of the variables k_t, η and ϕ with respect to the legs "0", "1" and "2". To do so we introduce a rotation about the y-axis of the Breit frame (or hadronic centre-of-mass frame) and write the components of the vector $\mathbf{k}$ (three-momentum of the gluon) in the rotated frame, in which the $+z$-axis becomes parallel to the three-momentum of leg (l). The rotation angle is θ_l in the $x-z$ plane, where θ_l is the angle between the $+z$-axis and the three-momentum of leg (l). Thus we can write:

$$\begin{pmatrix} k_t \cos\phi \\ k_t \sin\phi \\ k_t \sinh\eta \end{pmatrix} = \begin{pmatrix} \cos\theta_l & 0 & -\sin\theta_l \\ 0 & 1 & 0 \\ \sin\theta_l & 0 & \cos\theta_l \end{pmatrix} \begin{pmatrix} k_t^{(l)} \cos\phi^{(l)} \\ k_t^{(l)} \sin\phi^{(l)} \\ k_t^{(l)} \sinh\eta^{(l)} \end{pmatrix}. \tag{6.2.7}$$

From this we arrive at:

$$k_t = k_t^{(l)} \sqrt{\left[\cos\theta_l \cos\phi^{(l)} - \sin\theta_l \sinh\eta^{(l)}\right]^2 + \left[\sin\phi^{(l)}\right]^2}, \tag{6.2.8}$$

$$\begin{aligned} \sin\phi &= \frac{\sin\phi^{(l)}}{\sqrt{\left[\cos\theta_l \cos\phi^{(l)} - \sin\theta_l \sinh\eta^{(l)}\right]^2 + \left[\sin\phi^{(l)}\right]^2}} \\ &= \frac{\cosh\eta_l \sin\phi^{(l)} / \sinh\eta^{(l)}}{\sqrt{\left[1 - \sinh\eta_l \cos\phi^{(l)} / \sinh\eta^{(l)}\right]^2 + \left[\cosh\eta_l \sin\phi^{(l)} / \sinh\eta^{(l)}\right]^2}}. \end{aligned} \tag{6.2.9}$$

Thus we deduce that for a soft and collinear emission to the incoming leg ("0") we have in the E_t-weighted scheme[1]:

$$\Delta\phi^{(0)} = k_t^{(0)} / p_t \left|\sin\phi^{(0)}\right|, \tag{6.2.10}$$

while for a soft and collinear emission to legs "1" and "2" we have:

$$\Delta\phi^{(1),(2)} \simeq \frac{2}{3} k_t^{(1),(2)} / p_t \cosh^2(\eta_{1,2}) \exp(-2\eta^{(1),(2)}) \left|\sin^3\phi^{(1),(2)}\right|, \tag{6.2.11}$$

where η_l is the rapidity of leg (l) with respect to the z-axis. Thus eq. (6.2.6) is satisfied.

[1]Eqs. (6.2.10) and (6.2.11) are useful in determining the "radiator" for the resummed result [111] (see appendix B). They can also be used to implement our observable into CAESAR [111] (see later).

The above implies that the observable in the E_t-weighted scheme is continuously global. This means that no non-global component is present and the resummed result to NLL accuracy has no dependence on the jet algorithm [47]. This is the recombination scheme used by the H1 collaboration to measure this observable [32]. However if one employs a recombination scheme in which the four-momentum of the jet is defined by the addition of four-momenta of particles in the jet, then our observable becomes non-global. In this case one would need to calculate the additional non-global component as well as the dependence on the jet algorithm. The DØ collaboration employed the latter recombination scheme to measure the observable [30, 31].

In the next section we perform a resummation to NLL accuracy. We specify to the DIS case and generalise our results to hadronic collisions in a later section. We also assume the jets are recombined using the E_t-weighted scheme.

6.3 Factorisation and resummation

To calculate the resummed distribution we begin by factorising the integrated distribution for events with $\Delta\phi < \Delta$ for some Δ as follows:

$$\Sigma(\Delta) \equiv \int_0^{\Delta} \frac{d\sigma}{dx\, dQ^2\, d\Delta\phi} d\Delta\phi = \sum_{a=q,g} \int d\mathcal{B}\sigma_{\mathcal{B}}^a \sum_n \int dP_n^a \left[\theta\left(\Delta - \Delta\phi\right) - 1\right], \quad (6.3.1)$$

from which the differential distribution $d\sigma/(dx\, dQ^2\, d\Delta\phi)$ can be obtained by differentiation at $\Delta = \Delta\phi$. In eq. (6.3.1) the term (-1) accounts for the virtual corrections contribution, dP_n^a is the differential probability of the classical independent emission of n gluons in the soft and collinear regime with an incoming parton a ($a = q$ for quark and $a = g$ for gluon), where for the case $q \to qg$, with g being leg "2" [51, 52, 53, 80]:

$$dP_n^q = \frac{1}{n!} \prod_i^n \frac{dk_{t,i}}{k_{t,i}} d\eta_i \frac{d\phi_i}{2\pi} \frac{N_c}{2} \left(w_{02}(k_i) + w_{12}(k_i) - \frac{1}{N_c^2} w_{01}(k_i) \right), \quad (6.3.2)$$

and for the case $g \to q\bar{q}$:

$$dP_n^g = \frac{1}{n!} \prod_i^n \frac{dk_{t,i}}{k_{t,i}} d\eta_i \frac{d\phi_i}{2\pi} \frac{N_c}{2} \left(w_{02}(k_i) - \frac{1}{N_c^2} w_{12}(k_i) + w_{01}(k_i) \right), \quad (6.3.3)$$

with:

$$w_{kj}(k) = \frac{\alpha_s(k^2_{\perp,k,j})}{2\pi} 2k_t^2 \frac{p_k.p_j}{k.p_k\, k.p_j}. \tag{6.3.4}$$

In eqs. (6.3.2) and (6.3.3) $k_{\perp,k,j}$ is the invariant transverse momentum of the emission with respect to the dipole in consideration. In fact $k^2_{\perp,k,j} = 4k_t^2/w_{kj}(k)$ for the dipole "kj".

In eq. (6.3.1) $\sigma^a_{\mathcal{B}}$ is the Born cross-section for the production of two hard partons in DIS with an incoming parton a. It is given by[2]:

$$d\mathcal{B}\sigma^q_{\mathcal{B}} = \sum_{\delta=T,L} \frac{2\pi\alpha^2_{\rm em}}{Q^4} \frac{\alpha_s(\mu_r)}{2\pi} \frac{d\xi}{\xi} dz C_F \varphi_\delta(y) C_{\delta,q}(\xi, z, E_{\rm min}) q\left(\frac{x}{\xi}, \mu_f^2\right), \tag{6.3.5}$$

$$d\mathcal{B}\sigma^g_{\mathcal{B}} = \sum_{\delta=T,L} \frac{2\pi\alpha^2_{\rm em}}{Q^4} \frac{\alpha_s(\mu_r)}{2\pi} \frac{d\xi}{\xi} dz T_f \varphi_\delta(y) C_{\delta,g}(\xi, z, E_{\rm min}) g\left(\frac{x}{\xi}, \mu_f^2\right), \tag{6.3.6}$$

where all the variables and constants have the same meaning as those defined in section 2.3 and μ_r and μ_f are the renormalisation and factorisation scales, which we chose to equal either Q or p_t. The index δ denotes the transverse and longitudinal pieces and the functions $\varphi_\delta(y)$ are given by:

$$\varphi_T(y) = 1 + (1-y)^2, \tag{6.3.7}$$

$$\varphi_L(y) = 2(1-y). \tag{6.3.8}$$

In eq. (6.3.5) and (6.3.6) we only consider events with $p_t > E_{\rm min}$, with $E_{\rm min}$ being some cut-off scale, so the coefficient functions have an explicit dependence on $E_{\rm min}$ through the theta function $\theta(p_t - E_{\rm min})$, with $p_t = Q\sqrt{z(1-z)(1-\xi)/\xi}$.

We factorise the theta function by introducing the transformation:

$$\theta\left(\Delta - \Delta\phi\right) = \frac{1}{\pi}\int_{-\infty}^{+\infty} \frac{db}{b} \sin(b\Delta) \prod_i^n \exp\left(ib\frac{k_{t,i}}{p_t}\left[\sin\phi_i - \theta_{i1}\phi_i - \theta_{i2}(\pi - \phi_i)\right]\right). \tag{6.3.9}$$

Thus the resummed result is given by:

$$\Sigma(\Delta) = \int d\mathcal{B}\sigma_{\mathcal{B}} \frac{1}{\pi}\int_{-\infty}^{+\infty} \frac{db}{b} \sin(b\Delta) \exp(-R(\bar{b})), \tag{6.3.10}$$

where we suppressed the index a (the radiator explicitly depends on the index a),

[2]This is presented in detail in subsection 2.3.2.

and (to NLL accuracy) [75]:

$$\begin{aligned} R &= -\int dP \left[\exp\left(ib\frac{k_t}{p_t}\left|\sin\phi - \theta_1\phi - \theta_2(\pi-\phi)\right|\right) - 1\right], \\ &= \int dP\theta\left(k_t - \frac{p_t}{\alpha\bar{b}}\right), \end{aligned} \tag{6.3.11}$$

where $\alpha = |\theta_1\phi + \theta_2(\pi-\phi) - \sin\phi|$, with $\theta_j = \theta\left(R^2 - (\eta-\eta_j)^2 - (\phi-\phi_j)^2\right)$, and $\bar{b} = |b|e^{\gamma_E}$. Hence for the b integral we can replace $\int_{-\infty}^{+\infty} \to 2\int_0^{+\infty}$.

We present the result for the radiator and the expansion of the resummed result to $\mathcal{O}(\alpha_s^2)$ in appendix B. Furthermore, to account for the contribution of hard collinear emissions to the incoming leg we evolve the PDFs as described in appendix B, which results in the substitutions: $q_a(x/\xi, \mu_f^2) \to q_a(x/\xi, \mu_f^2/\bar{b}^2)$ (where $q_q(x,\mu_f^2) = q(x,\mu_f^2)$ and $q_g(x,\mu_f^2) = g(x,\mu_f^2)$). Thus the Born weight $\sigma_{\mathcal{B}}$ becomes explicitly dependent on b and we move it inside the b integral. We also rescale $\bar{b} \to b$ such that we write the result as:

$$\Sigma(\Delta) = \int d\mathcal{B}\frac{2}{\pi}\int_0^{+\infty}\frac{db}{b}\sigma_{\mathcal{B}}(\mu_f^2/b^2)\sin(b\overline{\Delta})e^{-R(b)}, \tag{6.3.12}$$

with $\overline{\Delta} = \Delta e^{-\gamma_E}$.

6.4 Result in Δ space

In contrast to Q_t distributions (such as that we studied in chapter 4) the result in Δ space, evaluated using the saddle point method, has a divergence at $R'(1/\Delta) = 1$ of the same nature to that we discussed in subsection 4.3.1 (see appendix B for the derivative of the radiator). This corresponds to a quite high value of Δ (for the illustrative value of $Q/p_t = 6$ and for an incoming gluon we arrive at $\Delta \sim 0.13$) and thus the result in this way is not suitable for phenomenological purposes. We remind the reader that in section 4.3.1 we found that the divergence for the Q_t distribution occurs at $R'(Q/Q_t) = 2$ (which corresponds to a very small value of Q_t). This enabled most of the Q_t range to be safely studied.

An alternative approach which we highlighted in section 4.3 can be used in this case, that is to evaluate the b integral numerically. As we already pointed out in section 4.3 the radiator has a Landau pole singularity which can be overcome by

making the replacement $b \to b^* = b/\sqrt{1+b^2/b_{\rm lim}^2}$ in both the radiator and PDFs, where we choose $b_{\rm lim} = \mu_f/Q_0$, with Q_0 being a cut-off scale[3]. Furthermore we freeze the radiator for values of b^* below "1", i.e. we evaluate the integral over b from 0 to $b_{\rm min}$, where $b_{\rm min} = b_{\rm lim}/\sqrt{b_{\rm lim}^2 - 1}$, freezing the radiator at the value "0", and then integrate over b from $b_{\rm min}$ up to $b_{\rm max}$, where $b_{\rm max} = \exp(1/(2\beta_0\alpha_s(\mu_r^2)))$, using the full expression for the radiator.

Thus we can write the expression to be used in the numerical code as follows:

$$\Sigma(\Delta) = \int d\mathcal{B}\left(\sigma_{\mathcal{B}}(\mu_f^2)\frac{2}{\pi}\mathrm{Si}(\overline{\Delta}b_{\rm min}) + \frac{2}{\pi}\int_{b_{\rm min}}^{b_{\rm max}}\frac{db}{b}\sin(b\overline{\Delta})\sigma_{\mathcal{B}}(\mu_f^2/b^{*2})e^{-R(b^*)}\right), \quad (6.4.1)$$

with Si being the "sin integral" function, defined by $\mathrm{Si}(x) = \int_0^x \sin(t)/t\, dt$.

6.5 Matching

For an ideal matching one would need to compute the fixed-order result for the distribution analytically in order to obtain the constant coefficients $\boldsymbol{C}_1^q$ and $\boldsymbol{C}_1^g$ (in analogy to the constant term $\boldsymbol{C}_1$ for the Q_t distribution, which is presented in appendix A.1). The resummed result would then be given by eq. (6.4.1) with the replacement (after restoring the index a):

$$\sigma_{\mathcal{B}}^a(\mu_f^2/b^{*2}) \to \sigma_{\mathcal{B}}^a(\mu_f^2)\frac{\boldsymbol{C}_0^{\,a}\otimes\boldsymbol{q}(x/\xi,\mu_f^2/b^{*^2}) + \alpha_s(\mu_r)/(2\pi)\,\boldsymbol{C}_1^{\,a}\otimes\boldsymbol{q}(x/\xi,\mu_f^2)}{q_a(x/\xi,\mu_f^2)}, \quad (6.5.1)$$

where the matrices $\boldsymbol{C}_0^{\,a}$ are presented in appendix B.4.2, and for $\sigma_{\mathcal{B}}^a(\mu_f^2)$ we just set $b^* \to 1$ in eq. (6.5.1).

Currently the leading-order analytical result is not available. It is only possible to obtain the term $C_1 = C_1^q + C_1^g$, where:

$$C_1^a = \int d\mathcal{B}\sigma_{\mathcal{B}}^a(\mu_f^2)\frac{\boldsymbol{C}_1^{\,a}\otimes\boldsymbol{q}(x/\xi,\mu_f^2)}{q_a(x/\xi,\mu_f^2)}, \quad (6.5.2)$$

from NLOJET++ by subtracting the logarithms at $\mathcal{O}(\alpha_s)$. For optimal results of the matching we would need to separate the quark and gluon channel contributions to C_1 (i.e. calculate or extract C_1^q and C_1^g) in order to write the resummed result using

[3]We choose Q_0 such that the scale of PDFs (μ_f/b^*) is always above the minimum required by the PDF data set we use (CTEQ6M [112]), $Q_0 = 1$GeV.

eq. (6.5.1) (which affects $\mathcal{O}(\alpha_s^2 \ln^2(1/\Delta))$ terms in the expansion of the resummed result).

The matching is complicated not only by not having a fixed-order analytical result, but also by not having an analytical NLL resummed result in Δ space. Both these problems were overcome when we studied the Q_t distribution in chapter 4, however here we do encounter both these difficulties. In fact for the dijet azimuthal correlation distribution a decent matching would need to be carried out in b space rather than Δ space, which means the matching would also need to be performed numerically.

Since we do not have an analytical fixed-order result we combine the resummed result to NLOJET++ results in Δ space in the following way[4]:

$$\Sigma_{\text{mat}}(\Delta) = \Sigma(\Delta)\left[1 + \left(\Sigma_e^{(1)} - \Sigma_r^{(1)}\right)/\Sigma_0\right] + \left(\Sigma_e^{(2)} - \Sigma_r^{(2)}\right)\widetilde{\Sigma}(\Delta), \tag{6.5.3}$$

where now the result has a form similar to that in eq. (3.4.1). Here $\Sigma(\Delta)$ is the resummed result, $\Sigma_r^{(1)}$ and $\Sigma_r^{(2)}$ are the first and second order terms in the expansion of the resummed result and Σ_0 is the Born cross-section. Expressions for Σ_0, $\Sigma_r^{(1)}$ and $\Sigma_r^{(2)}$ are presented in appendix B.4.2. Here $\Sigma_e^{(1)}$ and $\Sigma_e^{(2)}$ are the first and second order coefficients of the NLOJET++ predictions for the integrated distribution. The form-factor $\widetilde{\Sigma}$ is given by:

$$\widetilde{\Sigma}(\Delta) = \left(\sum_a \int d\mathcal{B}\sigma_{\mathcal{B}}^a \exp[-R_{\text{DL}}^a(1/\Delta)]\right)/\Sigma_0, \tag{6.5.4}$$

with R_{DL} being the double logarithmic piece of the radiator which is presented in appendix B.4.2 (with the substitution $\bar{b} \to 1/\Delta$). Once again the introduction of this form-factor is ad-hoc and only affects our result at subleading accuracy. Its role here is analogous to that for the Q_t distribution we presented in chapter 4, that is to eliminate the effect of subleading $\mathcal{O}(\alpha_s^2 L)$ terms, which we do not control, at small Δ. Furthermore since we do not account for the coefficients C_1^q and C_1^g, the $\mathcal{O}(\alpha_s^2 L^2)$ terms are not fully controlled[5]. However these terms are also suppressed by the form-factor.

[4]The matching to NLOJET++ we provide here can be improved by separating quark and gluon channel contributions. We leave this for our forthcoming work [38].

[5]In chapter 4 we controlled all $\mathcal{O}(\alpha_s^2 L^2)$ terms since we computed the term $\boldsymbol{C}_1$.

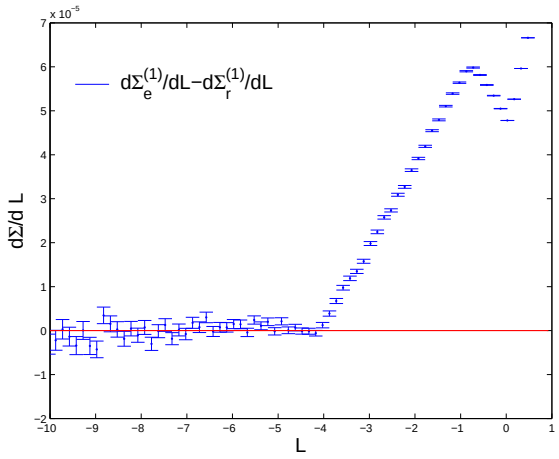

Figure 6.1: Subtraction of the logarithms from NLOJET++ predictions. The difference $d(\Sigma_e^{(1)} - \Sigma_r^{(1)})/d\ln\Delta$ tends to zero when $\Delta \to 0$. This indicates an agreement between our results and NLOJET++ predictions.

6.6 Results and discussion

In this section we present a result for the matched distribution and discuss the theoretical uncertainties in our prediction.

In fig. 6.1 we present a comparison between the terms $d\Sigma_e^{(1)}/dL$ and $d\Sigma_r^{(1)}/dL$, where $L = \ln(\Delta)$. We notice that there is an agreement between NLOJET++ predictions and our results at small Δ (since the difference vanishes), indicating that the terms H_{11} and H_{12}, which respectively represent the coefficients of $\ln(1/\Delta)$ and $\ln^2(1/\Delta)$ in the expansion of the resummed result to $\mathcal{O}(\alpha_s)$ (see appendix B.4.2), agree with those in NLOJET++ results. Thus the subtraction $\Sigma_e^{(1)} - \Sigma_r^{(1)}$ contains no logarithmic dependence and (formally) tends to the constant $\alpha_s/(2\pi)C_1$ when $\Delta \to 0$.

We also note that all the coefficients of logarithms that we control (H_{11}, H_{12}, H_{23} and H_{24}, which are presented in appendix B.4.2) have been checked against those predicted by CAESAR [111] and we have an agreement. We did not however consider the computation of the resummed result using CAESAR since (as we stated before) the divergence at $R' = 1$ (using the saddle point method, which is implemented by CAESAR) corresponds to a high value of Δ.

In fig. 6.2 we present our results for the matched result compared to NLO-

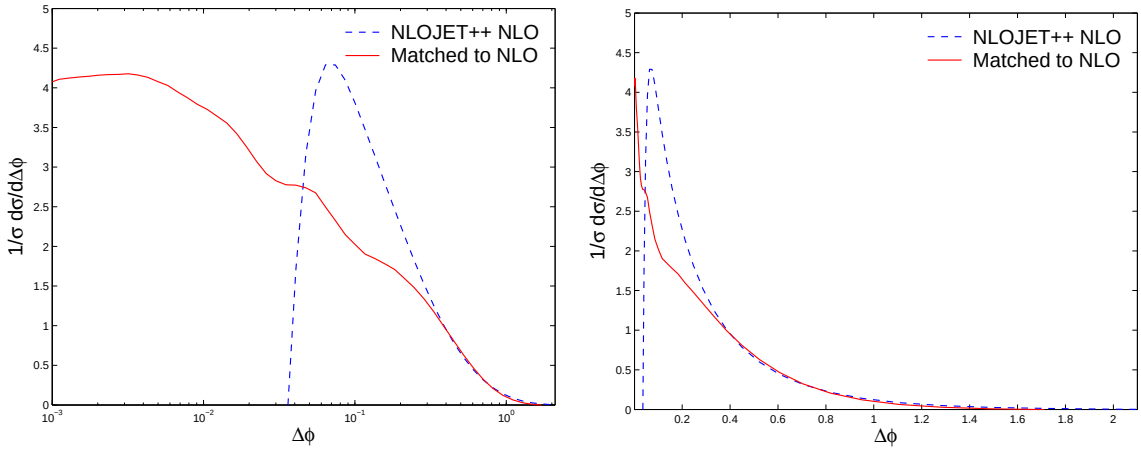

Figure 6.2: Preliminary matched-resummed result compared to the NLO prediction. CTEQ6M [112] PDFs are used.

JET++ predictions. We plot the differential distribution $1/\sigma\, d\sigma/d\Delta\phi$, which is normalised to the total NLO cross-section σ. The differential distribution is obtained by differentiating $\Sigma(\Delta)$ at $\Delta = \Delta\phi$ (see eq.(6.3.1)). The NLO result diverges when $\Delta\phi \to 0$, while the matched result tends to a constant. The difference between the matched and resummed result at small $\Delta\phi$ is a constant factor, which amounts to $\Sigma_{\rm mat} \approx (1 + \alpha_s/(2\pi)C_1)\Sigma$. The results here were obtained using: $Q = 20$ GeV, $\mu_r = \mu_f = Q$, $E_{\rm min} = 5$GeV, $x = 0.01$ and $|\eta_{1,2}| < 1$.

The matching prescription we presented above results in some theoretical uncertainties. The most significant one is the lack of knowledge about the terms C_1^q and C_1^g since we do not control all the $\mathcal{O}(\alpha_s^2 L^2)$ logarithms in the expansion of the resummed result. In addition we have uncertainties associated with factorisation and renormalisation scales, fixed higher-order corrections (due to large differences between leading and next-to-leading order results) and the numerical b-space integration. We leave the analyses of these issues for our forthcoming work [38].

6.7 Dijet azimuthal correlations in hadronic collisions

We report below the result for the dijet azimuthal correlation distribution in hadronic collisions. This has been measured at DØ using the jet recombination scheme in

which the four-momentum of a jet is obtained by the sum over the four-momenta of particles in the jet [30, 31] (we refer to this scheme as the "four-momentum" scheme). Here we report the result which uses eq. (6.2.2) and briefly discuss the result in the other scheme.

In the "E_t-weighted" scheme the observable $\Delta\phi$ has exactly the same expression as that in the DIS case (i.e. eq. (6.2.5)). The resummed result is given by [111]:

$$\Sigma(\Delta) = \int d\widetilde{\mathcal{B}} \frac{2}{\pi} \int_0^\infty \frac{db}{b} \widetilde{\sigma}_{\mathcal{B}}(\mu_f^2/b^2) \sin(b\overline{\Delta}) e^{-\widetilde{R}(b)} \mathcal{S}(b)\,, \tag{6.7.1}$$

where $\widetilde{\sigma}_{\mathcal{B}}(b)$ is the Born cross-section for the production of two hard partons in hadronic collisions, which also contains PDFs from both incoming legs evolved to μ_f^2/b^2, and $d\widetilde{\mathcal{B}}$ is the corresponding phase-space. We have suppressed the sum over various channels. Here $\widetilde{R}$ is the radiator and is presented in eq. (B.4.15) in appendix B. The function $\mathcal{S}$ is given by:

$$\mathcal{S}(b) = \mathrm{Tr}[\mathbf{H} e^{-\zeta(\lambda)\mathbf{\Gamma}^\dagger} \mathbf{S} e^{-\zeta(\lambda)\mathbf{\Gamma}}]/\mathrm{Tr}(\mathbf{HS})\,, \tag{6.7.2}$$

where $\mathbf{H}$, $\mathbf{\Gamma}$ and $\mathbf{S}$ are the hard, anomalous dimension and soft matrices. These depend on the kinematics of the process [57, 58, 59, 60]. The matrices $\mathbf{H}$ and $\mathbf{S}$ are identical to those we presented in section 3.5. The matrix $\mathbf{\Gamma}$ contains integrations over directions in the entire phase-space, as apposed to those in section 3.5, which are performed in a limited region of the phase-space. Here the matrix $\mathbf{\Gamma}$ has the form given in eq. (3.5.12) but with:

$$S = 0, \tag{6.7.3}$$

$$T = \ln \frac{-\hat{t}}{\hat{s}} + i\pi, \tag{6.7.4}$$

$$U = \ln \frac{-\hat{u}}{\hat{s}} + i\pi, \tag{6.7.5}$$

with $\hat{s}$, $\hat{u}$ and $\hat{t}$ being the Mandelstam variables which are defined just after eq. (3.5.5). In eq. (6.7.2) the single logarithmic function $\zeta(\lambda)$ (with $\lambda = \alpha_s(Q^2)\beta_0 \ln(b)$) accounts for soft wide-angle emissions and is presented in eq. (B.4.12) in appendix B.

We can further our study by looking at the hadronic collisions case using the same jet definition as that used by the DØ collaboration ("four-momentum" scheme). Here

the four-momentum of a jet is given by:

$$p^{\mu}_{\text{jet}} = \sum_{i \in \text{jet}} p^{\mu}_{i}, \tag{6.7.6}$$

where the sum runs over the four-momenta of all particles in the jet. Thus:

$$\Delta\phi \approx \sum_{i \notin \text{outgoing jets}} k_{t,i} \sin\phi_i / p_t, \tag{6.7.7}$$

where the sum runs over particles which are not clustered to the outgoing jets. Hence the observable in this scheme is non-global and the analysis of the resummed result, to NLL accuracy, requires the inclusion of the non-global component in addition to the impact of the k_t algorithm on the resummation, similar to that we discussed in chapter 5.

Both of these components are currently not available. However the current indication is that the effect of these pieces may not be significant [20, 113], particularly since these pieces contain only single logarithms while the distribution is dominated by double logarithms originating from soft and collinear emissions to the incoming legs. In any case one could estimate these components preliminarily in a similar way to that we presented in section 5.5. We leave this to our forthcoming work.

6.8 Conclusions

In the present chapter we have, for the first time, dealt with the resummation of the dijet azimuthal correlation distribution both in DIS and hadronic collisions to NLL accuracy. We used the "E_t-weighted" scheme to define the azimuths of the final-state particles, which lead to the simplification of the calculation since the observable is global in this case. However in the "four-momentum" scheme the observable is non-global and formally the resummation is not complete to NLL accuracy. The full estimate of the resummed result in the latter case is an avenue for future work.

We have also provided a matched result to fixed-order NLO predictions using NLOJET++. We found an agreement between our resummed prediction expanded to first order in α_s and NLOJET++ results. There is also an agreement between the coefficients of the logarithms we control and those estimated by the CAESAR program. The matching we provided here can be improved by separating the incoming

quark and gluon channel contributions to the term we referred to as C_1. We leave this for our forthcoming work.

Another step one can take towards more accurate predictions for this observable is to study the non-perturbative effects, which are expected to be of the "intrinsic k_t" type. Furthermore the sensitivity to small-x effects may be present and this observable forms a good testing ground for these effects.

In addition to being a means towards better understanding of the resummation of jet-defined quantities, the analysis we carried out here should enable, in the near future, the comparison of our predictions with data and other approaches, such as that of ref. [35] which implements unintegrated PDFs.

In the next chapter we study the power corrections to the energy flow distribution in hadronic collisions.

Chapter 7

Aspects of power corrections in hadron-hadron collisions

7.1 Introduction

The principle issue that limits the accuracy of theoretical predictions in QCD is the presence of non-perturbative physics responsible for the confinement of quarks and gluons (hadronisation). The success of perturbative QCD, despite a lack of quantitative understanding of the confinement process, is a major achievement that is based on identifying infrared and collinear-safe observables [72] which are as insensitive as possible to non-perturbative effects such as hadronisation. In such instances the role of non-perturbative hadronisation effects is reduced to the level of corrections to the perturbative estimates which take the form of an inverse-power law in the hard scale Q, $1/Q^p$, where p depends on the observable. For some observables, such as the total cross-section in e^+e^- annihilation to jets, where $p = 4$, the corrections in question are insignificant and can safely be ignored in comparisons to data. For other observables such as event-shape variables [46, 47] it was noted however, as we stated before, that the power corrections scale as $1/Q$ and obscure the perturbative analysis significantly.

Over the past decade, theoretical efforts essentially based on renormalons (see ref. [81] and references therein) have given a clearer picture of the origin and role of power corrections. Within the renormalon model these corrections are shown to be

related to a factorial divergence of the perturbative QCD expansion at high orders and the consequent error in truncating what is in fact an asymptotic series [81]. This observation allows one to estimate power corrections from a lowest-order Feynman graph, modified to incorporate the relevant subset of higher-order terms (renormalon bubble insertions).

From a phenomenological viewpoint the most widely used formulation of the renormalon model is one that uses a dispersive representation of the running coupling [44], thereby introducing a dispersive variable m that plays the role of a fake gluon mass. This scale is a natural trigger for power corrections arising in the infrared regime for observables that are otherwise dominated by a hard scale Q. The most appealing feature of the dispersive approach is the hypothesis of a universal infrared-finite coupling $\alpha_{\rm eff}$. The size of the power corrections in this approach are governed by moments of this universal coupling: $\int_0^{+\infty} dm^2/m^2 \alpha_{\rm eff}(m^2)(m^2/Q^2)^p$. For most event-shape variables (for example) $p = 1/2$ [46], and the relevant coupling moment or equivalently the related quantity α_0 (which we introduced in section 3.6) has been extracted from data for different event shapes in both e^+e^- annihilation and DIS [42, 43]. The values of α_0 thus obtained have generally confirmed the universality hypothesis to within the expected uncertainties due to missing higher-order corrections [46]. These studies have not only enabled successful studies of several observables, but also lent credence to the notion that the QCD coupling may be a meaningful (finite and universal) concept all the way down to the smallest energy scales, and have thus renewed hope of a better understanding of the confinement domain from first principles of QCD.

The successes of renormalon-inspired studies have thus far been limited to observables which involve just two hard partons at Born level such as event shapes in $e^+e^- \to$ two jets and DIS $(1+1)$ jets. Some of the most interesting QCD observables however do not fall into the above class. Examples include three-jet event shapes in e^+e^- annihilation and DIS [51, 52, 53, 54], dijet event shapes in hadron collisions [114] and single-jet inclusive cross-sections at hadron colliders [55]. These observables contain more than two hard partons at Born level and additionally pertain to processes that have gluons at Born level where one may question the extension

of the dispersive approach, which (strictly speaking) was formulated for observables involving only quarks at the Born level [81]. The program of understanding power corrections has not been put to test in such situations which will be of importance at the LHC, for instance, although some progress is being made on the phenomenological side for three-jet event shapes [54]. In fact for the case of observables involving four hard partons at the Born level there are as yet no complete theoretical predictions for power corrections.

Applying the renormalon model, in many such cases, reduces (as for e^+e^- annihilation to jets or DIS event shapes) to an analysis of soft gluon radiation with transverse momenta $k_t \sim \Lambda_{\rm QCD}$, which are associated with a universal infrared-finite coupling. Given the rich structure (colour and geometry-dependence) of soft gluon radiation for processes like dijet production in hadron collisions, it is indeed enticing to see how a perturbative structure may influence predictions for power corrections as predicted by the renormalon model. Signs of perturbatively calculable colour structure in the non-perturbative power-behaved component would strongly suggest that the renormalon-inspired picture of these corrections is an extension of soft gluon radiation, with a modified but universal coupling, thereby conclusively establishing the model.

In this chapter we provide a calculation of the power correction to the transverse energy (E_t) flow away from jets accompanying hard dijet production in hadron collisions. A variant of this observable (the "pedestal" height) was suggested several years ago by Marchesini and Webber as a means of separating perturbative bremsstrahlung from the contribution of the soft underlying event in hadron collisions [107]. To date however a satisfactory understanding of the away-from-jet energy flow has proved elusive. In the region of small E_t the distribution $d\sigma/dE_t$ contains large logarithms of the form $\alpha_s^n \ln^{n-1}(P_t/E_t)/E_t$, where P_t is the hard scale (jet transverse momenta) of the problem. As we mentioned in earlier chapters, these logarithms can only be resummed in the large N_c limit [21, 22, 76] which limits the accuracy of perturbative estimates that can be made in this case alongside the lack of any estimates of the NLL contributions. One may also expect power corrections of the form $1/P_t$ to the resummed distribution as for the case of event-shape distributions in e^+e^- annihila-

tion and DIS. Once again there is no estimate for these power corrections and it is this that we aim to provide here. Combining the power corrections we compute with resummed E_t flow distributions gives a more complete theoretical account which should facilitate comparisons to experiment.

While at hadron colliders the ever-present soft underlying event may obstruct clean studies of power-behaved corrections arising from the bremsstrahlung component of the E_t flow, our calculations here are also easily adapted to the case of rapidity gaps in dijet photoproduction at HERA, and are in principle more readily tested in that environment. Moreover there are theoretical ideas concerning observables such as inclusive jet cross-sections at hadron colliders, where it may be possible to disentangle the underlying event from the non-perturbative physics in the bremsstrahlung component, due to a singular $1/R$ (R being a jet radius parameter) behaviour of the latter [55]. A full estimate of this piece however involves a calculation similar to the one we introduce here and thus the present calculations can be used as a guide in moving towards better estimates of the inclusive jet cross-sections as well. Another related class of observables, to which the techniques we use here are directly applicable, is the important case of event shapes at hadronic colliders [114]. Resummed perturbative estimates already exist for these quantities and identical considerations to those of this chapter will be required when dealing with the issue of power corrections. While other problems such as lack of knowledge about next-to-leading logarithms also need to be addressed, the calculation of the power correction is ultimately an important ingredient which, as we stressed above, also serves as a case study for hadron-hadron observables more generally.

This chapter is organised as follows. In the following section we define the observable more precisely and review the perturbative result in Mellin space conjugate to E_t, which involves colour matrices in the resummed anomalous dimensions [57, 58, 59, 60]. We then compute the power correction to each of the matrix elements of the anomalous dimension by considering the appropriate combination of dipoles involved in that matrix element. The calculation of the power correction in each dipole term is performed using the appropriate scale of the running coupling (the invariant transverse momentum of the dipole, $k_\perp$ [51, 52, 53, 79]). The final step

is to take the inverse Mellin transform of the result, for which it proves convenient to diagonalise the power-corrected anomalous dimension matrices. We find that the power correction to the E_t distribution is not a simple shift of the resummed distribution by a fixed amount proportional to $1/P_t$ as is the case for event shapes in $e^+e^- \to$ two jets and DIS (to a good approximation).

7.2 Resummed perturbative result

Here we outline the resummed result for the E_t flow distribution, specialising for simplicity (as in chapter 5) to the case of a slice in rapidity of width $\Delta\eta$, which we take to be centred at $\eta = 0$ (the rapidity η is defined with respect to the beam axis). The observable we compute is once again the distribution:

$$\Sigma(P_t, E_t) = \frac{1}{\sigma}\int_0^{E_t} \frac{d\sigma}{dE_t'} dE_t', \qquad E_t = \sum_{i\in\Omega} E_{t,i}, \tag{7.2.1}$$

where σ is the total cross-section for dijet production in hadronic collisions, Ω denotes the rapidity slice and E_t is obtained by summing over all objects (partons/jets) in the gap.

As we have stated many times now, the resummed prediction $\Sigma(P_t, E_t)$ up to SL accuracy (resumming all the terms $\alpha_s^n \ln^n(P_t/E_t)$), can be thought of as comprising two distinct pieces with different dynamical origins: global and non-global.

The global component, which we discussed at length in section 3.5, [21, 22] is a result of considering multiple soft emissions, both real and virtual, attached just to the primary or Born hard partons. Due to infrared-safety of the observable real and virtual emissions cancel below the scale E_t, while real emissions above this scale are vetoed. Thus the resummed result for this piece is just the summation of virtual graphs above the scale E_t, attached to the primary hard partons [57, 58, 59, 60]. In actual fact the factorisation of real emissions and the consequent cancellation with virtual ones takes place in Mellin space conjugate to E_t, analogous to that we presented in section 3.3. This complication can be ignored for the leading logarithmic terms, but to analyse the impact of power corrections on the resummed distribution we need to compute the result in Mellin space and then invert the transform to E_t

space. To be more precise the perturbative resummed result (considering just the global term for now) reads:

$$\Sigma(P_t, E_t) = \int \frac{d\nu}{2\pi i\nu} e^{\nu E_t} \mathcal{R}(\nu), \tag{7.2.2}$$

where ν is the Mellin variable conjugate to E_t and the integration contour is taken, in the usual manner, parallel to the imaginary axis and to the right of all singularities of the integrand. We have:

$$\mathcal{R}(\nu) = \mathrm{Tr}\left(\mathbf{H} e^{-\mathbf{\Gamma}^\dagger(\nu)} \mathbf{S} e^{-\mathbf{\Gamma}(\nu)}\right) / \Sigma_0. \tag{7.2.3}$$

In the above $\mathbf{\Gamma}$ is essentially an "anomalous dimension matrix" and $\mathbf{H}$ and $\mathbf{S}$ are the hard and soft matrices which we introduced in section 3.5 for the case $q\bar{q} \to q\bar{q}$. The matrix elements H_{ij} represent the product[1] of the Born amplitude in colour channel i and its complex conjugate in colour channel j, and the matrix $\mathbf{S}$ represents the normalisation arising from the colour algebra (i.e. the elements $c_i^*.c_j$, which we introduced in section 3.5). The squared matrix element for the Born scattering in this notation is just $\Sigma_0 = \mathrm{Tr}(\mathbf{HS})$. We shall return to the detailed structure of $\mathbf{\Gamma}$ in the next section.

We now turn to the second piece of resummed distribution: the non-global contribution. The above result, resumming essentially virtual corrections above the veto scale E_t which dress the hard scattering, is not the complete description at single-logarithmic accuracy [21, 22]. An additional non-global piece $\mathcal{S}(P_t, E_t)$, which is different than that in the two-jet case, arises (starting at the two-gluon emission level, $\mathcal{O}(\alpha_s^2)$) and is also single-logarithmic. The dynamical origin of this piece, as we explained in earlier chapters, is multiple soft energy-ordered radiation with an arbitrary complex geometry ("hedgehog" configurations of soft gluons, similar to that in fig 3.3, as opposed to emissions strongly ordered in angle). As we emphasised before, it has thus far been possible to treat this term only in the large N_c approximation, which limits the accuracy of perturbative calculations in the present instance.

However it has been pointed out and clarified in a series of papers [18, 19, 20, 108] (including the work we presented in chapter 5) that the role of the non-global com-

[1]This is analogous to $\mathcal{M}_j^\dagger \mathcal{M}_i$, with the colour-averaging factor $1/N_c^2$ and sum over spins, where $\mathcal{M}_i$ and $\mathcal{M}_j$ stand for the components of the vector $\mathbf{M}$ in eq. (3.5.3).

ponent can be significantly reduced by defining the observable in terms of soft jets rather than individual hadrons in the gap. This can be achieved by running a clustering algorithm on the final states such that all objects are included in jets. We have shown that the clustering procedure (with a large cluster radius $R = 1$) virtually eliminates the non global component while giving rise to additional global terms [20] that were at most modest corrections to the pure virtual dressing as represented here by eq. (7.2.3). Moreover the power corrections associated to the non-global component of the result would start at a higher-order in α_s (albeit potentially accompanied by logarithms of P_t/E_t) which we ignore. This was also the procedure employed for the case of non-global DIS event shapes [46], where power corrections were computed in the exponentiated single-gluon piece of the resummed distribution, which was a phenomenological success. For all these reasons we shall choose to concentrate for the rest of this chapter on the global component (eq. (7.2.3)), ignoring the non-global component.

In the following section we explicate the structure of $\mathbf{\Gamma}$ in terms of the various hard colour dipoles from which one considers soft gluons to be emitted according to the usual antenna pattern. Non-perturbative power corrections are then computed on a dipole-by-dipole basis, adapting the procedure for a $q\bar{q}$ dipole developed for the case of e^+e^- annihilation to two jets. Having obtained the power corrections to $\mathbf{\Gamma}(\nu)$ we then invert the Mellin transform to examine the result for the E_t distribution.

7.3 The anomalous dimension and power corrections

We first write down the structure of the resummed anomalous dimension matrix $\mathbf{\Gamma}(\nu)$ and then note that it contains an integral over the running coupling which is formally divergent. Making the ansatz of a universal infrared-finite coupling cures this divergence and introduces calculable power corrections to the perturbative anomalous dimensions. In what follows and for the rest of this chapter we specialise to the case of the sub-process $q\bar{q} \to q\bar{q}$ since identical considerations are involved for all other sub-processes.

First we summarise the results we obtained in section 3.5. For the sub-process $q\left(p_1,r_1\right)+\bar{q}\left(p_2,r_2\right)\rightarrow q\left(p_3,r_3\right)+\bar{q}\left(p_4,r_4\right)$, where p_i and r_i are respectively four-momenta and colour indices, we can choose to work in the t-channel singlet-octet colour basis:

$$c_1=\delta_{r_1r_3}\delta_{r_2r_4},\qquad c_2=\frac{1}{2}\left(\delta_{r_3r_4}\delta_{r_1r_2}-\frac{1}{N_c}\delta_{r_1r_3}\delta_{r_2r_4}\right). \tag{7.3.1}$$

For this basis we have:

$$\mathbf{S}=\begin{pmatrix} N_c^2 & 0 \\ 0 & \frac{N_c^2-1}{4} \end{pmatrix}, \tag{7.3.2}$$

and the anomalous dimension matrix $\mathbf{\Gamma}$ is:

$$\mathbf{\Gamma}=\begin{pmatrix} C_FT & \frac{C_F}{2N_c}(S-U) \\ S-U & C_FS-\frac{1}{2N_c}(T-2U+S) \end{pmatrix}. \tag{7.3.3}$$

In the above S, T and U are combinations of dipole contributions with each contribution given by the corresponding dipole antenna. Thus one has:

$$S = \tilde{w}_{12}+\tilde{w}_{34}, \tag{7.3.4}$$

$$T = \tilde{w}_{13}+\tilde{w}_{24}, \tag{7.3.5}$$

$$U = \tilde{w}_{23}+\tilde{w}_{14}, \tag{7.3.6}$$

where each dipole contribution $\tilde{w}_{ij}$ reads:

$$\tilde{w}_{ij}=\int\frac{d^3\vec{k}}{2\omega(2\pi)^3}g_s^2\frac{(p_i.p_j)}{(p_i.k)\,(p_j.k)}u(k_t,\nu). \tag{7.3.7}$$

In the above result we integrate the soft gluon emission probability, given by the dipole antenna pattern, over the gluon phase-space (with $\vec{k}$ and ω being respectively the three-momentum and energy of the gluon, as usual) with a "source" function $u(k_t,\nu)$ and $g_s^2=4\pi\alpha_s$. The source is a result of factorising the real soft emission phase-space in Mellin space (see for instance ref. [76]) and accounting additionally for virtual corrections:

$$u(k)=\left(1-e^{-\nu k_t}\right), \tag{7.3.8}$$

if the emission is in Ω and is zero elsewhere. The source thus represents the impact of real-virtual contributions which completely cancel, to our accuracy, for emissions

outside Ω. Now introducing the variables η and ϕ, respectively being the rapidity and azimuth of the emission with respect to the beam direction, one can write:

$$\tilde{w}_{ij} = \int \frac{dk_t}{k_t} \frac{\alpha_s(k^2_{\perp,i,j})}{2\pi} d\eta \frac{d\phi}{2\pi} \left(1 - e^{-\nu k_t}\right) f_{ij}(\eta, \phi), \tag{7.3.9}$$

with $f_{ij}(\eta, \phi)$ being the functional dependence on rapidity and azimuth that arises from the dipole antenna patterns and which we shall use below. We note that the argument of the running coupling for emission from a dipole is ([51, 52, 53, 79, 80]) $k^2_{\perp,i,j} = 2(p_i.k)(p_j.k)/(p_i.p_j)$, which is the transverse momentum of the gluon k with respect to the dipole axis in the dipole rest frame. This must be distinguished from k_t, the transverse momentum of the gluon with respect to the beam direction, which is the quantity that directly enters the observable definition. In fact we have, in terms of the functions f_{ij} introduced above, $k_{\perp,ij} = k_t\sqrt{2/f_{ij}}$.

7.3.1 Power corrections dipole-by-dipole

Now we proceed to an extraction of the leading power-behaved contribution. In order to do this we first note that the integral over k_t in eq. (7.3.9), which can be rewritten as one over the related variable $k_\perp$, is divergent if one uses the usual perturbative definition of α_s, due to the divergence of the running coupling at $k_\perp = \Lambda_{\rm QCD}$. In order to isolate and cure this pathological behaviour, as we did in section 3.6 for the two-jet case, we introduce the infrared-finite effective coupling ($\alpha_{\rm eff}$) and change the variable of integration from k_t to $k_\perp$ in eq. (7.3.9). We then follow the method of Dokshitzer and Webber [45] to write $\alpha_{\rm eff}(k^2_\perp) = \alpha_{s,\rm PT}(k^2_\perp) + \delta\alpha_{s,\rm NP}(k^2_\perp)$, where PT and NP stand for perturbative and non-perturbative respectively. In doing so we have assumed that the actual coupling $\alpha_{\rm eff}$ is in fact finite even at arbitrarily small $k_\perp$, and can be split into the usual perturbative component $\alpha_{s,\rm PT}$ and a modification $\delta\alpha_{s,\rm NP}$ which is due to non-perturbative effects. Both the perturbative and non-perturbative components separately diverge, but the divergences cancel in their sum due to the assumed finiteness of the physical coupling $\alpha_{\rm eff}$. Moreover, since we do not modify the perturbative results at large scales, the non-perturbative physics as represented by the modification $\delta\alpha_{s,\rm NP}$ must vanish above some infrared "matching" scale μ_I. Effectively the addition of the $\delta\alpha_{s,\rm NP}$ term represents removal

of the badly-behaved perturbative contribution below μ_I and its replacement with the well-behaved integral over the infrared-finite physical coupling $\alpha_{\rm eff}$.

Thus for the observable itself one has from dipole (ij):

$$\int_{k\in\Omega} d\eta \frac{d\phi}{2\pi} \frac{dk_{\perp,i,j}}{k_{\perp,i,j}} \frac{\alpha_{s,\rm PT}(k^2_{\perp,i,j})}{2\pi} \left(1 - e^{-\nu k_t}\right) f_{ij}(\eta,\phi) + \\ + \int_{k\in\Omega} d\eta \frac{d\phi}{2\pi} \frac{dk_{\perp,i,j}}{k_{\perp,i,j}} \frac{\delta\alpha_{s,\rm NP}(k^2_{\perp,i,j})}{2\pi} \left(1 - e^{-\nu k_t}\right) f_{ij}(\eta,\phi). \quad (7.3.10)$$

The integral involving the perturbative coupling represents the usual perturbative contribution from dipole (ij). The leading logarithmic perturbative contribution arises from the region where one can make the approximation:

$$\left(1 - e^{-\nu k_t}\right) \approx \theta\left(k_t - \frac{1}{\nu}\right). \quad (7.3.11)$$

The perturbative results were reported at length by Berger et al [78] (also presented in section 3.5). In what follows we shall consider in more detail the non-perturbative contribution from the integral involving $\delta\alpha_{s,\rm NP}$.

In order to evaluate the non-perturbative contribution we first consider that the leading such term arises from the region $\mu_I \ll 1/\nu$, which translates to a requirement on E_t to be above a few GeV. In this region one can expand the exponential in an exactly analogous way as for event-shape distributions [45]. The leading term is given by the first term in the expansion: $1 - \exp(-\nu k_t) \approx \nu k_t$, and this corresponds to a linear $1/P_t$ power correction. We ignore quadratic and higher power corrections that would scale as $1/P_t^2$ and beyond, once again following the case of event-shape variables. We also note that in the shape function approach [115, 116], where one may study non-perturbative effects even into the region $E_t \sim \Lambda_{\rm QCD}$, higher powers of ν need also to be retained. Working with just the leading term gives us the non-perturbative correction from the (ij) dipole which can then be written as:

$$\tilde{w}_{ij} = \tilde{w}_{ij}^{\rm PT} + \nu \mathcal{P} C_{ij}. \quad (7.3.12)$$

Here the non-perturbative quantity $\mathcal{P}$ is the first moment of the coupling modification $\delta\alpha_{s,\rm NP}$:

$$\mathcal{P} = \int_0^{\mu_I} \frac{dk_\perp}{k_\perp} k_\perp \frac{\delta\alpha_{s,\rm NP}(k_\perp^2)}{2\pi}, \quad (7.3.13)$$

which also enters $1/Q$ (Q being the hard scale) power corrections to event shapes and can be related to the parameter α_0, extracted from fits to event shape data, as (see eq. (3.6.3)):

$$\mathcal{P} = \frac{\mu_I}{2\pi}\left(\alpha_0(\mu_I) - \alpha_s(P_t^2) - \frac{\beta_0}{2\pi}\left(\ln\frac{P_t}{\mu_I} + \frac{K_F}{\beta_0} + 1\right)\alpha_s^2(P_t^2) + \mathcal{O}(\alpha_s^3)\right), \quad (7.3.14)$$

where $\alpha_0(\mu_I) = 1/\mu_I \int_0^{\mu_I} dk_\perp\, \alpha_{\rm eff}(k_\perp^2)$.

The coefficients C_{ij} represent the integral over directions:

$$C_{ij} = \int_{k\in\Omega} d\eta \frac{d\phi}{2\pi}\frac{1}{\sqrt{2}} f_{ij}^{3/2}, \quad (7.3.15)$$

where f_{ij} arises from the dipole antenna pattern as indicated in eq. (7.3.9), and a further factor proportional to $\sqrt{f_{ij}}$ comes from rewriting k_t in terms of $k_\perp$ as we stated before. The explicit form of the f_{ij} functions is reported in appendix C. Performing the integrals over η and ϕ in eq. (7.3.15) yields the coefficients C_{ij} that correspond to the non-perturbative contribution to $\tilde{w}_{ij}$ in eq. (7.3.12), which we do not explicitly display for economy of presentation.

Having computed the power corrections proportional to ν for each dipole, we can include these corrections to the anomalous dimension matrix in eq. (7.3.3), which can then be written as:

$$\mathbf{\Gamma} = \tau\mathbf{\Gamma}_{\rm PT} + \nu\mathcal{P}\mathbf{\Gamma}_{\rm NP}, \quad (7.3.16)$$

where the non-perturbative contribution $\mathbf{\Gamma}_{\rm NP}$ is built up by combining the dipole contributions C_{ij} as in the perturbative case. In the case of the perturbative term $\mathbf{\Gamma}_{\rm PT}$ we explicitly extracted the integral over the transverse momentum of the coupling:

$$\tau = \int_{1/\nu}^{P_t} \frac{dk_t}{k_t}\frac{\alpha_{s,\rm PT}(k_t^2)}{2\pi}, \quad (7.3.17)$$

which is analogous to that we introduced in eq. (3.3.7), and arises by making the substitution (7.3.11) in the first term of (7.3.10). Then the matrix $\mathbf{\Gamma}_{\rm PT}$ is the usual perturbative anomalous dimension containing integrals over gluon directions inside the region[2] Ω. In the following section we shall consider the evaluation of the inverse Mellin transform to take our results from ν space to E_t space.

[2]These integrals (referred to as W_{ij} in appendix C) are similar to those which yield the C_{ij} except that the functions f_{ij} are involved rather than $f_{ij}^{3/2}/\sqrt{2}$.

7.4 Power corrections in the E_t cross-section

After accommodating the leading power corrections (those expected to give rise to $1/P_t$ effects), eq. (7.2.2) assumes the explicit form:

$$\Sigma(P_t, E_t) = \int \frac{d\nu}{2\pi i\nu} e^{\nu E_t} \times \\ \times \mathrm{Tr}\left[\mathbf{H} \exp\left(-\tau \mathbf{\Gamma}^{\dagger}_{\mathrm{PT}} - \nu \mathcal{P} \mathbf{\Gamma}^{\dagger}_{\mathrm{NP}}\right) \mathbf{S} \exp\left(-\tau \mathbf{\Gamma}_{\mathrm{PT}} - \nu \mathcal{P} \mathbf{\Gamma}_{\mathrm{NP}}\right)\right] / \Sigma_0. \quad (7.4.1)$$

In order to invert the Mellin transform (perform the ν integral above) it is simplest to diagonalise the matrix $\tau \mathbf{\Gamma}_{\mathrm{PT}} + \nu \mathcal{P} \mathbf{\Gamma}_{\mathrm{NP}}$. In the basis in which the matrix $\mathbf{\Gamma}$ is diagonal the matrices $\mathbf{H}$ and $\mathbf{S}$ become $\widetilde{\mathbf{H}} = \mathbf{R}^{-1}\mathbf{H}\mathbf{R}^{-1\dagger}$ and $\widetilde{\mathbf{S}} = \mathbf{R}^{\dagger}\mathbf{S}\mathbf{R}$, where $\mathbf{R}$ is a matrix containing the eigenvectors of $\mathbf{\Gamma}$ as column entries. After diagonalisation we can write the result for $\Sigma(P_t, E_t)$ in terms of components as:

$$\Sigma(P_t, E_t) = \int \frac{d\nu}{2\pi i\nu} e^{\nu E_t} e^{-\lambda_i} \delta_{ij} \widetilde{H}_{jk} e^{-\lambda^*_k} \delta_{kl} \widetilde{S}_{li} / \Sigma_0, \quad (7.4.2)$$

where λ_i are the eigenvalues of the matrix $\mathbf{\Gamma}$. For the case of the $q\bar{q} \to q\bar{q}$ sub-process, which we use as an example, $\mathbf{\Gamma}$, $\widetilde{\mathbf{H}}$ and $\widetilde{\mathbf{S}}$ are 2×2 matrices and the above result can be written explicitly in terms of the elements of the various matrices as:

$$\Sigma(P_t, E_t) = \int \frac{d\nu}{2\pi i\nu} e^{\nu E_t} \frac{1}{\Sigma_0} \times \\ \times \left(\widetilde{H}_{11}\widetilde{S}_{11} e^{-(\lambda_1 + \lambda_1^*)} + \widetilde{H}_{12}\widetilde{S}_{21} e^{-(\lambda_1 + \lambda_2^*)} + \widetilde{H}_{21}\widetilde{S}_{12} e^{-(\lambda_1^* + \lambda_2)} + \widetilde{H}_{22}\widetilde{S}_{22} e^{-(\lambda_2 + \lambda_2^*)}\right), \quad (7.4.3)$$

where the above result contains both perturbative and non-perturbative contributions. To separate these we note that the eigenvalues can be expanded so as to retain only the first-order in ν correction to the perturbative value, which depends logarithmically on ν:

$$\lambda_i = \tau(\nu) \lambda_i^{\mathrm{PT}} + \nu \mathcal{P} \lambda_i^{\mathrm{NP}} + \mathcal{O}(\nu^2). \quad (7.4.4)$$

We emphasise here that while λ_i^{PT} are simply the eigenvalues of $\mathbf{\Gamma}_{\mathrm{PT}}$, λ_i^{NP} are *not* the eigenvalues of $\mathbf{\Gamma}_{\mathrm{NP}}$. Instead they are coefficients of the $\mathcal{O}(\nu)$ component of the expansion of the eigenvalues of $\tau \mathbf{\Gamma}_{\mathrm{PT}} + \nu \mathcal{P} \mathbf{\Gamma}_{\mathrm{NP}}$ and they depend on the components of both $\mathbf{\Gamma}_{\mathrm{NP}}$ and $\mathbf{\Gamma}_{\mathrm{PT}}$.

The matrices $\widetilde{\mathbf{H}}$ and $\widetilde{\mathbf{S}}$ also differ from their pure perturbative forms by corrections which depend on ν. Let us define the matrix $\mathbf{D}$ such that $D_{ij} = \widetilde{H}_{ij}\widetilde{S}_{ji}$. We expand the elements D_{ij} to first order in ν and write the result as:

$$\Sigma(E_t, P_t) = \sum_{i,j} \int \frac{d\nu}{2\pi i\nu} e^{\nu\left(E_t - \mathcal{P}\left[\lambda_i^{\mathrm{NP}} + \lambda_j^{*\mathrm{NP}}\right]\right)} \left(D_{ij}^{\mathrm{PT}} + \frac{\nu}{\tau(\nu)} \mathcal{P} D_{ij}^{\mathrm{NP}} \right) e^{-\tau(\nu)(\lambda_i^{\mathrm{PT}} + \lambda_j^{*\mathrm{PT}})} / \Sigma_0, \tag{7.4.5}$$

where the sum runs over the components of the matrix D_{ij} and we ignore higher-order terms in the expansion of $D_{ij}(\nu)$.

We ignore for the moment the correction terms involving D_{ij}^{NP} which shall be presently considered. We first write down the pure perturbative result $\Sigma^{\mathrm{PT}}(P_t, E_t)$ obtained by ignoring all non-perturbative components. Then performing the integral over ν (easily performed by contour integration) and retaining only leading perturbative logarithms we get:

$$\Sigma^{\mathrm{PT}}(P_t, E_t) = \sum_{i,j} D_{ij}^{\mathrm{PT}} e^{-\left(\lambda_i^{\mathrm{PT}} + \lambda_j^{*\mathrm{PT}}\right)\tau(E_t)} / \Sigma_0, \tag{7.4.6}$$

where the effect of the ν integration amounts to merely replacing ν by $1/E_t$. Including the non-perturbative correction to the eigenvalues we find by examining eq. (7.4.5) that the impact of the non-perturbative term amounts to a shift of the perturbative result in each of the terms in the sum in eq. (7.4.6):

$$E_t \to E_t - \mathcal{P}\left(\lambda_i^{\mathrm{NP}} + \lambda_j^{*\mathrm{NP}}\right). \tag{7.4.7}$$

Looking at the distribution in E_t, with E_t being measured in units of the hard scale P_t, amounts to a $1/P_t$ non-perturbative shift in each term in the sum above, as is the case for two-jet event-shape variables [115, 45]. However in contrast to the case of event shapes it should be clear that the overall impact of the power correction is not simply a shift of the perturbative distribution by a fixed amount since each term in the sum on the right hand side of eq. (7.4.6) receives its own characteristic shift depending on the sum of the eigenvalues $\lambda_i^{\mathrm{NP}} + \lambda_j^{*\mathrm{NP}}$ entering the term in question.

Moreover we have still not accounted for the non-perturbative contribution to the colour basis as contained in the D_{ij}^{NP} terms. To evaluate these one performs the contour integral in question which yields a power correction of the form $\mathcal{P}/E_t$.

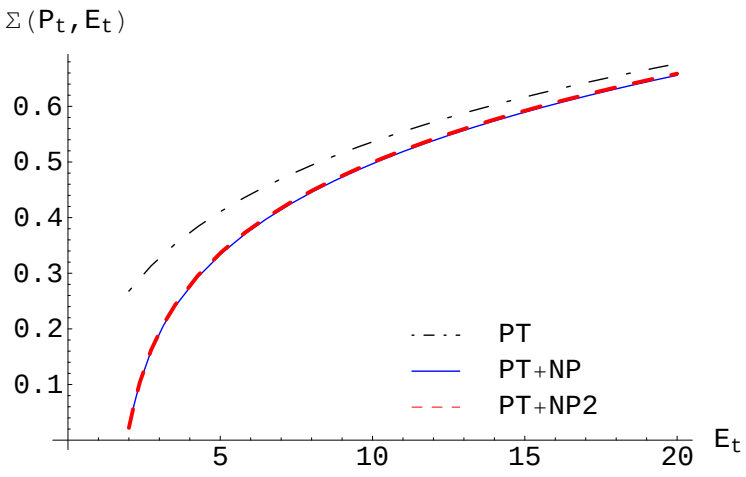

Figure 7.1: Power corrections to the energy flow distribution. PT stands for the pure perturbative result $\Sigma^{\rm PT}(P_t, E_t)$ as presented in eq. (7.4.6), PT+NP stands for the result including the non-perturbative correction and ignoring the terms $D_{ij}^{\rm NP}$, while PT+NP2 stands for the result presented in eq. (7.4.8).

Computing the full result for this piece we arrive at our final result for $\Sigma(P_t, E_t)$:

$$\Sigma(P_t, E_t) = \sum_{i,j} e^{-\Delta_{ij}^{\rm PT}\tau\left(E_t - \Delta_{ij}^{\rm NP}\right)} \times \\ \times \left[D_{ij}^{\rm PT} + D_{ij}^{\rm NP} \frac{\mathcal{P}}{E_t - \Delta_{ij}^{\rm NP}} \frac{1}{\tau\left(E_t - \Delta_{ij}^{\rm NP}\right)} G\left(\alpha_s, \frac{P_t}{E_t - \Delta_{ij}^{\rm NP}}\right) \right] / \Sigma_0, \quad (7.4.8)$$

where $\Delta_{ij}^{\rm NP} = \mathcal{P}(\lambda_i^{\rm NP} + \lambda_j^{*\rm NP})$ and $\Delta_{ij}^{\rm PT} = \lambda_i^{\rm PT} + \lambda_j^{*\rm PT}$, and the function G is approximately a constant of order $\alpha_s(P_t)$, varying very slowly with E_t over the range of E_t we consider here. It is a function of the logarithmic derivative of the single-log resummed perturbative result and hence scales as α_s. We also note the presence of $1/\tau(E_t - \Delta_{ij}^{\rm NP})$, which is a reflection of the fact that the correction terms (containing $D_{ij}^{\rm NP}$) go as ν/τ.

7.5 Results

In this section we illustrate the impact of non-perturbative power corrections on the energy flow distribution we discussed above.

In fig. 7.1 we show the result for $\Sigma(P_t, E_t)$. We present the pure perturbative result (eq. (7.4.6)), the result including non-perturbative corrections without the

$D_{ij}^{\rm NP}$ component (PT+NP) and the result presented in eq. (7.4.8) (PT+NP2).

The results above were obtained for the illustrative value of $p_t = 80$ GeV. We have performed the integration over the functions $f_{ij}^{3/2}$ for the non-perturbative component (given in eq. (7.3.15)) numerically. We also assumed that the rapidity gap has width $\Delta\eta = 1$.

We notice that the effect of the term $D_{ij}^{\rm NP}$ is in fact very small and thus we take this as an indication that neglected higher orders in the expansion of D_{ij} are even more suppressed. We also note that the corrections to the result are larger when E_t is small. Furthermore there is clearly no indication of a pure shift in the overall result as we stated before.

7.6 Conclusions

In this chapter we have revealed for the first time a calculation of the power corrections in hadronic collisions. We illustrated the computation for the energy flow distribution using the process $q\bar{q} \to q\bar{q}$. The generalisation to other channels is straightforward and only requires the numerical computation of the diagonalised anomalous dimensions and the corresponding hard and soft matrices.

We found that the result does not correspond to the usual shift found in studies of two-jet event shapes and energy flows (see section 3.6). The reason for this is the non-trivial colour algebra involved in the case of hadronic collisions.

The techniques we used here should enable better estimates of power corrections for observables which have a similar nature to the one we introduced here (such as the inclusive jet cross-section we mentioned earlier).

Once again our computation does not account for the Milan factor which we highlighted in section 3.6. As we mentioned there this factor has not been accounted for in the hadronic collisions case and a two-loop analysis is required in order to estimate it.

Chapter 8

Conclusions

In this thesis we have studied different aspects of soft gluon and non-perturbative effects in QCD observables. The aim was to achieve a better understanding of QCD dynamics which, for instance, dominate important physics at the LHC.

In chapter 4 we studied the distribution $1/\sigma\, d\sigma/dQ_t$, where Q_t is the modulus of the transverse momentum vector of particles in the current hemisphere of the DIS Breit frame. We resummed the large logarithms in the small Q_t region, to NLL accuracy, including the non-global logarithms involved and combined the result to NLO predictions. This observable, as we pointed out, is simply related to the Drell-Yan vector boson and predicted Higgs Q_t spectra at hadronic colliders.

Having obtained the theoretical prediction we compared our results to preliminary HERA predictions [89]. After obtaining the final form of the data we ought to be able to assess the role or absence of small-x (BFKL) effects, neglected in conventional resummation of such quantities. This we leave for our forthcoming phenomenological investigation.

We then revisited, in chapter 5, the impact of the k_t clustering algorithm on predictions of energy flows into gaps between hard jets. We analytically computed the dependence of the primary emission term on the jet algorithm, which gave significantly more insight than a previous numerical study of the same. We also pointed out that the non-global component of the answer is reduced even more significantly by the clustering than suggested previously in the literature. We provided improved predictions for the latest ZEUS photoproduction data, assessing the impact of our

latest findings.

As a future avenue the proper calculation of the clustering-dependent component in hadronic collisions and dijet photoproduction (together with a prediction for the non-global component) should be straightforward.

Next we studied the azimuthal correlation distribution for dijet production in QCD hard processes in chapter 6. This observable is sensitive to soft and/or collinear emissions in the back-to-back region, giving rise to single and double logarithms. We provided resummed predictions to NLL accuracy for both DIS at HERA and hadronic collisions at the Tevatron and performed an NLO matching to NLOJET++ results in the DIS case.

The task of fully computing a matched result and comparing our predictions to HERA data, as we explained in chapter 6, is well on the way. Having done this we plan to compute the non-perturbative corrections and proceed with studying this observable using the jet definition employed by the DØ collaboration.

Finally in chapter 7 we studied the power corrections to the inter-jet energy flow distribution in hadronic collisions. The "usual" simple shift of the distribution does *not* manifest itself in this case because of the complicated colour algebra involved. We calculated the power corrections to this distribution using the renormalon-inspired techniques that were employed in e^+e^- annihilation into jets and DIS cases. We have illustrated the impact of such corrections in the simple case of $q\bar{q} \to q\bar{q}$, where we calculated the corresponding anomalous dimension matrices.

The next step in the analysis of these power correction is to compute the Milan factor, which requires a two-loop analysis of the argument of the coupling. Once this is done, and in light the work of chapter 5, one can provide the most accurate predictions which can be compared to energy flow data in hadronic collisions together with those from DIS photoproduction. This allows us to test many perturbative frameworks we have developed in this thesis, which are very important for the LHC, particularly the universality of non-perturbative effects manifested in the coupling moment.

Appendix A

Fixed-order result and the radiator for the DIS Breit current hemisphere Q_t distribution

A.1 Fixed-order result

In all what follows the symbols have the same meaning as those introduced in chapter 2 and chapter 4. The observable we study here is the modulus of the vectorial sum of transverse momenta of all particles in the current hemisphere $p_t = |\vec{p}_t| = \left|\sum_{i\in\mathcal{H}_c} \vec{k}_{t,i}\right|$. The momenta of particles in the Breit frame are given by:

$$P = \frac{Q}{2x}(1,0,0,-1), \tag{A.1.1}$$

$$p = \frac{Q}{2\xi}(1,0,0,-1), \tag{A.1.2}$$

$$q = Q(0,0,0,1), \tag{A.1.3}$$

$$r = \frac{Q}{2}(z_0,z_1,z_2,z_3), \tag{A.1.4}$$

$$k = \frac{Q}{2}(\overline{z}_0,\overline{z}_1,\overline{z}_2,\overline{z}_3), \tag{A.1.5}$$

where

$$z_1^2 + z_2^2 = \overline{z}_1^2 + \overline{z}_2^2 = -(\overline{z}_1 z_1 + \overline{z}_2 z_2) = z_\perp^2, \tag{A.1.6}$$

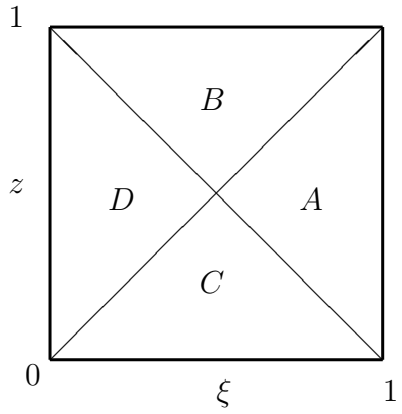

Figure A.1: The phase-space. See table A.1 for the values of p_t in different regions.

Region	**Particles in region**	p_t	QB_{zQ}
A	both outgoing particles	0	$Qz_\perp$
B and C	one outgoing particle	$Qz_\perp/2$	$Qz_\perp/2$
D	None	0	0

Table A.1: Values of p_t and QB_{zQ} in different regions of the phase-space.

and

$$z_0 = 2z - 1 + \frac{1-z}{\xi}, \tag{A.1.7}$$

$$\overline{z}_0 = 1 - 2z + \frac{z}{\xi}, \tag{A.1.8}$$

$$z_3 = 1 - \frac{1-z}{\xi}, \tag{A.1.9}$$

$$\overline{z}_3 = 1 - \frac{z}{\xi}, \tag{A.1.10}$$

$$z_\perp = 2\sqrt{\frac{z(1-z)(1-\xi)}{\xi}}. \tag{A.1.11}$$

The vectors $\vec{r}_t = Q/2(z_1, z_2)$ and $\vec{k}_t = Q/2(\overline{z}_1, \overline{z}_2)$ are the transverse momentum vectors of the outgoing particles. They are equal in magnitude and opposite in direction. Their modulus is $Qz_\perp/2$.

At $\mathcal{O}(\alpha_s)$ we identify four distinct regions of the phase-space each with a different distribution of particles as shown in fig. A.1 and summarised in table A.1.

A.1.1 A relation between p_t and the jet broadening

It proves convenient for the calculation of the Q_t distribution at $\mathcal{O}(\alpha_s)$ to consider the *jet broadening* [87]. This is defined as:

$$B_{zQ} = \frac{\sum_{i\in\mathcal{H}_c} |\vec{p}_i \times \vec{n}|}{Q}, \tag{A.1.12}$$

where $\vec{n}$ is a unit vector along the z-axis. The values of the jet broadening in different regions of the phase-space are shown in table A.1.

Clearly $QB_{zQ} = p_t$ in regions "B", "C" and "D". Thus one can subtract the contribution of region "A" to the jet broadening leading-order distribution to get the Q_t one.

A.1.2 Setting-up the calculation of the cross-section

The integrated cross-section for events with $p_t < Q_t$ is obtained by restricting the phase-space in eq. (2.3.4) with a theta function of the form $\theta(Q_t - p_t)$. One can write:

$$\begin{aligned}\frac{1}{\sigma_0}\sigma^{(1)}(Q_t, Q, x) = \frac{1}{q(x,Q^2)}\frac{\alpha_s}{2\pi}\int_x^1 \frac{d\xi}{\xi}\Bigg\{ & C_F q\left(\frac{x}{\xi}, Q^2\right)\mathcal{F}_{2,q}\left(\xi, \frac{Q}{Q_t}\right) + \\ & + T_f g\left(\frac{x}{\xi}, Q^2\right)\mathcal{F}_{2,g}\left(\xi, \frac{Q}{Q_t}\right) - \frac{y^2}{1+(1-y)^2}\Bigg[C_F q\left(\frac{x}{\xi}, Q^2\right)\mathcal{F}_{L,q}\left(\xi, \frac{Q}{Q_t}\right) + \\ & + T_f g\left(\frac{x}{\xi}, Q^2\right)\mathcal{F}_{L,g}\left(\xi, \frac{Q}{Q_t}\right)\Bigg]\Bigg\},\end{aligned} \tag{A.1.13}$$

where

$$\mathcal{F}_{i,j}\left(\xi, \frac{Q}{Q_t}\right) = \int_0^1 dz C_{i,j}(\xi, z)\,\theta\left(Q_t - p_t\right), \tag{A.1.14}$$

and $C_{i,j}$ are the coefficient functions (see equations (2.3.5) to (2.3.8)). Our aim here is to solve the integral in eq. (A.1.13) neglecting terms that vanish when $Q_t \to 0$, which we do not require. We are particularly interested in extracting the logarithms and the term $\boldsymbol{C}_1$ that appears in eq. (4.3.2). Terms which we neglect are supplied to the distribution by matching to NLO results.

To work with real emissions alone we exploit the unitarity relation:

$$\sigma^{(1)}_{p_t<Q_t} = \sigma^{(1)}_{\text{tot}} - \sigma^{(1)}_{p_t>Q_t}, \tag{A.1.15}$$

where $\sigma^{(1)}_{\rm tot}$ is the total leading-order cross-section. The term $\sigma^{(1)}_{p_t>Q_t}$, which represents the integrated distribution for events with $p_t > Q_t$ at $\mathcal{O}(\alpha_s)$, does not acquire virtual corrections.

The jet broadening fixed-order results have been calculated by Dasgupta and Salam [87]. We use those results and subtract the contribution of region "A" to get the Q_t distribution. We have:

$$\sigma^{(1)}_{B_{zQ}<B} = \sigma^{(1)}_{\rm tot} - \left(\sigma^{(1)}_{B_{zQ}>B}(\text{region B}) + \sigma^{(1)}_{B_{zQ}>B}(\text{region C}) + \sigma^{(1)}_{B_{zQ}>B}(\text{region A})\right), \tag{A.1.16}$$

$$\sigma^{(1)}_{p_t<Q_t} = \sigma^{(1)}_{\rm tot} - \left(\sigma^{(1)}_{p_t>Q_t}(\text{region B}) + \sigma^{(1)}_{p_t>Q_t}(\text{region C})\right). \tag{A.1.17}$$

Hence:

$$\sigma^{(1)}_{p_t<Q_t} = \sigma^{(1)}_{B_{zQ}<B} + \sigma^{(1)}_{B_{zQ}>B}(\text{region A}), \tag{A.1.18}$$

where $B = Q_t/Q$.

We now compute the integrated distribution with $B_{zQ} > Q_t/Q$ in region A, which we denote by $\sigma^{(1)}_A$. Let $\sigma^{(1)}_{A,i,j}$ represent the contribution to $\sigma^{(1)}_A$ of F_2/x ($i = 2$) or F_L ($i = L$), with j standing for the incoming gluon ($j = g$) or quark ($j = q$) channel contributions such that:

$$\sigma^{(1)}_A = \frac{1}{q(x,Q^2)}\frac{\alpha_s}{2\pi}\times \\ \times\left(C_F\sigma^{(1)}_{A,2,q} + T_f\sigma^{(1)}_{A,2,g} - \frac{y^2}{1+(1-y)^2}\left[C_F\sigma^{(1)}_{A,L,q} + T_f\sigma^{(1)}_{A,L,g}\right]\right). \tag{A.1.19}$$

Using table A.1 and eq. (A.1.11) one can write:

$$\sigma^{(1)}_{A,i,j}(Q_t,Q,x) = \int_{\frac{1}{2}}^{1}\frac{d\xi}{\xi}q_j\left(\frac{x}{\xi},Q^2\right)\int_{1-\xi}^{\xi}dz\; C_{i,j}(\xi,z)\times \\ \times\,\theta\left(\frac{4z(1-z)(1-\xi)}{\xi} - \frac{Q_t^2}{Q^2}\right). \tag{A.1.20}$$

We have used the fact that[1] $1/2 < \xi < 1$ and $1-\xi < z < \xi$ in region "A" according to fig. A.1. The theta function imposes the conditions: $\xi < 1/(1+Q_t^2/Q^2)$ (and hence $Q_t < Q$ since $\xi > 1/2$) and: $\xi_{\rm min} < z < \xi_{\rm max}$, where:

$$\xi^{\rm max}_{\rm min} = \frac{1}{2}\left(1 \pm \sqrt{1 - \frac{(Q_t/Q)^2\xi}{1-\xi}}\right). \tag{A.1.21}$$

[1]Strictly speaking we also have $\xi > x$, which means that a theta function $\theta(1-x/\xi)$ is embodied in PDFs.

The condition on z we mentioned just before eq. (A.1.21) can only be applied if $\xi > 1 - Q_t/(2Q)$, since we already have $1-\xi < z < \xi$. Thus the integral splits into two parts:

$$\sigma^{(1)}_{A,i,j}(Q_t,Q,x) = \int_{\frac{1}{2}}^{1-\frac{Q_t}{2Q}} \frac{d\xi}{\xi} q_j\left(\frac{x}{\xi},Q^2\right)\int_{1-\xi}^{\xi} dz C_{i,j}(\xi,z) + \\ + \int_{1-\frac{Q_t}{2Q}}^{\frac{1}{1+(Q_t/Q)^2}} \frac{d\xi}{\xi} q_j\left(\frac{x}{\xi},Q^2\right)\int_{\xi_{\min}}^{\xi_{\max}} dz C_{i,j}(\xi,z). \quad \text{(A.1.22)}$$

A.1.3 Quark contribution

The quark contribution to F_2/x is given by:

$$\sigma^{(1)}_{A,2,q}(Q_t,Q,x) = \int_{\frac{1}{2}}^{1-\frac{Q_t}{2Q}} \frac{d\xi}{\xi} q\left(\frac{x}{\xi},Q^2\right)\int_{1-\xi}^{\xi} dz \left(\frac{z^2+\xi^2}{(1-\xi)(1-z)} + 6z\xi + 2\right) + \\ + \int_{1-\frac{Q_t}{2Q}}^{\frac{1}{1+(Q_t/Q)^2}} \frac{d\xi}{\xi} q\left(\frac{x}{\xi},Q^2\right)\int_{\xi_{\min}}^{\xi_{\max}} dz \left(\frac{z^2+\xi^2}{(1-\xi)(1-z)} + 6z\xi + 2\right). \quad \text{(A.1.23)}$$

Performing the z integral we get:

$$\sigma^{(1)}_{A,2,q}(Q_t,Q,x) = \int_{\frac{1}{2}}^{1-\frac{Q_t}{2Q}} \frac{d\xi}{\xi} q\left(\frac{x}{\xi},Q^2\right)\left(-\frac{1+\xi^2}{1-\xi}\ln\frac{1-\xi}{\xi} - \frac{12\xi^3-10\xi^2+1}{2(1-\xi)}\right) + \\ + \int_{1-\frac{Q_t}{2Q}}^{\frac{1}{1+(Q_t/Q)^2}} \frac{d\xi}{\xi} q\left(\frac{x}{\xi},Q^2\right)\left\{-\frac{6\xi^2-2\xi-1}{2(1-\xi)}\sqrt{1-\frac{(Q_t/Q)^2\xi}{1-\xi}} - \right. \\ \left. - \frac{1+\xi^2}{1-\xi}\left[\ln\left(1-\sqrt{1-\frac{(Q_t/Q)^2\xi}{1-\xi}}\right) - \ln\left(1+\sqrt{1-\frac{(Q_t/Q)^2\xi}{1-\xi}}\right)\right]\right\}. \quad \text{(A.1.24)}$$

In order to separate the large logarithms we use eq. (2.5.6) to write:

$$\int_0^1 f(\xi)g(\xi)d\xi = \int_0^1 f(1)g(\xi)d\xi + \int_0^1 f(\xi)[g(\xi)]_+ d\xi, \quad \text{(A.1.25)}$$

with $f(\xi)$ and $g(\xi)$ being a smooth function and a divergent function which has a singularity of the form $1/(1-\xi)$ at $\xi = 1$. The first term in the right hand side of eq. (A.1.25) contains logarithms of $(1-\xi)$ and the second one is regularised by the plus prescription which we introduced in eq. (2.5.6). We use this in eq. (A.1.24) and we

set $Q_t \to 0$ in the regularised part arriving at:

$$\sigma^{(1)}_{A,2,q}(Q_t,Q,x) = \int_x^1 \frac{d\xi}{\xi} q\left(\frac{x}{\xi},Q^2\right)\Bigg\{\delta(1-\xi)\Bigg(2\ln^2\frac{Q}{Q_t} + 4\ln 2\ln\frac{Q}{Q_t} - \\ - 3\ln\frac{Q}{Q_t} + 2\ln^2 2 - \frac{3}{2}\ln 2 + 3 - \frac{\pi^2}{2}\Bigg) - (1+\xi^2)\left[\frac{\theta(2\xi-1)}{1-\xi}\ln\frac{1-\xi}{\xi}\right]_+ - \\ - (12\xi^3 - 10\xi^2 + 1)\left[\frac{\theta(2\xi-1)}{2(1-\xi)}\right]_+\Bigg\}. \quad \text{(A.1.26)}$$

A.1.4 Gluon contribution

The gluon contribution to F_2/x is given by:

$$\sigma^{(1)}_{A,2,g}(Q_t,Q,x) = \int_{\frac{1}{2}}^{1-\frac{Q_t}{2Q}} \frac{d\xi}{\xi} g\left(\frac{x}{\xi},Q^2\right)\int_{1-\xi}^{\xi} dz\Bigg\{[\xi^2+(1-\xi)^2]\times \\ \times\frac{z^2+(1-z)^2}{z(1-z)} + 8\xi(1-\xi)\Bigg\} + \int_{1-\frac{Q_t}{2Q}}^{\frac{1}{1+(Q_t/Q)^2}} \frac{d\xi}{\xi} g\left(\frac{x}{\xi},Q^2\right)\times \\ \times\int_{\xi_{\min}}^{\xi_{\max}} dz\left\{[\xi^2+(1-\xi)^2]\frac{z^2+(1-z)^2}{z(1-z)} + 8\xi(1-\xi)\right\}, \quad \text{(A.1.27)}$$

which simplifies to:

$$\sigma^{(1)}_{A,2,g}(Q_t,Q,x) = \int_{\frac{1}{2}}^{1-\frac{Q_t}{2Q}} \frac{d\xi}{\xi} g\left(\frac{x}{\xi},Q^2\right)\Bigg\{-24\xi^3+36\xi^2-16\xi+2- \\ -(4\xi^2-4\xi+2)\ln\frac{1-\xi}{\xi}\Bigg\} + \int_{1-\frac{Q_t}{2Q}}^{\frac{1}{1+(Q_t/Q)^2}} \frac{d\xi}{\xi} g\left(\frac{x}{\xi},Q^2\right)\Bigg\{2(1+2\xi^2-2\xi)\times \\ \times\left[\ln\left(1+\sqrt{1-\frac{(Q_t/Q)^2\xi}{1-\xi}}\right) - \left(1-\sqrt{1-\frac{(Q_t/Q)^2\xi}{1-\xi}}\right)\right] - \\ -2(1+6\xi^2-6\xi)\sqrt{1-\frac{(Q_t/Q)^2\xi}{1-\xi}}\Bigg\}. \quad \text{(A.1.28)}$$

There are no singularities in this equation[2]. One can check this by expanding the integrals as in eq. (A.1.25). Therefore we just set Q_t to zero everywhere arriving at:

$$\sigma^{(1)}_{A,2,g}(Q_t,Q,x) = \int_x^1 \frac{d\xi}{\xi} g\left(\frac{x}{\xi},Q^2\right)\Bigg[(-24\xi^3+36\xi^2-16\xi+2)\theta(2\xi-1) - \\ -(4\xi^2-4\xi+2)\theta(2\xi-1)\ln\frac{1-\xi}{\xi}\Bigg]. \quad \text{(A.1.29)}$$

[2]This can be seen by noting that there are no soft singularities for this channel (as we stated just after eq. (2.3.11)). The only logarithms that arise for this channel come from the region where the incoming gluon splits into a collinear quark/anti-quark pair, which happens only in regions B and C.

A.1.5 Longitudinal quark contribution

Following the same steps as before we find that the quark contribution to F_L is given by:

$$\sigma^{(1)}_{A,L,q}(Q_t,Q,x) = \int_{\frac{1}{2}}^{1-\frac{Q_t}{2Q}} \frac{d\xi}{\xi} q\left(\frac{x}{\xi},Q^2\right) 2\xi\,(2\xi-1) + \\ + \int_{1-\frac{Q_t}{2Q}}^{\frac{1}{1+(Q_t/Q)^2}} \frac{d\xi}{\xi} q\left(\frac{x}{\xi},Q^2\right) 2\xi\sqrt{1-\frac{Q_t^2/Q^2\xi}{1-\xi}}. \quad \text{(A.1.30)}$$

This also has no singularities. We have:

$$\sigma^{(1)}_{A,L,q}(Q_t,Q,x) = \int_x^1 \frac{d\xi}{\xi} q\left(\frac{x}{\xi},Q^2\right) 2\xi\,(2\xi-1)\,\theta\,(2\xi-1)\,. \quad \text{(A.1.31)}$$

A.1.6 Longitudinal gluon contribution

The longitudinal gluon contribution is given by:

$$\sigma^{(1)}_{A,L,g}(Q_t,Q,x) = \int_x^1 \frac{d\xi}{\xi} g\left(\frac{x}{\xi},Q^2\right) 8\xi(1-\xi)(2\xi-1)\theta\,(2\xi-1)\,. \quad \text{(A.1.32)}$$

A.1.7 The final answer

The leading-order cross-section for events with $p_t < Q_t$ is given by eq. (A.1.13) where, after using (A.1.18), we arrive at:

$$\mathcal{F}_{2,q}\left(\xi,\frac{Q}{Q_t}\right) = \delta(1-\xi)\left[-2\ln^2\frac{Q}{Q_t}+\frac{3}{2}\ln 2-\frac{\pi^2}{6}\right] - \\ - 2\frac{1+\xi^2}{(1-\xi)_+}\ln\frac{Q}{Q_t}+\frac{1+\xi^2}{1-\xi}\ln\xi-(1+\xi^2)\left[\frac{\ln(1-\xi)}{1-\xi}\right]_+ + \frac{6\xi^2-2\xi-1}{2(1-\xi)_+} - \\ - (1+\xi^2)\left[\frac{\theta(2\xi-1)}{1-\xi}\ln\frac{1-\xi}{\xi}\right]_+ - (12\xi^3-10\xi^2+1)\left[\frac{\theta(2\xi-1)}{2(1-\xi)}\right]_+, \quad \text{(A.1.33)}$$

$$\mathcal{F}_{2,g}\left(\xi,\frac{Q}{Q_t}\right) = -[\xi^2+(1-\xi^2)]\left[4\ln\frac{Q}{Q_t}-2+2\ln\frac{1-\xi}{\xi}\right] - 8\xi(1-\xi) + \\ + (-24\xi^3+36\xi^2-16\xi+2)\theta\,(2\xi-1) - (4\xi^2-4\xi+2)\theta\,(2\xi-1)\ln\frac{1-\xi}{\xi}, \quad \text{(A.1.34)}$$

$$\mathcal{F}_{L,q} = 2\xi\,(2\xi-1)\,\theta\,(2\xi-1)\,, \quad \text{(A.1.35)}$$

and:

$$\mathcal{F}_{L,g} = 8\xi\,(2\xi-1)\,(1-\xi)\theta\,(2\xi-1)\,, \quad \text{(A.1.36)}$$

where we use the results for the leading-order B_{zQ} distribution from ref. [87]. In obtaining the last two equations we exploit the fact that the leading-order B_{zQ} distribution does not acquire any longitudinal contributions [87].

The above results are only valid in the DIS factorisation scheme [117] and can only be used with PDFs which are defined in that scheme. To go to the $\overline{\rm MS}$ scheme we add[3] the leading-order $\overline{\rm MS}$ coefficient functions [118] (see also ref. [88]) to the functions $\mathcal{F}_{2,j}$. We get:

$$\begin{aligned}\mathcal{F}_{2,q}^{\overline{\rm MS}}\left(\xi,\frac{Q}{Q_t}\right) &= \delta(1-\xi)\left[-2\ln^2\frac{Q}{Q_t}+3\ln\frac{Q}{Q_t}+\frac{3}{2}\ln 2-\frac{\pi^2}{2}-\frac{9}{2}\right]- \\ &\quad -2\left[\frac{1+\xi^2}{1-\xi}\right]_+\ln\frac{Q}{Q_t}+1-\xi-(1+\xi^2)\left[\frac{\theta(2\xi-1)}{1-\xi}\ln\left(\frac{1-\xi}{\xi}\right)\right]_+- \\ &\quad -(12\xi^3-10\xi^2+1)\left[\frac{\theta(2\xi-1)}{2(1-\xi)}\right]_+, \qquad \text{(A.1.37)}\end{aligned}$$

$$\begin{aligned}\mathcal{F}_{2,g}^{\overline{\rm MS}}\left(\xi,\frac{Q}{Q_t}\right) &= -4[\xi^2+(1-\xi)^2]\ln\frac{Q}{Q_t}+4\xi(1-\xi)+ \\ &\quad +\left\{2(2\xi-1)(-6\xi^2+6\xi-1)-2[\xi^2+(1-\xi)^2]\ln\frac{1-\xi}{\xi}\right\}\theta\left(2\xi-1\right). \qquad \text{(A.1.38)}\end{aligned}$$

In eq. (A.1.37) we use the fact that:

$$\frac{1+\xi^2}{(1-\xi)_+} \;=\; \left(\frac{1+\xi^2}{1-\xi}\right)_+ - \frac{3}{2}\delta(1-\xi). \qquad \text{(A.1.39)}$$

The $(2n_f+1)\times 1$ matrices $\boldsymbol{C}_0$ and $\boldsymbol{C}_1$ are defined such that their transposes are given by:

$$\boldsymbol{C}_0^T(z) = \begin{pmatrix} e_u^2\,\delta(1-z) \\ e_u^2\,\delta(1-z) \\ \vdots \\ 0 \end{pmatrix}, \qquad \text{(A.1.40)}$$

and:

$$\boldsymbol{C}_1^T(z) = \begin{pmatrix} C_F\,e_u^2\left\{\mathcal{F}_{2,q}^{\overline{\rm MS}}(z,1)-\frac{y^2}{1+(1-y)^2}\mathcal{F}_{L,q}(z,1)\right\} \\ C_F\,e_u^2\left\{\mathcal{F}_{2,q}^{\overline{\rm MS}}(z,1)-\frac{y^2}{1+(1-y)^2}\mathcal{F}_{L,q}(z,1)\right\} \\ \vdots \\ T_f\left\{\mathcal{F}_{2,g}^{\overline{\rm MS}}(z,1)-\frac{y^2}{1+(1-y)^2}\mathcal{F}_{L,g}(z,1)\right\} \end{pmatrix}. \qquad \text{(A.1.41)}$$

[3]We exclude the longitudinal pieces in the addition because they are scheme-independent.

A.2 The radiator

The radiator for the Q_t distribution we studied in chapter 4 is given by:

$$R(Q/Q_t) = Lg_1(\alpha_s L) + g_2(\alpha_s L)\,, \tag{A.2.1}$$

where $L = \ln(Q/Q_t)$ and in the $\overline{\text{MS}}$ scheme we have:

$$g_1(\alpha_s L) = -\frac{C_F}{\pi\beta_0}\left[1 + \frac{\ln(1-2\lambda)}{2\lambda}\right], \tag{A.2.2}$$

$$\begin{aligned} g_2(\alpha_s L) = \frac{3C_F}{4\pi\beta_0}\ln(1-2\lambda) + \frac{C_F K_F}{4\pi^2\beta_0^2}\left[\ln(1-2\lambda) + \frac{2\lambda}{1-2\lambda}\right] - \\ - \frac{C_F\beta_1}{2\pi\beta_0^3}\left[\frac{2\lambda + \ln(1-2\lambda)}{1-2\lambda} + \frac{1}{2}\ln^2(1-2\lambda)\right], \end{aligned} \tag{A.2.3}$$

with $\lambda = \alpha_s(Q^2)\beta_0 L$ and:

$$\beta_1 = \frac{17C_A^2 - 5C_A n_f - 3C_F n_f}{24\pi^2}\,. \tag{A.2.4}$$

In obtaining this we use eq.(4.2.12) and the two-loop QCD β function to replace the scale of α_s with Q^2 and moved from the CMW [74] scheme to the $\overline{\text{MS}}$ scheme (see e.g. ref. [87]). The derivative of the radiator with respect to $\ln b$ at $\bar{b}\,Q = Q/Q_t$ is given by:

$$R'(Q/Q_t) = \frac{2C_F}{\pi\beta_0}\frac{\lambda}{1-2\lambda}\,. \tag{A.2.5}$$

The expansion of the resummed result (eq.(4.3.3)) to $\mathcal{O}(\bar{\alpha}_s)$ and $\mathcal{O}(\bar{\alpha}_s^2)$, which is needed in eq. (4.4.1), yields:

$$\sigma_r^{(1)}/\sigma_0 = G_{11}L + G_{12}L^2 - 2\frac{\boldsymbol{C}_0 \otimes \boldsymbol{P}^{(0)} \otimes \boldsymbol{q}(x,Q^2)}{q(x,Q^2)}L + \frac{\boldsymbol{C}_1 \otimes \boldsymbol{q}(x,Q^2)}{q(x,Q^2)}\,, \tag{A.2.6}$$

$$\begin{aligned} \sigma_r^{(2)}/\sigma_0 = G_{22}L^2 + G_{23}L^3 + \frac{1}{2}G_{12}^2L^4 + \\ + \frac{\boldsymbol{C}_1 \otimes \boldsymbol{q}(x,Q^2)}{q(x,Q^2)}\left(G_{11}L + G_{12}L^2\right) + 2\frac{\boldsymbol{C}_0 \otimes \boldsymbol{P}^{(0)} \otimes \boldsymbol{P}^{(0)} \otimes \boldsymbol{q}(x,Q^2)}{q(x,Q^2)}L^2 - \\ - 2\left((G_{11} + 2\pi\beta_0)L^2 + G_{12}L^3\right)\frac{\boldsymbol{C}_0 \otimes \boldsymbol{P}^{(0)} \otimes \boldsymbol{q}(x,Q^2)}{q(x,Q^2)}\,, \end{aligned} \tag{A.2.7}$$

where $\boldsymbol{P}^{(0)}$ is the matrix of leading-order splitting functions (defined in eqs. (2.5.2) to (2.5.5)) and the coefficients G_{mn} are given in table A.2. In the above we exploit eq. (2.5.13). One can clearly see that the expansion of the resummed result to $\mathcal{O}(\alpha_s)$ reproduces the leading-order result given by eq. (A.1.13).

G_{12}	$-2\,C_F$
G_{11}	$3\,C_F$
G_{23}	$-6\,C_F^2 - \frac{16}{3}\pi\,C_F\beta_0$
G_{22}	$-\frac{\pi^2}{3}C_F C_A + \frac{9}{2}\,C_F^2 - 2\,C_F K_F + 6\,\pi\,C_F\beta_0$

Table A.2: The coefficients G_{nm} that enter the fixed-order expansion of the resummed result.

Appendix B

The radiator for the dijet azimuthal correlation distribution in DIS

We present here the radiator for the dijet azimuthal correlation distribution in DIS. We do this for the process $q(0) \to q(1) + g(2)$ and generalise the result at the end. In all what follows all symbols have the same meaning as those introduced in chapter 6.

B.1 Dipole "02"

We write the contribution of this dipole to the radiator, I_{02}, as follows:

$$I_{02} = \frac{N_c}{2} \int \frac{dk_\perp}{k_\perp} \frac{\alpha_s(k_\perp^2)}{2\pi} d\eta \frac{d\phi}{2\pi} 2k_t^2 \frac{p_0.p_2}{p_0.k\, p_2.k} \theta\left[k_t - \frac{p_t}{\alpha\bar{b}}\right] \theta\left[p_t - k_t\right], \tag{B.1.1}$$

with

$$k_\perp^2 = 2\frac{(k.p_0)(k.p_2)}{p_0.p_2} = 2k_t^2 \frac{\cosh(\eta_2 - \eta) + \cos\phi}{e^{\eta_2 - \eta}}. \tag{B.1.2}$$

Hence:

$$I_{02} = N_c \int \frac{dk_\perp}{k_\perp} \frac{\alpha_s(k_\perp^2)}{2\pi} d\eta \frac{d\phi}{2\pi} \frac{1}{r^2} \theta\left[k_\perp - \frac{p_t\sqrt{2}r}{\alpha\bar{b}}\right] \theta\left[\sqrt{2}rp_t - k_\perp\right], \tag{B.1.3}$$

where we define:

$$r^2 = \frac{\cosh(\eta_2 - \eta) + \cos\phi}{e^{\eta_2 - \eta}}. \tag{B.1.4}$$

The soft and collinear enhancement around leg "2" comes from the phase-space where $\eta - \eta_2 = \phi - \pi = 0$. For this reason we define:

$$\eta - \eta_2 = \rho \sin\theta, \tag{B.1.5}$$

$$\phi - \pi = \rho \cos\theta, \tag{B.1.6}$$

such that we arrive at:

$$I_{02} = N_c \int \frac{dk_\perp}{k_\perp} \frac{\alpha_s(k_\perp^2)}{2\pi} \rho d\rho \frac{d\theta}{2\pi} \frac{1}{r^2} \theta \left[k_\perp - \frac{p_t \sqrt{2} r}{\alpha \bar{b}} \right] \theta \left[\sqrt{2} r p_t - k_\perp \right]. \tag{B.1.7}$$

Evaluating the integral over $k_\perp$ we find:

$$N_c \int_{p_t r\sqrt{2}/\alpha\bar{b}}^{p_t r\sqrt{2}} \frac{dk_\perp}{k_\perp} \frac{\alpha_s(k_\perp^2)}{2\pi} = \frac{C_A}{4\pi\beta_0} \left[\ln(1+2\alpha_s\beta_0 \ln(r\sqrt{2})) - \ln\left(1 + 2\alpha_s\beta_0 \ln\frac{r\sqrt{2}}{\alpha\bar{b}}\right) + \right.$$
$$\left. + \frac{\beta_1}{\beta_0}\alpha_s \left(\frac{1+\ln(1+2\alpha_s\beta_0\ln(r\sqrt{2}))}{1+2\alpha_s\beta_0\ln(r\sqrt{2})} - \frac{1+\ln\left(1+2\alpha_s\beta_0\ln\frac{r\sqrt{2}}{\alpha\bar{b}}\right)}{1+2\alpha_s\beta_0\ln\frac{r\sqrt{2}}{\alpha\bar{b}}} \right) \right]. \tag{B.1.8}$$

The calculation of the contribution of dipole "02" to the radiator proceeds in the following way. We first expand $1/r^2 = 2/\rho^2$. We perform the η and ϕ integrations in the whole phase-space using the definition $\alpha = |\sin\phi|$ and then subtract the contribution from the circles of radius R (in the $\eta - \phi$ plane) which are centred at the outgoing legs, and add their contribution with $\alpha = |\sin\phi - \phi|$ or $|\sin\phi - \pi + \phi|$ accordingly. Then we add the contribution from higher-order terms in the expansion of $1/r^2$.

B.1.1 Contribution with $\alpha = |\sin\phi|$ in the whole phase-space

To NLL accuracy we can write result for the $k_\perp$ integral in eq. (B.1.8) as follows:

$$\frac{C_A}{4\pi\beta_0} \left[\ln\left(1 + 2\alpha_s\beta_0 \ln\rho\right) - \ln\left(1 + 2\alpha_s\beta_0 \ln\frac{1}{\cos\theta\bar{b}}\right) + \right.$$
$$\left. + \frac{\beta_1}{\beta_0}\alpha_s \left(\frac{1+\ln(1+2\alpha_s\beta_0\ln\rho)}{1+2\alpha_s\beta_0\ln\rho} - \frac{1+\ln\left(1+2\alpha_s\beta_0\ln\frac{1}{b}\right)}{1+2\alpha_s\beta_0\ln\frac{1}{b}} \right) \right], \tag{B.1.9}$$

where we use the symmetry of the θ integral and chose the region $-\pi/2 < \theta < \pi/2$ such that $|\cos\theta| = \cos\theta$. Here we replace $d\theta/(2\pi) \to d\theta/\pi$. From eq. (B.1.7) one can deduce that $\alpha\bar{b} > 1$, a condition that can be applied to the ρ integral such that $\rho > g(\bar{b})/\cos\theta$, with $g(\bar{b})$ being the function that satisfies $\sin(g) = 1/\bar{b}$. To NLL

accuracy it suffices to write $g(\bar{b}) = 1/\bar{b}$ for this case. The upper limit on the ρ integral is $\pi/\cos\theta$. Thus we may write the contribution under consideration, $I_{02}^{\rm all}$, as:

$$I_{02}^{\rm all} = \frac{C_A}{4\pi\beta_0}\int_{-\pi/2}^{\pi/2}\frac{d\theta}{\pi}\int_{g/\cos\theta}^{\pi/\cos\theta}\frac{2}{\rho}d\rho \times k_\perp \text{ integral}, \tag{B.1.10}$$

where "$k_\perp$ intergal" stands for the result appearing in eq. (B.1.9). The above integral can be solved and one can remove all subleading terms leaving only up to NLL terms. We write the result for this as:

$$I_{02}^{\rm all} = \frac{C_A}{4\pi\beta_0}\Bigg[-\frac{\beta_1}{\beta_0^2}\left(\frac{1}{2}\ln^2(1-2\lambda)+\frac{\ln(1-2\lambda)+2\lambda}{1-2\lambda}\right)-L\frac{2\lambda+\ln(1-2\lambda)}{\lambda}- \\ -2\ln 2\left(\frac{2\lambda}{1-2\lambda}+\ln(1-2\lambda)\right)-2\ln\pi\ln(1-2\lambda)\Bigg], \tag{B.1.11}$$

with $\lambda = \alpha_s(p_t^2)\beta_0 L$ and $L = \ln\bar{b}$. We have used the fact that $\int_{-\pi/2}^{\pi/2} d\theta/\pi \ln(\sec\theta) = \ln 2$. Next we calculate the contribution from the region around leg "2" with $\alpha = |\sin\phi|$ (which we shall subtract later).

B.1.2 Contribution with $\alpha = |\sin\phi|$ around leg "2"

We now calculate the contribution of the region around leg "2" with $\alpha = |\sin\phi|$, $I_{02}^{-\rm c2}$, i.e. perform the following integral:

$$I_{02}^{-\rm c2} = \frac{C_A}{4\pi\beta_0}\int_{-\pi/2}^{\pi/2}\frac{d\theta}{\pi}\int_{g/\cos\theta}^{R}\frac{2}{\rho}d\rho \times k_\perp \text{ integral}. \tag{B.1.12}$$

The result to NLL accuracy reads:

$$I_{02}^{-\rm c2} = \frac{C_A}{4\pi\beta_0}\Bigg[-\frac{\beta_1}{\beta_0^2}\left(\frac{1}{2}\ln^2(1-2\lambda)+\frac{\ln(1-2\lambda)+2\lambda}{1-2\lambda}\right)-L\frac{2\lambda+\ln(1-2\lambda)}{\lambda}- \\ -4\ln 2\frac{\lambda}{1-2\lambda}-2\ln R\ln(1-2\lambda)\Bigg]. \tag{B.1.13}$$

Next we calculate the contribution of the region around leg "2" with $\alpha = |\sin\phi - \pi + \phi|$.

B.1.3 Contribution with $\alpha = |\sin\phi - \pi + \phi|$ around leg "2"

We now calculate the term:

$$I_{02}^{+\rm c2} = \frac{C_A}{4\pi\beta_0}\int_{-\pi/2}^{\pi/2}\frac{d\theta}{\pi}\int_{g/\cos\theta}^{R}\frac{2}{\rho}d\rho \times k_\perp \text{ integral}, \tag{B.1.14}$$

where now g satisfies $g - \sin g = 1/\bar{b}$, which to NLL accuracy gives: $g = \sqrt[3]{6/\bar{b}}$. The result for the "$k_\perp$ integral" now has the form:

$$\frac{C_A}{4\pi\beta_0}\Bigg[\ln\left(1+2\alpha_s\beta_0\ln\rho\right) - \ln\left(1+2\alpha_s\beta_0\ln\frac{6}{\rho^2\cos^3\theta\bar{b}}\right) + \\ + \frac{\beta_1}{\beta_0}\alpha_s\left(\frac{1+\ln(1+2\alpha_s\beta_0\ln\rho)}{1+2\alpha_s\beta_0\ln\rho} - \frac{1+\ln\left(1+2\alpha_s\beta_0\ln\frac{1}{\rho^2\bar{b}}\right)}{1+2\alpha_s\beta_0\ln\frac{1}{\rho^2\bar{b}}}\right)\Bigg]. \quad \text{(B.1.15)}$$

The result reads:

$$I_{02}^{+\mathrm{c2}} = \frac{C_A}{4\pi\beta_0}\Bigg[L\left(\frac{1-2\lambda}{2\lambda}\ln(1-2\lambda) - \frac{3-2\lambda}{2\lambda}\ln\left(1-\frac{2}{3}\lambda\right)\right) + \\ + \frac{\beta_1}{2\beta_0^2}\left(\frac{1}{2}\ln^2(1-2\lambda) - \frac{3}{2}\ln^2\left(1-\frac{2}{3}\lambda\right) + \ln(1-2\lambda) - 3\ln\left(1-\frac{2}{3}\lambda\right)\right) - \\ - (\ln 3 + 4\ln 2)\left(\ln\left(1-\frac{2}{3}\lambda\right) - \ln(1-2\lambda)\right) - 2\ln R\ln(1-2\lambda)\Bigg]. \quad \text{(B.1.16)}$$

The last term in the equation just above cancels that in $I_{02}^{-\mathrm{c2}}$, thus there is no dependence of the radiator on the radius parameter R.

Since there are no singularities around leg "1" in the case of dipole "02" one can deduce that the addition and subtraction of the contributions around leg "1" with the corresponding definitions of the observable cancel each other. We therefore discard the calculation of this piece.

B.1.4 Soft and collinear enhancement around leg "0"

To calculate the contribution from higher-order terms in the expansion of $1/r^2$ (which correspond to soft and collinear emissions from the incoming leg) we restore the integral in consideration to its original form, eq. (B.1.3), and subtract the piece we already calculated. We thus write the contribution of the remaining terms, $I_{02}^{(0)}$, as:

$$I_{02}^{(0)} = N_c\int\frac{dk_\perp}{k_\perp}\frac{\alpha_s(k_\perp^2)}{2\pi}d\eta\frac{d\phi}{2\pi}\left(\frac{1}{r^2} - \frac{2}{(\eta-\eta_2)^2+(\phi-\pi)^2}\right)\times \\ \times\,\theta\left[k_\perp - \frac{p_t r\sqrt{2}}{\alpha\bar{b}}\right]\theta\left[p_t r\sqrt{2} - k_\perp\right]\theta\left[\eta - \ln\frac{k_t\xi}{Q}\right]. \quad \text{(B.1.17)}$$

In this equation we introduce the cut-off on η, $\theta\left[\eta - \ln(k_t\xi/Q)\right]$ (which only contributes for soft and collinear emissions to the incoming leg), originating from the

requirement that $\omega < E_0$, with ω and E_0 being the energies of the soft gluon and the incoming leg respectively.

The singularities around $\eta - \eta_2 = \phi - \pi = 0$ cancel between the two terms in this subtraction. To avoid such singularities we introduce a small cut-off ϵ on the integral over η around η_2 and show that this cancels as anticipated. Let us start by evaluating the ϕ and η integrals. We have:

$$\begin{aligned}\int_{\ln\frac{k_t\xi}{Qe^{B_0}}}^{+\infty} d\eta \int_0^{2\pi} \frac{d\phi}{2\pi}\frac{1}{r^2} &= 2\eta_2 - 2\ln\frac{k_t\xi}{Q} + 2B_0 - 2\ln 2 - 2\ln\epsilon \\ &= 2\ln\frac{Q_{02}^2}{p_t^2} - 2\ln\frac{k_t}{p_t} + 2B_0 - 2\ln 2 - 2\ln\epsilon, \quad \text{(B.1.18)}\end{aligned}$$

where $Q_{ij}^2 = 2p_i.p_j$ and we use the fact that $\eta_i = \ln(2\xi p_i.p_0/(Qp_t))$. To account for hard collinear emissions to the incoming leg we have replaced Q by Qe^{B_0} (see e.g refs. [88, 111]) in this equation, where B_i stands for the "hard collinear factor" for leg "i". We have:

$$\begin{aligned}B_i &= -\frac{3}{4}, && \text{for quark legs,} \\ B_i &= -\frac{11C_A - 4T_R n_f}{12C_A}, && \text{for gluon legs.} \quad \text{(B.1.19)}\end{aligned}$$

Note that we neglect the dependence of the theta functions containing r on η and ϕ, which is valid to NLL accuracy (see below).

The integral over η and ϕ of the subtracted term gives:

$$\int_{-\infty}^{+\infty} d\eta \int_0^{2\pi} \frac{d\phi}{2\pi}\frac{2}{(\eta_2-\eta)^2 + (\pi-\phi)^2} = 2\ln\pi - 2\ln\epsilon, \quad \text{(B.1.20)}$$

where we use the freedom to set $k_t \to 0$ in the theta function $\theta[\eta - \ln(k_t\xi/Q)]$ since this term is regular as $\eta \to -\infty$ (i.e. the theta function we just mentioned contributes below NLL accuracy in this case). Clearly the terms containing $\ln\epsilon$ cancel between the contributions in eqs. (B.1.18) and (B.1.20) and we are left with the following integral over $k_\perp$:

$$I_{02}^{(0)} = \frac{C_A}{2\pi}\int \frac{dk_\perp}{k_\perp}\alpha_s(k_\perp^2)\left(2\ln\frac{Q_{02}^2}{p_t^2} + 2B_0 - 2\ln 2 - 2\ln\pi - 2\ln\frac{k_\perp}{p_t}\right)\times \\ \times\,\theta\left[k_\perp - \frac{p_t}{\alpha\bar{b}}\right]\theta\left[p_t - k_\perp\right], \quad \text{(B.1.21)}$$

where we set $r \to 1/\sqrt{2}$, which is valid to NLL accuracy in the region where $\eta \to -\infty$. The $k_\perp$ integration over the first four terms in right hand side of the above equation

gives the result:

$$-\frac{C_A}{4\pi\beta_0}\ln(1-2\lambda)\left(2\ln\frac{Q_{02}^2}{p_t^2}+2B_0-2\ln 2-2\ln\pi\right). \tag{B.1.22}$$

Notice that the term containing $\ln\pi$ will cancel that in eq. (B.1.11). The integral over the term which contains $\ln k_\perp/p_t$ gives:

$$\frac{C_A}{4\pi\beta_0}\Bigg[-\frac{\beta_1}{\beta_0^2}\left(\frac{1}{2}\ln^2(1-2\lambda)+\frac{\ln(1-2\lambda)+2\lambda}{1-2\lambda}\right)-L\frac{2\lambda+\ln(1-2\lambda)}{\lambda}- \\ -2\ln\frac{1}{\alpha^2}\frac{\lambda}{1-2\lambda}\Bigg]. \tag{B.1.23}$$

Averaging[1] over ϕ using $\alpha=|\sin\phi|$ (we are away from legs "1" and "2" and thus we are safe to use the $|\sin\phi|$ definition of the observable) and assembling the result we get:

$$I_{02}^{(0)}=\frac{C_A}{4\pi\beta_0}\Bigg[-\frac{\beta_1}{\beta_0^2}\left(\frac{1}{2}\ln^2(1-2\lambda)+\frac{\ln(1-2\lambda)+2\lambda}{1-2\lambda}\right)-L\frac{2\lambda+\ln(1-2\lambda)}{\lambda}- \\ -4\ln 2\frac{\lambda}{1-2\lambda}-2\ln(1-2\lambda)\left(\ln\frac{Q_{02}^2}{p_t^2}+B_0-\ln 2-\ln\pi\right)\Bigg]. \tag{B.1.24}$$

Note that since we now include hard collinear emissions to the incoming legs PDFs must be evolved to the scale $\mu_f^2/\bar{b}^2$.

B.1.5 The final result for dipole "02"

Assembling all the bits of the answer we arrive at the final result for dipole "02": $I_{02}=I_{02}^{\text{all}}-I_{02}^{-c2}+I_{02}^{+c2}+I_{02}^{(0)}$. Thus we arrive at the following result:

$$I_{02}=\frac{C_A}{4\pi\beta_0}\Bigg[L\left(\frac{1-2\lambda}{2\lambda}\ln(1-2\lambda)-\frac{3-2\lambda}{2\lambda}\ln\left(1-\frac{2}{3}\lambda\right)\right)+ \\ +\frac{\beta_1}{2\beta_0^2}\left(\frac{1}{2}\ln^2(1-2\lambda)-\frac{3}{2}\ln^2\left(1-\frac{2}{3}\lambda\right)+\ln(1-2\lambda)-3\ln\left(1-\frac{2}{3}\lambda\right)\right)- \\ -(\ln 3+4\ln 2)\left(\ln\left(1-\frac{2}{3}\lambda\right)-\ln(1-2\lambda)\right)- \\ -\frac{\beta_1}{\beta_0^2}\left(\frac{1}{2}\ln^2(1-2\lambda)+\frac{\ln(1-2\lambda)+2\lambda}{1-2\lambda}\right)-L\frac{2\lambda+\ln(1-2\lambda)}{\lambda}- \\ -4\ln 2\frac{\lambda}{1-2\lambda}-2\ln(1-2\lambda)\left(\ln\frac{Q_{02}^2}{p_t^2}+B_0\right)\Bigg]. \tag{B.1.25}$$

[1] This means we replace $\ln(1/\alpha^2)\to\int_0^{2\pi}d\phi/(2\pi)\ln(1/\alpha^2)$. This is valid to NLL accuracy.

B.2 Dipole "01"

The result for this dipole is the same as that for dipole "02" with the substitutions $C_A \to -1/C_A$ and $Q_{02} \to Q_{01}$.

B.3 Dipole "12"

The expression for the contribution of dipole "12" to the radiator, I_{12}, has the form given in eq. (B.1.3) but now with:

$$\frac{1}{r^2} = \frac{1+\cosh\Delta\eta}{\cosh(\eta-\eta_1)+\cosh(\eta-\eta_2)}\left(\frac{1}{\cosh(\eta-\eta_2)+\cos\phi}+\frac{1}{\cosh(\eta-\eta_1)-\cos\phi}\right), \tag{B.3.1}$$

where $\Delta\eta = \eta_2 - \eta_1$. We first use the same definition for ρ and θ as before and concentrate on the first term of eq. (B.3.1). One can expand:

$$\rho\frac{1+\cosh\Delta\eta}{\cosh(\eta-\eta_1)+\cosh(\eta-\eta_2)}\frac{1}{\cosh(\eta-\eta_2)+\cos\phi} = \frac{2}{\rho}+\mathcal{O}(1). \tag{B.3.2}$$

To NLL accuracy it suffices to consider $r = \rho/\sqrt{2}$ in the expression for the $k_\perp$ integral in this case (eq. (B.1.8) with r being defined in eq. (B.3.1)). Thus the result for integrating over $k_\perp$, η and ϕ (using only the first term in the expansion of $1/r^2$) is identical to that for dipole "02" (i.e. $I_{02}^{\text{all}} - I_{02}^{-c2} + I_{02}^{+c2}$). Thus we write the result as:

$$\begin{aligned} I_{12}^{\text{sc}} = 2\times\frac{C_A}{4\pi\beta_0}\Bigg[& L\left(\frac{1-2\lambda}{2\lambda}\ln(1-2\lambda)-\frac{3-2\lambda}{2\lambda}\ln\left(1-\frac{2}{3}\lambda\right)\right)+ \\ & +\frac{\beta_1}{2\beta_0^2}\left(\frac{1}{2}\ln^2(1-2\lambda)-\frac{3}{2}\ln^2\left(1-\frac{2}{3}\lambda\right)+\ln(1-2\lambda)-3\ln\left(1-\frac{2}{3}\lambda\right)\right)- \\ & -(\ln 3+4\ln 2)\left(\ln\left(1-\frac{2}{3}\lambda\right)-\ln(1-2\lambda)\right)-2\,(\ln\pi+\ln 2)\ln(1-2\lambda)\Bigg], \end{aligned} \tag{B.3.3}$$

where I_{12}^{sc} stands for the contribution from the soft and collinear region to both legs "1" and "2" and the factor 2 accounts for the fact that we get the same result for the second term in the expression of $1/r^2$ in eq. (B.3.1).

We now treat higher-order terms in the expansion (B.3.2). We write the contribution form these terms as:

$$I_{12}^{\text{sw}} = 2\times\frac{C_A}{2\pi}\int\frac{dk_\perp}{k_\perp}\alpha_s(k_\perp^2)\int_{-\infty}^{+\infty}d\eta\int_0^{2\pi}\frac{d\phi}{2\pi}\left(\frac{1}{r_1^2}-\frac{2}{(\eta_2-\eta)^2+(\pi-\phi)^2}\right), \tag{B.3.4}$$

where $I_{12}^{\rm sw}$ stands for the contribution from the soft wide-angle region to both legs "1" and "2", $1/r_1^2$ stands for the first term in eq. (B.3.1) and the factor 2 stands for the fact that we get the same result by considering the second term in eq. (B.3.1). Integrating over the first term in eq. (B.3.4) we get:

$$-2\times\frac{C_A}{4\pi\beta_0}\ln(1-2\lambda)\left(2\ln\cosh\frac{\Delta\eta}{2}-2\ln\epsilon\right). \tag{B.3.5}$$

The second term in eq. (B.3.4) gives:

$$-2\times\frac{C_A}{4\pi\beta_0}\ln(1-2\lambda)(2\ln\pi-2\ln\epsilon), \tag{B.3.6}$$

where we introduce a cut-off around $\eta=\eta_2$, which cancels when subtracting the two terms. Below we write the full result for this dipole.

B.3.1 The final result for dipole "12"

Assembling the result for dipole I_{12} we arrive at:

$$\begin{aligned}I_{12}=2\times\frac{C_A}{4\pi\beta_0}\Bigg[&L\left(\frac{1-2\lambda}{2\lambda}\ln(1-2\lambda)-\frac{3-2\lambda}{2\lambda}\ln\left(1-\frac{2}{3}\lambda\right)\right)+\\&+\frac{\beta_1}{2\beta_0^2}\left(\frac{1}{2}\ln^2(1-2\lambda)-\frac{3}{2}\ln^2\left(1-\frac{2}{3}\lambda\right)+\ln(1-2\lambda)-3\ln\left(1-\frac{2}{3}\lambda\right)\right)-\\&-(\ln3+4\ln2)\left(\ln\left(1-\frac{2}{3}\lambda\right)-\ln(1-2\lambda)\right)-2\ln\frac{Q_{12}}{p_t}\ln(1-2\lambda)\Bigg],\end{aligned} \tag{B.3.7}$$

where we use the fact that $2\cosh(\Delta\eta/2)=Q_{12}/p_t$.

B.4 The assembled result

The assembled result for all dipole contributions is given by[2]:

$$
\begin{aligned}
R(\bar{b}) = \frac{C_1+C_2}{2\pi\beta_0}\Bigg[& L\left(\frac{1-2\lambda}{2\lambda}\ln(1-2\lambda) - \frac{3-2\lambda}{2\lambda}\ln\left(1-\frac{2}{3}\lambda\right)\right) + \\
& + \frac{\beta_1}{2\beta_0^2}\left(\frac{1}{2}\ln^2(1-2\lambda) - \frac{3}{2}\ln^2\left(1-\frac{2}{3}\lambda\right) + \ln(1-2\lambda) - 3\ln\left(1-\frac{2}{3}\lambda\right)\right) - \\
& - (\ln 3 + 4\ln 2)\left(\ln\left(1-\frac{2}{3}\lambda\right) - \ln(1-2\lambda)\right)\Bigg] + \\
& + \frac{C_0}{2\pi\beta_0}\Bigg[- \frac{\beta_1}{\beta_0^2}\left(\frac{1}{2}\ln^2(1-2\lambda) + \frac{\ln(1-2\lambda)+2\lambda}{1-2\lambda}\right) - L\frac{2\lambda+\ln(1-2\lambda)}{\lambda} - \\
& - 4\ln 2\frac{\lambda}{1-2\lambda}\Bigg] - \\
& - \frac{1}{2\pi\beta_0}\ln(1-2\lambda)\left(C_A\ln\frac{Q_{qg}^2}{p_t^2} - \frac{1}{C_A}\frac{Q_{q\bar{q}}^2}{p_t^2} + C_A\ln\frac{Q_{\bar{q}g}^2}{p_t^2} + 2C_0B_0\right), \quad \text{(B.4.1)}
\end{aligned}
$$

where C_i represents the colour factor of the i^{th} leg ($C_i = C_F$ for quarks and $C_i = C_A$ for gluons) and B_0 accounts for hard collinear emissions to the incoming leg "0".

Changing the coupling from the CMW scheme [74] to the $\overline{\text{MS}}$ scheme results in the addition of the terms:

$$
\frac{K_F}{2\pi\beta_0}\left(\frac{C_1+C_2}{2\pi\beta_0}\left[\frac{3}{2}\ln\left(1-\frac{2}{3}\lambda\right) - \frac{1}{2}\ln(1-2\lambda)\right] + \frac{C_0}{2\pi\beta_0}\left[\ln(1-2\lambda) + 2\frac{\lambda}{1-2\lambda}\right]\right), \quad \text{(B.4.2)}
$$

to the radiator. Similarly changing the scale of the coupling from p_t to Q results in the additions of the terms:

$$
\ln\frac{Q^2}{p_t^2}\left(\frac{C_1+C_2}{2\pi\beta_0}\left[\frac{3}{2}\ln\left(1-\frac{2}{3}\lambda\right) - \frac{1}{2}\ln(1-2\lambda)\right] + \frac{C_0}{2\pi\beta_0}\left[\ln(1-2\lambda) + 2\frac{\lambda}{1-2\lambda}\right]\right), \quad \text{(B.4.3)}
$$

where λ becomes $\alpha_s(Q^2)\beta_0 L$. Finally we account for hard collinear emissions to the outgoing legs by simply adding the SL function [111]:

$$
-\frac{1}{\pi\beta_0}\ln\left(1-\frac{2}{3}\lambda\right)\left[C_1B_1 + C_2B_2\right], \quad \text{(B.4.4)}
$$

to the radiator. We can alternatively express the final result for the radiator in the

[2]We also generalise to the case of arbitrary incoming leg.

standard form:

$$R(\bar{b}) = (C_1+C_2)\left[Lr_1(\alpha_s L) + r_2(\alpha_s L) + r_1'(\alpha_s L)\left(-\ln 3 - 4\ln 2 + 3\ln\frac{Q}{p_t}\right)\right] + \\ + C_0\left[LR_1(\alpha_s L) + R_2(\alpha_s L) + R_1'(\alpha_s L)\left(-\ln 2 + \ln\frac{Q}{p_t}\right)\right] + \\ + \zeta(\lambda)\left(C_A \ln\frac{Q_{gq}Q_{gq'}}{Q_{qq'}Q} + 2C_F\ln\frac{Q_{qq'}}{Q}\right) + \zeta(\lambda)C_0B_0 + \zeta(\lambda/3)(C_1B_1+C_2B_2), \tag{B.4.5}$$

where:

$$r_1 = \frac{1}{2\pi\beta_0}\left[\frac{1-2\lambda}{2\lambda}\ln(1-2\lambda) - \frac{3-2\lambda}{2\lambda}\ln\left(1-\frac{2}{3}\lambda\right)\right], \tag{B.4.6}$$

$$r_2 = \frac{\beta_1}{4\pi\beta_0^3}\left[\frac{1}{2}\ln^2(1-2\lambda) - \frac{3}{2}\ln^2\left(1-\frac{2}{3}\lambda\right) + \ln(1-2\lambda) - 3\ln\left(1-\frac{2}{3}\lambda\right)\right] + \\ + \frac{K_F}{8\pi^2\beta_0^2}\left[3\ln\left(1-\frac{2}{3}\lambda\right) - \ln(1-2\lambda)\right], \tag{B.4.7}$$

$$R_1 = -\frac{1}{2\pi\beta_0}\frac{2\lambda+\ln(1-2\lambda)}{\lambda}, \tag{B.4.8}$$

$$R_2 = -\frac{\beta_1}{2\pi\beta_0^3}\left[\frac{1}{2}\ln^2(1-2\lambda) + \frac{\ln(1-2\lambda)+2\lambda}{1-2\lambda}\right] + \\ + \frac{K_F}{4\pi^2\beta_0^2}\left[\ln(1-2\lambda) + \frac{2\lambda}{1-2\lambda}\right], \tag{B.4.9}$$

$$r_1' = \frac{\partial r_1}{\partial\ln\bar{b}} = \frac{1}{2\pi\beta_0}\left[\ln\left(1-\frac{2}{3}\lambda\right) - \ln(1-2\lambda)\right], \tag{B.4.10}$$

$$R_1' = \frac{\partial R_1}{\partial\ln\bar{b}} = \frac{1}{2\pi\beta_0}\frac{4\lambda}{1-2\lambda}, \tag{B.4.11}$$

$$\zeta(\lambda) = -\frac{1}{\pi\beta_0}\ln(1-2\lambda). \tag{B.4.12}$$

The derivative of the radiator, to NLL accuracy, is given by:

$$R' = \frac{\partial R}{\partial\ln\bar{b}} = (C_1+C_2)\left(-\ln 3 - 4\ln 2 + 3\ln\frac{Q}{p_t}\right)r_1' + C_0\left(-\ln 2 + \ln\frac{Q}{p_t}\right)R_1', \tag{B.4.13}$$

and the double logarithmic piece of the radiator is:

$$R_{\rm DL}(\bar{b}) = (C_1+C_2)Lr_1(\alpha_s L) + C_0LR_1(\alpha_s L). \tag{B.4.14}$$

B.4.1 Radiator for the hadronic collisions case

The radiator in the case of hadronic collisions can be expressed as:

$$\begin{aligned}\widetilde{R}(\bar{b}) = (C_2+C_3)\left[Lr_1(\alpha_s L)+r_2(\alpha_s L)+r_1'(\alpha_s L)\left(-\ln 3-4\ln 2+3\ln\frac{Q}{p_t}\right)\right]+\\ +(C_0+C_1)\left[LR_1(\alpha_s L)+R_2(\alpha_s L)+R_1'(\alpha_s L)\left(-\ln 2+\ln\frac{Q}{p_t}\right)\right]+\\ +\zeta(\lambda)(C_1B_1+C_0B_0)+\zeta(\lambda/3)(C_2B_2+C_3B_3)+\\ +\zeta(\lambda)\left(C_0+C_1+C_2+C_3\right)\ln\frac{Q_{12}}{Q}, \quad \text{(B.4.15)}\end{aligned}$$

where the subscripts 0, 1, 2 and 3 stand for the two incoming legs and the two outgoing legs respectively. This can easily be obtained by observing the expression for the observable when a single soft and collinear emission to leg "l" is considered (see eqs. (6.2.10) and (6.2.11)) [111].

B.4.2 Expansion of the resummed result

We can express the expansion of the resummed result (in the DIS case) to $\mathcal{O}(\alpha_s^2)$ in b space as follows:

$$\sigma_{\mathcal{B}}^a(\mu_f^2/\bar{b}^2)e^{-R(\bar{b})} = \sigma_{\mathcal{B}}^a(\mu_f^2)(1+\bar{\alpha}_s\sigma_r^{(1)}+\bar{\alpha}_s^2\sigma_r^{(2)}), \quad \text{(B.4.16)}$$

where a stands for quark or gluon channels (as in eq. (6.3.1)), $\bar{\alpha}_s = \alpha_s/(2\pi)$ and:

$$\begin{aligned}\sigma_r^{(1)} &= h_{11}L + h_{12}L^2, & \text{(B.4.17)}\\ \sigma_r^{(2)} &= h_{22}L^2 + h_{23}L^3 + h_{24}L^4, & \text{(B.4.18)}\end{aligned}$$

with

$$\begin{aligned}h_{11} &= G_{11} - 2\frac{\boldsymbol{C}_0^a \otimes \boldsymbol{P}^{(0)} \otimes \boldsymbol{q}(x/\xi,\mu_f^2)}{q_a(x/\xi,\mu_f^2)}, & \text{(B.4.19)}\\ h_{12} &= G_{12}, & \text{(B.4.20)}\\ h_{22} &= G_{22} - 2\left[G_{11}+2\pi\beta_0\right]\frac{\boldsymbol{C}_0^a \otimes \boldsymbol{P}^{(0)} \otimes \boldsymbol{q}(x/\xi,\mu_f^2)}{q_a(x/\xi,\mu_f^2)} +\\ &\quad +2\frac{\boldsymbol{C}_0^a \otimes \boldsymbol{P}^{(0)} \otimes \boldsymbol{P}^{(0)} \otimes \boldsymbol{q}(x/\xi,\mu_f^2)}{q_a(x/\xi,\mu_f^2)} + \frac{1}{2}G_{11}^2, & \text{(B.4.21)}\\ h_{23} &= G_{23} - 2G_{12}\frac{\boldsymbol{C}_0^a \otimes \boldsymbol{P}^{(0)} \otimes \boldsymbol{q}(x/\xi,\mu_f^2)}{q_a(x/\xi,\mu_f^2)} + G_{11}G_{12}, & \text{(B.4.22)}\\ h_{24} &= \frac{1}{2}G_{12}^2, & \text{(B.4.23)}\end{aligned}$$

where we exploit eq. (2.5.13). Here the matrix $\boldsymbol{C}_0^q$ is equal to $\boldsymbol{C}_0$ which we introduced in appendix A.1, while $\boldsymbol{C}_0^g$ (this also has $2n_f+1$ dimensions) is defined such that its transpose is given by:

$$\boldsymbol{C}_0^{g,T}(z) = \begin{pmatrix} 0 \\ 0 \\ \vdots \\ \delta(1-z) \end{pmatrix}. \tag{B.4.24}$$

The coefficients G_{nm} are given by:

$$\begin{aligned}
G_{11} &= -\Bigg[4C_0B_0 + \frac{4}{3}\left(C_1B_1 + C_2B_2\right) + 4\left(C_A \ln\frac{Q_{gq}Q_{gq'}}{Q_{qq'}Q} + 2C_F\ln\frac{Q_{qq'}}{Q}\right) + \\
&\quad +4C_0\left(-\ln 2 + \ln\frac{Q}{p_t}\right) + \frac{4}{3}\left(-\ln 3 - 4\ln 2 + 3\ln\frac{Q}{p_t}\right)(C_1+C_2)\Bigg], &\text{(B.4.25)}\\
G_{12} &= -2\left(C_0 + \frac{C_1+C_2}{3}\right), &\text{(B.4.26)}\\
G_{22} &= -8\pi\beta_0\left(C_0B_0 + \frac{C_1B_1+C_2B_2}{9}\right) - 2K_F\left(C_0 + \frac{C_1+C_2}{3}\right) + \\
&\quad -8\pi\beta_0\left(2C_0\left[-\ln 2 + \ln\frac{Q}{p_t}\right] + \frac{4}{9}(C_1+C_2)\left[-\ln 3 - 4\ln 2 + 3\ln\frac{Q}{p_t}\right]\right) + \\
&\quad -8\pi\beta_0\left(C_A\ln\frac{Q_{gq}Q_{gq'}}{Q_{qq'}Q} + 2C_F\ln\frac{Q_{qq'}}{Q}\right), &\text{(B.4.27)}\\
G_{23} &= -\frac{8\pi\beta_0}{3}\left(2C_0 + \frac{4}{9}(C_1+C_2)\right). &\text{(B.4.28)}
\end{aligned}$$

The formal expansion of the resummed distribution to $\mathcal{O}(\alpha_s^2)$ in Δ space is expressed as:

$$\Sigma_r(\Delta) = \Sigma_0 + \Sigma_r^{(1)} + \Sigma_r^{(2)}, \tag{B.4.29}$$

where Σ_0 is the Born cross-section for dijet production in DIS. We have:

$$\begin{aligned}
\Sigma_0 &= \sum_{a=q,g} d\mathcal{B}\sigma_{\mathcal{B}}^a(\mu_f^2), &\text{(B.4.30)}\\
\Sigma_r^{(1)} &= H_{11}\ln\frac{1}{\Delta} + H_{12}\ln^2\frac{1}{\Delta}, &\text{(B.4.31)}\\
\Sigma_r^{(2)} &= H_{22}\ln^2\frac{1}{\Delta} + H_{23}\ln^3\frac{1}{\Delta} + H_{24}\ln^4\frac{1}{\Delta}, &\text{(B.4.32)}
\end{aligned}$$

with $H_{ij} = \bar{\alpha}_s^i \sum_{a=q,g} d\mathcal{B}\sigma_{\mathcal{B}}^a(\mu_f^2)h_{ij}$ for all but the H_{22} term. For H_{22} we have:

$$H_{22} = \bar{\alpha}_s^2 \sum_{a=q,g} d\mathcal{B}\sigma_{\mathcal{B}}^a(\mu_f^2)(h_{22} + \pi^2/4\, G_{12}^2). \tag{B.4.33}$$

Appendix C

The functions f_{ij}

We present here expressions for the functions f_{ij} which are needed in chapter 7. We define η_3 and η_4 to be the rapidities of the outgoing hard legs. We specify the kinematics of the particles as follows:

$$p_1 = x_1\sqrt{s}/2\,(1,0,0,-1)\,, \tag{C.0.1}$$

$$p_2 = x_2\sqrt{s}/2\,(1,0,0,1)\,, \tag{C.0.2}$$

$$p_3 = P_t\,(\cosh\eta_3, 1, 0, \sinh\eta_3)\,, \tag{C.0.3}$$

$$p_4 = P_t\,(\cosh\eta_4, -1, 0, \sinh\eta_4)\,, \tag{C.0.4}$$

$$k = k_t\,(\cosh\eta, \cos\phi, \sin\phi, \sinh\eta)\,, \tag{C.0.5}$$

where s is the hadronic centre-of-mass energy squared, related to $\hat{s}$ (the partonic centre-of-mass energy squared) by $\hat{s} = x_1x_2s$, with x_1 x_2 being the momentum fractions of the incoming protons, carried by the struck partons "1" and "2" respectively.

The functions $f_{ij}(\eta,\phi) = k_t^2\, p_i.p_j/(p_i.k\, p_j.k)$, are given by:

$$f_{12} = 2, \tag{C.0.6}$$

$$f_{13} = \frac{e^{\eta_3-\eta}}{\cosh(\eta_3-\eta)-\cos\phi}, \tag{C.0.7}$$

$$f_{14} = \frac{e^{\eta_4-\eta}}{\cosh(\eta_4-\eta)+\cos\phi}, \tag{C.0.8}$$

$$f_{23} = \frac{e^{-\eta_3+\eta}}{\cosh(\eta_3-\eta)-\cos\phi}, \tag{C.0.9}$$

$$f_{24} = \frac{e^{-\eta_4+\eta}}{\cosh(\eta_4-\eta)+\cos\phi}, \tag{C.0.10}$$

$$f_{34} = \frac{\cosh(\eta_3-\eta_4)+1}{(\cosh(\eta_3-\eta)-\cos\phi)(\cosh(\eta_4-\eta)+\cos\phi)}. \tag{C.0.11}$$

We present below the results for $W_{ij} = \int_\Omega d\eta d\phi/(2\pi) f_{ij}$ which enter the perturbative part of the anomalous dimension matrix:

$$W_{12} = 2\Delta\eta, \tag{C.0.12}$$

$$W_{13} = \left|\Delta\eta + \ln\frac{\sinh(\eta_3 + \Delta\eta/2)}{\sinh(\eta_3 - \Delta\eta/2)}\right|, \tag{C.0.13}$$

$$W_{14} = \left|\Delta\eta + \ln\frac{\sinh(\eta_4 + \Delta\eta/2)}{\sinh(\eta_4 - \Delta\eta/2)}\right|, \tag{C.0.14}$$

$$W_{23} = \left|\Delta\eta - \ln\frac{\sinh(\eta_3 + \Delta\eta/2)}{\sinh(\eta_3 - \Delta\eta/2)}\right|, \tag{C.0.15}$$

$$W_{24} = \left|\Delta\eta - \ln\frac{\sinh(\eta_4 + \Delta\eta/2)}{\sinh(\eta_4 - \Delta\eta/2)}\right|, \tag{C.0.16}$$

$$W_{34} = -2\left|\ln\left[\frac{\cosh\left(\frac{\Delta\eta-\eta_3-\eta_4}{2}\right)}{\cosh\left(\frac{\Delta\eta+\eta_3+\eta_4}{2}\right)}\right]\right| + W_{13} + W_{24}. \tag{C.0.17}$$

The last equation is only valid if $\eta_3\eta_4 > 0$. If $\eta_3\eta_4 < 0$ then $W_{34} = W_{13} + W_{14}$. In the above we assume that the gap Ω is centred at $\eta = 0$ with width $\Delta\eta$ and that it stretches over all azimuths.

The non-perturbative components $C_{ij} = \int_\Omega d\eta d\phi/(2\pi) f_{ij}^{3/2}/\sqrt{2}$, are easily computed numerically.

Bibliography

[1] A. Tricoli, A. M. Cooper-Sarkar and C. Gwenlan, *Uncertainties on W and Z production at the LHC*, *In the proceedings of HERA and the LHC: A Workshop on the Implications of HERA for LHC Physics, Hamburg, Germany, 17-21 Jan 2005* [hep-ex/0509002].

[2] G. Bozzi, S. Catani, D. de Florian and M. Grazzini, *Transverse-momentum resummation and the spectrum of the Higgs boson at the LHC*, *Nucl. Phys.* **B 737** (2006) 73 [hep-ph/0508068].

[3] D. de Florian, M. Grazzini and Z. Kunszt, *Higgs production with large transverse momentum in hadronic collisions at next-to-leading order*, *Phys. Rev. Lett.* **82** (1999) 5209 [hep-ph/9902483].

[4] V. S. Fadin, E. A. Kuraev and L. N. Lipatov, *On the Pomeranchuk Singularity in Asymptotically Free Theories*, *Phys. Lett.* **B 60** (1975) 50.

[5] E. A. Kuraev, L. N. Lipatov and V. S. Fadin, *Multi - Reggeon Processes in the Yang-Mills Theory*, *Sov. Phys. JETP* **44** (1976) 443 [Zh. Eksp. Teor. Fiz. **71** (1976) 840].

[6] E. A. Kuraev, L. N. Lipatov and V. S. Fadin, *The Pomeranchuk Singularity in Nonabelian Gauge Theories*, *Sov. Phys. JETP* **45** (1977) 199 [Zh. Eksp. Teor. Fiz. **72** (1977) 377].

[7] I. I. Balitsky and L. N. Lipatov, *The Pomeranchuk Singularity in Quantum Chromodynamics*, *Sov. J. Nucl. Phys.* **28** (1978) 822 [Yad. Fiz. **28** (1978) 1597].

[8] S. Berge, P. Nadolsky, F. Olness and C. P. Yuan, *Transverse momentum resummation at small x for the Tevatron and LHC*, *Phys. Rev.* **D 72** (2005) 033015 [hep-ph/0410375].

[9] P. Nadolsky, D. R. Stump and C. P. Yuan, *Semi-inclusive hadron production at HERA: The effect of QCD gluon resummation*, *Phys. Rev.* **D 61** (2000) 014003 [Erratum-*ibid.* **D 64** (2001) 059903] [hep-ph/9906280].

[10] M. Dasgupta and Y. Delenda, *The Q_t distribution of the Breit current hemisphere in DIS as a probe of small-x broadening effects*, *J. High Energy Phys.* **08** (2006) 080 [hep-ph/0606285].

[11] K. H. Streng, T. F. Walsh and P. M. Zerwas, *Quark and gluon jets in the Breit frame of lepton-nucleon scattering*, *Zeit. Phys.* **C2** (1979) 237 [DESY 79/10].

[12] R. D. Peccei and R. Rückl, *Energy flow and energy correlations in deep inelastic scattering*, *Nucl. Phys.* **B 162** (1980) 125.

[13] L. V. Gribov, Y. L. Dokshitzer, S. I. Troian and V. A. Khoze, *Manifestation of quantum chromodynamic coherence in deep inelastic scattering*, *Sov. Phys. JETP* **67** (1988) 1303 [Zh. Eksp. Teor. Fiz. **94** (1988) 12].

[14] S. Catani, Y. L. Dokshitzer, M. H. Seymour and B. R. Webber, *Longitudinally-Invariant $k_\perp$-Clustering Algorithms for Hadron-Hadron Collisions*, *Nucl. Phys.* **B 406** (1993) 187 [CERN-TH.6775/93].

[15] S. D. Ellis and D. E. Soper, *Successive combination jet algorithm for hadron collisions*, *Phys. Rev.* **D 48** (1993) 3160 [hep-ph/9305266].

[16] M. Cacciari and G. P. Salam, *Dispelling the N^3 myth for the k_t jet-finder*, *Phys. Lett.* **B 641** (2006) 57 [hep-ph/0512210].

[17] G. P. Salam and G. Soyez, *A practical Seedless Infrared-Safe Cone jet algorithm*, *J. High Energy Phys.* **05** (2007) 086 [arXiv: 0704.0292].

[18] R. B. Appleby and M. H. Seymour, *Non-global logarithms in inter-jet energy flow with k_t clustering requirement*, *J. High Energy Phys.* **12** (2002) 063 [hep-ph/0211426].

[19] A. Banfi and M. Dasgupta, *Problems in resumming interjet energy flows with k_t clustering*, *Phys. Lett.* **B 628** (2005) 49 [hep-ph/0508159].

[20] Y. Delenda, R. Appleby, A. Banfi and M. Dasgupta, *On QCD resummation with k_t clustering*, *J. High Energy Phys.* **12** (2006) 044 [hep-ph/0610242].

[21] M. Dasgupta and G. P. Salam, *Resummation of non-global QCD observables*, *Phys. Lett.* **B 512** (2001) 323 [hep-ph/0104277].

[22] M. Dasgupta and G. P. Salam, *Accounting for coherence in interjet E_t flow: A case study*, *J. High Energy Phys.* **03** (2002) 017 [hep-ph/0203009].

[23] B. Abbott et al. [DØ Collaboration], *Probing hard color-singlet exchange in $p\bar{p}$ collisions at $\sqrt{s} = 630$ GeV and 1800 GeV*, *Phys. Lett.* **B 440** (1998) 189 [hep-ex/9809016].

[24] F. Abe et al. [CDF Collaboration], *Dijet production by color-singlet exchange at the Fermilab Tevatron*, *Phys. Rev. Lett.* **80** (1998) 1156 [FERMILAB-PUB-97-283-E].

[25] F. Abe et al. [CDF Collaboration], *Events with a rapidity gap between jets in $\bar{p}p$ collisions at $\sqrt{s} = 630$ GeV*, *Phys. Rev. Lett.* **81** (1998) 5278 [FERMILAB-PUB-98-334-E].

[26] M. Derrick et al. [ZEUS Collaboration], *Rapidity Gaps between Jets in Photoproduction at HERA*, *Phys. Lett.* **B 369** (1996) 55 [hep-ex/9510012].

[27] C. Adloff et al. [H1 Collaboration], *Energy flow and rapidity gaps between jets in photoproduction at HERA*, *Eur. Phys. J.* **C 24** (2002) 517 [hep-ex/0203011].

[28] S. Chekanov et al. [ZEUS Collaboration], *Photoproduction of events with rapidity gaps between jets at HERA*, *Eur. Phys. J.* **C 50** (2007) 283 [hep-ex/0612008].

[29] J. R. Forshaw, A. Kyrieleis and M. H. Seymour, *Super-leading logarithms in non-global observables in QCD?*, *J. High Energy Phys.* **08** (2006) 059 [hep-ph/0604094].

[30] V. M. Abazov et al. [DØ Collaboration], *Measurement of dijet azimuthal decorrelations at central rapidities in $p\bar{p}$ collisions at $\sqrt{s} = 1.96$ TeV*, *Phys. Rev. Lett.* **94** (2005) 221801 [hep-ex/0409040].

[31] M. Zielinski [DØ Collaboration], *DØ measurement of the dijet azimuthal decorrelations*, *AIP Conf. Proc* **842** (2006) 265 [hep-ex/0602019].

[32] M. Hansson [H1 Collaboration], *Decorrelation of Dijets at Low x and Q^2*, *Prepared for 14th International Workshop on Deep Inelastic Scattering (DIS 2006), Tsukuba, Japan, 20-24 Apr 2006* [H1prelim-06-032].

[33] A. Aktas et al. [H1 Collaboration], *Inclusive dijet production at low Bjorken-x in deep inelastic scattering*, *Eur. Phys. J.* **C 33** (2004) 477 [hep-ex/0310019].

[34] A. Szczurek, N. N. Nikolaev, W. Schafer and J. Speth, *Mapping the proton unintegrated gluon distribution in dijets correlations in real and virtual photoproduction at HERA*, *Phys. Lett.* **B 500** (2001) 254 [hep-ph/0011281].

[35] M. Hansson and H. Jung, *Towards precision determination of uPDFs*, *To appear in the proceedings of 15^{th} International Workshop on Deep-Inelastic Scattering and Related Subjects (DIS 2007), Munich, Germany, 16-20 Apr 2007* [arXiv: 0707.4276].

[36] A. J. Askew, D. Graudenz, J. Kwiecinski and A. D. Martin, *Dijet production at HERA as a probe of BFKL dynamics*, *Phys. Lett.* **B 338** (1994) 92 [hep-ph/9407337].

[37] J. Kwiecinski, A. D. Martin and A. M. Stasto, *Predictions for dijet production in DIS using small x dynamics*, *Phys. Lett.* **B 459** (1999) 644 [hep-ph/9904402].

[38] A. Banfi, M. Dasgupta and Y. Delenda, *Dijet azimuthal correlations in QCD hard processes*, in preparation.

[39] Z. Nagy and Z. Trocsanyi, *Multi-jet cross sections in deep inelastic scattering at next-to-leading order*, *Phys. Rev. Lett.* **87** (2001) 082001 [hep-ph/0104315].

[40] Z. Nagy and Z. Trocsanyi, *Three-jet event-shapes in lepton proton scattering at next-to-leading order accuracy*, *Phys. Lett.* **B 634** (2006) 498 [hep-ph/0511328].

[41] B. R. Webber, *Hadronization*, *In the proceedings of Zuoz 1994 Summer School on Hadronic Aspects of Collider Physics, Zuoz, Switzerland, 1994, pp49* [hep-ph/9411384].

[42] S. Kluth, *Power corrections in electron positron annihilation: Experimental review*, *In the Proceedings of FRIF workshop on first principles non-perturbative QCD of hadron jets, LPTHE, Paris, France, 12-14 Jan 2006, pp R002* [hep-ex/0606046].

[43] T. Kluge, *Review of power corrections in DIS*, *In the Proceedings of FRIF workshop on first principles non-perturbative QCD of hadron jets, LPTHE, Paris, France, 12-14 Jan 2006, pp R003* [hep-ex/0606053].

[44] Y. L. Dokshitzer, G. Marchesini and B. R. Webber, *Dispersive Approach to Power-Behaved Contributions in QCD Hard Processes*, *Nucl. Phys.* **B 469** (1996) 93 [hep-ph/9512336].

[45] Y. L. Dokshitzer and B. R. Webber, *Power corrections to event shape distributions*, *Phys. Lett.* **B 404** (1997) 321 [hep-ph/9704298].

[46] M. Dasgupta and G. P. Salam, *Event shapes in e^+e^- annihilation and deep inelastic scattering*, *J. Phys.* **G 30** (2004) R143 [hep-ph/0312283].

[47] M. Dasgupta and G. P. Salam, *Resummed event-shape variables in DIS*, *J. High Energy Phys.* **08** (2002) 032 [hep-ph/0208073].

[48] Y. L. Dokshitzer and B. R. Webber, *Calculation of power corrections to hadronic event shapes*, *Phys. Lett.* **B 352** (1995) 451 [hep-ph/9504219].

[49] M. Dasgupta and B. R. Webber, *Power corrections to event shapes in deep inelastic scattering*, *Eur. Phys. J.* **C 1** (1998) 539 [hep-ph/9704297].

[50] A. Guffanti and G. E. Smye, *Non-perturbative effects in the W and Z transverse momentum distribution*, *J. High Energy Phys.* **10** (2000) 025 [hep-ph/0007190].

[51] A. Banfi, Y. L. Dokshitzer, G. Marchesini and G. Zanderighi, *Near-to-planar 3-jet events in and beyond QCD perturbation theory*, *Phys. Lett.* **B 508** (2001) 269 [hep-ph/0010267].

[52] A. Banfi, Y. L. Dokshitzer, G. Marchesini and G. Zanderighi, *Non-perturbative QCD analysis of near-to-planar three-jet events*, *J. High Energy Phys.* **03** (2001) 007 [hep-ph/0101205].

[53] A. Banfi, Y. L. Dokshitzer, G. Marchesini and G. Zanderighi, *QCD analysis of D-parameter in near-to-planar three-jet events*, *J. High Energy Phys.* **05** (2001) 040 [hep-ph/0104162].

[54] A. Banfi, *Three-jet event-shapes: first NLO+NLL+1/Q results*, *To appear in the proceedings of* 15^{th} *International Workshop on Deep-Inelastic Scattering and Related Subjects (DIS 2007), Munich, Germany, 16-20 Apr 2007* [arXiv: 0706.2722].

[55] M. Cacciari, M. Dasgupta, L. Magnea and G. Salam, *Power corrections for jets at hadron colliders*, *To appear in the proceedings of* 15^{th} *International Workshop on Deep-Inelastic Scattering and Related Subjects (DIS 2007), Munich, Germany, 16-20 Apr 2007* [arXiv: 0706.3157].

[56] M. Dasgupta and Y. Delenda, *Aspects of power corrections in hadron-hadron collisions*, *submitted to J. High Energy Phys.* [arXiv: 0709.3309]

[57] J. Botts and G. Sterman, *Hard Elastic Scattering in QCD: Leading Behavior*, *Nucl. Phys.* **B 325** (1989) 62 [ITP-SB-89-7].

[58] N. Kidonakis and G. Sterman, *Subleading logarithms in QCD hard scattering*, *Phys. Lett.* **B 387** (1996) 867.

[59] N. Kidonakis and G. Sterman, *Resummation for QCD hard scattering*, *Nucl. Phys.* **B 505** (1997) 321 [hep-ph/9705234].

[60] N. Kidonakis, G. Oderda and G. Sterman, *Evolution of color exchange in QCD hard scattering*, *Nucl. Phys.* **B 531** (1998) 365 [hep-ph/9803241].

[61] J. C. Collins, D. E. Soper and G. Sterman, *Factorization for Short Distance Hadron - Hadron Scattering*, *Nucl. Phys.* **B 261** (1985) 104.

[62] J. C. Collins, D. E. Soper and G. Sterman, *Factorization of Hard Processes in QCD*, *Adv. Ser. Direct. High Energy Phys.* **5** (1988) 1 [hep-ph/0409313].

[63] J. C. Collins, D. E. Soper and G. Sterman, *Soft Gluons and Factorization*, *Nucl. Phys.* **B 308** (1988) 833 [ITP-SB-87-69].

[64] J. C. Collins, D. E. Soper and G. Sterman, *Factorization is not violated*, *Phys. Lett.* **B 438** (1998) 184 [hep-ph/9806234].

[65] V. N. Gribov and L. N. Lipatov, *Deep inelastic e p scattering in perturbation theory*, *Sov. J. Nucl. Phys.* **15** (1972) 438 [*Yad. Fiz.* **15** (1972) 781].

[66] L. N. Lipatov, *The parton model and perturbation theory*, *Sov. J. Nucl. Phys.* **20** (1975) 94 [*Yad. Fiz.* **20** (1974) 181].

[67] G. Altarelli and G. Parisi, *Asymptotic Freedom in Parton Language*, *Nucl. Phys.* **B 126** (1977) 298 [LPTENS-77-6].

[68] Y. L. Dokshitzer, *Calculation of the Structure Functions for Deep Inelastic Scattering and e^+e^- Annihilation by Perturbation Theory in Quantum Chromodynamics (In Russian)*, *Sov. Phys. JETP* **46** (1977) 641 [*Zh. Eksp. Teor. Fiz.* **73** (1977) 1216].

[69] H. D. Politzer, *Reliable Perturbative Results for Strong Interactions?*, *Phys. Rev. Lett.* **30** (1973) 1346.

[70] D. J. Gross and F. Wilczek, *Asymptotically Free Gauge Theories. 1*, *Phys. Rev.* **D 8** (1973) 3633 [FERMILAB-PUB-73-049-THY].

[71] R. D. Peccei and R. Rückl, *Energy flow and energy correlations in deep inelastic scattering*, *Nucl. Phys.* **B 162** (1980) 125 [MPI-PAE/PTh 21/79].

[72] G. Sterman and S. Weinberg, *Jets From Quantum Chromodynamics*, *Phys. Rev. Lett.* **39** (1977) 1436 [HUTP-77/A044].

[73] A. Bassetto, M. Ciafaloni and G. Marchesini, *Jet Structure and Infrared Sensitive Quantities in Perturbative QCD*, *Phys. Rept.* **100** (1983) 201.

[74] S. Catani, B. R. Webber and G. Marchesini, *QCD coherent branching and semi-inclusive processes at large x*, *Nucl. Phys.* **B 349** (1991) 635 [CAVENDISH-HEP-90-11].

[75] P. E. L. Rakow and B. R. Webber, *The Quark Form-Factor in Quantum Chromodynamics*, *Nucl. Phys.* **B 187** (1981) 254.

[76] A. Banfi, G. Marchesini and G. Smye, *Away-from-jet energy flow*, *J. High Energy Phys.* **08** (2002) 006 [hep-ph/0206076].

[77] S. Catani, L. Trentadue, G. Turnock and B. R. Webber, *Resummation of large logarithms in e^+e^- event shape distributions*, *Nucl. Phys.* **B 407** (1993) 3 [CERN-TH-6640-92].

[78] C. F. Berger, T. Kucs and G. Sterman, *Energy flow in interjet radiation*, *Phys. Rev.* **D 65** (2002) 094031 [hep-ph/0110004].

[79] A. Banfi, G. Marchesini, Y. L. Dokshitzer and G. Zanderighi, *QCD analysis of near-to-planar 3-jet events*, *J. High Energy Phys.* **07** (2000) 002 [hep-ph/0004027]

[80] S. Catani and M. Grazzini, *Infrared factorization of tree level QCD amplitudes at the next-to-next-to-leading order and beyond*, *Nucl. Phys.* **B 570** (2000) 287 [hep-ph/9908523].

[81] M. Beneke, *Renormalons*, *Phys. Rept.* **317** (1999) 1 [hep-ph/9807443].

[82] Y. L. Dokshitzer, A. Lucenti, G. Marchesini and G. P. Salam, *Universality of $1/Q$ corrections to jet-shape observables rescued*, *Nucl. Phys.* **B 511** (1998) 396 [Erratum-*ibid.* **B 593** (2001) 729] [hep-ph/9707532].

[83] Y. L. Dokshitzer, A. Lucenti, G. Marchesini and G. P. Salam, *On the universality of the Milan factor for* $1/Q$ *power corrections to jet shapes*, *J. High Energy Phys.* **05** (1998) 003 [hep-ph/9802381].

[84] M. Dasgupta and B. R. Webber, *Two-loop enhancement factor for* $1/Q$ *corrections to event shapes in deep inelastic scattering*, *J. High Energy Phys.* **10** (1998) 001 [hep-ph/9809247].

[85] S. Alekhin et al., *HERA and the LHC - A workshop on the implications of HERA for LHC physics: Proceedings Part A* [hep-ph/0601012]; *Proceedings Part B* [hep-ph/0601013].

[86] J. C. Collins, D. E. Soper and G. Sterman, *Transverse Momentum Distribution in Drell-Yan Pair and W And Z Boson Production*, *Nucl. Phys.* **B 250** (1985) 199 [CERN-TH-3923].

[87] M. Dasgupta and G. P. Salam, *Resummation of the jet broadening in DIS*, *Eur. Phys. J.* **C 24** (2002) 213 [hep-ph/0110213].

[88] V. Antonelli, M. Dasgupta and G. P. Salam, *Resummation of thrust distributions in DIS*, *J. High Energy Phys.* **02** (2000) 001 [hep-ph/9912488].

[89] T. Kluge, private communication.

[90] S. Catani and M. H. Seymour, *The Dipole Formalism for the Calculation of QCD Jet Cross Sections at Next-to-Leading Order*, *Phys. Lett.* **B 378** (1996) 287 [hep-ph/9602277].

[91] S. Catani and M. H. Seymour, *A general algorithm for calculating jet cross sections in NLO QCD*, *Nucl. Phys.* **B 485** (1997) 291 [Erratum-*ibid.* **B 510** (1998) 503] [hep-ph/9605323].

[92] M. Dasgupta and Y. Delenda, work in progress.

[93] G. Parisi and R. Petronzio, *Small Transverse Momentum Distributions in Hard Processes*, *Nucl. Phys.* **B 154** (1979) 427 [CERN-TH-2627].

[94] R. K. Ellis and S. Veseli, *W and Z transverse momentum distributions: Resummation in q_T-space*, *Nucl. Phys.* **B 511** (1998) 649 [hep-ph/9706526].

[95] S. Frixione, P. Nason and G. Ridolfi, *Problems in the resummation of soft-gluon effects in the transverse-momentum distributions of massive vector bosons in hadronic collisions*, *Nucl. Phys.* **B 542** (1999) 311 [hep-ph/9809367].

[96] J. w. Qiu and X. f. Zhang, *QCD prediction for heavy boson transverse momentum distributions*, *Phys. Rev. Lett.* **86** (2001) 2724 [hep-ph/0012058].

[97] J. w. Qiu and X. f. Zhang, *Role of the nonperturbative input in QCD resummed Drell-Yan Q_T-distributions*, *Phys. Rev.* **D 63** (2001) 114011 [hep-ph/0012348].

[98] C. T. H. Davies, B. R. Webber and W. J. Stirling, *Drell-Yan Cross-Sections at Small Transverse Momentum*, *Nucl. Phys.* **B 256** (1985) 413 [CERN-TH-3987/84].

[99] G. A. Ladinsky and C. P. Yuan, *The Nonperturbative Regime in QCD Resummation for Gauge Boson Production at Hadron Colliders*, *Phys. Rev.* **D 50** (1994) 4239 [hep-ph/9311341].

[100] F. Landry, R. Brock, P. M. Nadolsky and C. P. Yuan, *Tevatron Run-1 Z boson data and Collins-Soper-Sterman resummation formalism*, *Phys. Rev.* **D 67** (2003) 073016 [hep-ph/0212159].

[101] A. V. Konychev and P. M. Nadolsky, *Universality of the Collins-Soper-Sterman nonperturbative function in gauge boson production*, *Phys. Lett.* **B 633** (2006) 710 [hep-ph/0506225].

[102] G. Turnock, *Energy-energy correlation distribution in e^+e^- annihilation*, Cambridge University Ph. D. thesis (1992) [Cavendish-HEP-92/3].

[103] S. Catani, G. Turnock, B. R. Webber and L. Trentadue, *Thrust distribution in e^+e^- annihilation*, *Phys. Lett.* **B 263** (1991) 491 [CAVENDISH-HEP-91-3].

[104] A. D. Martin, R. G. Roberts, W. J. Stirling and R. S. Thorne, *Physical gluons and high-E_T jets*, *Phys. Lett.* **B 604** (2004) 61 [hep-ph/0410230].

[105] S. Tafat, *Nonperturbative corrections to the Drell-Yan transverse momentum distribution*, *J. High Energy Phys.* **05** (2001) 004 [hep-ph/0102237].

[106] F. Landry, R. Brock, G. Ladinsky and C. P. Yuan, *New fits for the non-perturbative parameters in the CSS resummation formalism*, *Phys. Rev.* **D 63** (2001) 013004 [hep-ph/9905391].

[107] G. Marchesini and B. R. Webber, *Associated transverse energy in hadronic jet production*, *Phys. Rev.* **D 38** (1988) 3419 [NSF-ITP-88-67].

[108] R. B. Appleby and M. H. Seymour, *The resummation of inter-jet energy flow for gaps-between-jets processes at HERA*, *J. High Energy Phys.* **09** (2003) 056 [hep-ph/0308086].

[109] N. Kidonakis, G. Oderda and G. Sterman, *Threshold resummation for dijet cross sections*, *Nucl. Phys.* **B 525** (1998) 299 [hep-ph/9801268].

[110] A. Banfi, G. Marchesini and G. Smye, *Azimuthal correlation in DIS*, *J. High Energy Phys.* **04** (2002) 024 [hep-ph/0203150].

[111] A. Banfi, G. P. Salam and G. Zanderighi, *Principles of general final-state resummation and automated implementation*, *J. High Energy Phys.* **03** (2005) 073 [hep-ph/0407286].

[112] J. Pumplin, D. R. Stump, J. Huston, H. L. Lai, P. Nadolsky and W. K. Tung, *New generation of parton distributions with uncertainties from global QCD analysis*, *J. High Energy Phys.* **07** (2002) 012 [hep-ph/0201195].

[113] A. Banfi and M. Dasgupta, *Dijet rates with symmetric E_t cuts*, *J. High Energy Phys.* **01** (2004) 027 [hep-ph/0312108].

[114] A. Banfi, G. P. Salam and G. Zanderighi, *Resummed event shapes at hadron hadron colliders*, *J. High Energy Phys.* **08** (2004) 062 [hep-ph/0407287].

[115] G. P. Korchemsky and G. Sterman, *Power corrections to event shapes and factorization*, *Nucl. Phys.* **B 555** (1999) 335 [hep-ph/9902341].

[116] A. V. Belitsky, G. P. Korchemsky and G. Sterman, *Energy flow in QCD and event shape functions*, *Phys. Lett.* **B 515** (2001) 297 [hep-ph/0106308].

[117] G. Altarelli, R. K. Ellis and G. Martinelli, *Leptoproduction and Drell-Yan Processes Beyond the Leading Approximation in Chromodynamics*, *Nucl. Phys.* **B 143** (1978) 521 [Erratum-*ibid.* **B 146** (1978) 544] [MIT-CTP-723].

[118] W. A. Bardeen, A. J. Buras, D. W. Duke and T. Muta, *Deep Inelastic Scattering Beyond the Leading Order in Asymptotically Free Gauge Theories*, *Phys. Rev.* **D 18** (1978) 3998 [FERMILAB-PUB-78-042-THY].